Tampere University

MIIKA AHOPELTO

Towards Automation and Improved Fuel Economy with System Architecture Design of a Non-Road Working Machine

Tampere University Dissertations 147

Tampere University Dissertations 147

MIIKA AHOPELTO

Towards Automation and Improved Fuel Economy with System Architecture Design of a Non-Road Working Machine

ACADEMIC DISSERTATION
To be presented, with the permission of
the Faculty of Engineering and Natural Sciences
of Tampere University,
for public discussion in the K1702
of the Konetalo building, Korkeakoulunkatu 6, Tampere,
on 29 November 2019, at 12 o'clock.

ACADEMIC DISSERTATION
Tampere University, Faculty of Engineering and Natural Sciences
Finland

Responsible supervisor and Custos	Professor Kalevi Huhtala Tampere University Finland	
Pre-examiners	PhD. Reno Filla Scania CV AB Sweden	Professor Juha Pyrhönen LUT University Finland
Opponents	Assoc. Professor Kari Tammi Aalto University Finland	Professor Juha Pyrhönen LUT University Finland

The originality of this thesis has been checked using the Turnitin OriginalityCheck service.

Cover design: Roihu Inc.

ISBN 978-952-03-1289-3 (print)
ISBN 978-952-03-1290-9 (pdf)
ISSN 2489-9860 (print)
ISSN 2490-0028 (pdf)
http://urn.fi/URN:ISBN:978-952-03-1290-9

PunaMusta Oy – Yliopistopaino
Tampere 2019

PREFACE

This dissertation was carried out at the Laboratory of Automation and Hydraulics (AUT, formerly IHA) at Tampere University. The beginning of the research was funded by the Academy of Finland and Doctoral Program of Concurrent Mechanical Engineering (DPCME). The finalising of the research and summarising of the results was funded by the Doctoral School of Industry Innovations (DSII) of Tampere University of Technology in cooperation with Bosch Rexroth AG. Further, this thesis was financially supported by the Wärtsilä Relief Foundation of Tampere University of Technology, KAUTE Foundation and Henry Ford Foundation.

I would like to express my deepest gratitude to my supervisor, Prof. Kalevi Huhtala, for his guidance, support and patience, as well for providing facilities for this study over the years. I thank Dr. Steffen Mutschler (Bosch Rexroth) for his comments and support while finalizing this study. I am grateful to Prof. Seppo Tikkanen for the discussions and review of my dissertation. The pre-examination feedback from Prof. Juha Pyrhönen and Dr. Reno Filla is highly appreciated.

Especially, I would like to express my gratitude to my colleagues Ville Ahola, Joni Backas, Reza Ghabcheloo, Mikko Huova, Mika Hyvönen, Timo Julkunen, Juha Järä, Miikka Ketonen, Antti Kolu, Tomi Krogerus, Jussi Tervonen, Jarno Uusisalo and Antti Vuohioja for fruitful discussion and teamwork in building and designing the machine discussed in this thesis.

Finally, I am grateful to my parents Satu-Maaria and Väinö, and to my brother and sisters Samuel, Josefina, Annika and Annuliina, for their support over the years, and especially to Saija, my love, for her understanding and patience during the final stages of my studies.

Miika Ahopelto, Tampere, November 2019

ABSTRACT

Increasing levels of automation and interest in fuel economy have been affecting the system design of non-road working machines. Both fuel economy and automation have been active research areas in non-road working machines. It is unlikely that in the near future electrification will solve the energy challenges of machines operating for long periods in forests, mines or fields. Therefore, it is necessary to increase the fuel efficiency of such machines with conventional technology, taking into account the fact that automation, along with the diversity of subcontractors and performance requirements, has increased the complexity of these machines.

A modular abstraction layer architecture is proposed for the machine level to support the development of automation and comparison of fuel economy. The architecture is developed and selected on the premise that a machine is operated with different automation levels between manual and autonomous operation and employs alternative control methods for different operation conditions. The designed system architecture is compared with alternative approaches by using trade-off analysis with defined scoring functions.

For improving fuel economy and demonstrating the capability of the designed architecture, a modular power management architecture is realised to meet the performance requirements of the machine. This architecture breaks the system down into smaller modules to facilitate design and development. Further, the architecture separates control of the power sources from the consumers, providing a new degree of freedom in designing the subsystems, as the consumer modules are not coupled with the engine.

The improvement in fuel economy is based on the MinRpm control strategy, which is integrated with the power management architecture. The objective of MinRpm is to minimise the rotational speed of the engine, which leads to the engine operating with higher partial loads and in a higher fuel efficiency region. In addition, the components and subsystems that use relative constant torque use less energy when

the rotational speed is lower. Devices of this kind are typically fans, fixed displacement pumps and oil coolers, in which the torque demand is not highly dependent on the rotational speed of the engine. The proposed modular power management architecture with the MinRpm control strategy does not require any new components to make improvements in fuel economy, which, in turn, reduces the implementation costs.

In both simulations and in experimental tests with a municipal wheel loader, the control method resulted in fuel savings of 11 to 22% compared with a series-production machine on the market. The comparison is realised by integrating the emulated series-production machine control with the same system architecture that was developed for the power management system with MinRpm approach. Therefore, both control methods are realised with the same wheel loader, which eliminates discrepancy of the component properties.

Realisation of the alternative control methods in the designed system architecture demonstrates the compatibility needed when the machine is operated with different operating modes from manual to autonomous. Before fully autonomous machines become real, a different level of automation is needed to perform efficiently and safely in all operation conditions. Therefore, the designed system architecture is capable of rerouting control signals and control flows, while safety features are guaranteed when the control mode is changed.

CONTENTS

List of Figures

List of Tables

NOMENCLATURE

Symbols

Roman symbols	**Description**	**Unit**
a_i	Member of Matrix $\boldsymbol{A}$	-
A	Area	m2
$\boldsymbol{A}$	Matrix A	-
A_{A}	Area of A-chamber	m2
A_{B}	Area of B-chamber	m2
b_i	Member of Matrix $\boldsymbol{B}$	-
b_{v}	Viscous friction coefficient	kg/s
$\boldsymbol{B}$	Matrix B	-
c_0	Machine specific constant	1/m
C_{air}	Aerodynamic drag coefficient	-
C_{press}	Pressure based gain	-
$C_{\mathrm{press,filt}}$	Filtered pressure-based gain	-
f_{roll}	Tire rolling resistance coefficient	-
F_{acc}	Acceleration force	N
F_{air}	Air drag	N
F_{c}	Coulomb friction force	N
F_{cyl}	Cylinder force	N
$F_{\mathrm{drivetrain}}$	Drive train friction force	N
F_{roll}	Rolling resistance	N
F_{slope}	Slope resistance	N
F_{FL}	Force of the front-left tire	N
F_{FR}	Force of the front-right tire	N
F_{RL}	Force of the rear-left tire	N
F_{RR}	Force of the rear-right tire	N

g	Gravity	m/s2
$i_{\Delta p}$	Tolerance of differential pressure	bar
i_q	Tolerance of flow rate	-
i_v	Tolerance of velocity	m/s
J	Inertia	kgm2
J_{A1}	Inertia of first shaft	kgm2
J_{A2}	Inertia of second shaft	kgm2
J_{Eff}	Effective inertia	kgm2
J_M	Inertia of hydraulic motor	kgm2
J_{tire}	Inertia of tire	kgm2
r_{fuel}	Fuel consumption rate	g/s
r_{tire}	Effective radius of tire	m
m	Mass	kg
m_{eff}	Effective mass	kg
n	Rotational speed of the engine	1/min
n_{tire}	Rotational speed of the tire	1/s
p	Pressure	Pa
$p_{cut-off}$	Cut-off pressure of the system	Pa
p_{loss}	Pressure loss	Pa
p_A	Pressure of A-chambers	Pa
p_B	Pressure of B-chambers	Pa
P	Power	W
P_{cyl}	Power of the cylinder	W
P_{in}	Power in	W
P_{loss}	Power loss	W
P_{st}	Steady-state power	W
P_{out}	Power out	W
Q	Flow rate	m3/s
Q_{in}	Flow rate in	m3/s
Q_{out}	Flow rate out	m3/s
Q_A	Input flow rate in the A-chamber	m3/s
Q_B	Input flow rate in the B-chamber	m3/s
t_0	Fixed time constant	s
T	Torque	Nm

T_{in}	Torque in	Nm
T_{out}	Torque out	Nm
v	Velocity	m/s
v_{cyl}	Velocity of cylinder	m/s
v_{src}	Searched velocity	m/s
v_{w}	Head-wind velocity	m/s
$\dot{v}$	Acceleration	m/s2
V	Maximum displacement	m3/rev

Greek symbols	**Description**	**Unit**
α_1	Gear ratio of the front and rear gear box	-
α_{gear}	Gear ratio of the gear box connected to the hydraulic motor	-
α_{final}	Final gear ratio	-
Δ	Differential, eg. Δp is differential pressure	-
ε	Displacement ratio	-
$\varepsilon_{\text{m,0}}$	Initial displacement ratio of the motor from predefined control sequence	-
$\varepsilon_{\text{p,0}}$	Initial displacement ratio of the pump from predefined control sequence	-
ρ_{air}	Density of air	kg/m
θ	Slope grade	rad
η	Efficiency	-
η_{hm}	Hydro-mechanical efficiency	-
η_{vol}	Volumetric efficiency	-
η_{tot}	Total efficiency	-
τ	Time constant	S
ω	Angular velocity	rad/s
ω_k	Current rotational speed	rad/s
ω_{k-1}	Previous rotational speed	rad/s
$\omega_{\text{ICE,0}}$	Initial angular velocity of the engine from predefined control sequence	rad/s
$\omega_{\text{ICE,refC}}$	Droop compensated reference for the engine	rad/s

$\dot{\omega}$	Angular acceleration	rad/s

Common subscripts	**Description**
act	Actual
Drive	Drive system
External	External
Extra	Extra
idle	Idle
ICE	Internal Combustion Engine
Implement	Implement system
Lift	Lift of the boom
m	Hydraulic motor
max	Maximum value
min	Minimum value
opt	Optimal
p	Hydraulic pump
pred	Predicted
ref	Reference
req	Request
serv	Served
Tilt	Tilt of the boom

ABBREVIATIONS

AFS	Articulated Frame Steering
BPC	Best Point Control
BSFC	Brake Specific Fuel Consumption
BTE	Brake Thermal Efficiency
CAN	Controller Area Network
CO	Carbon Monoxide
CO2	Carbon Dioxide
CVT	Continuously Variable Transmission
DA	Drive and Anti-stall
DPF	Diesel Particulate Filter
DVS	Digital Valve System
DFCU	Digital Flow Control Unit
ECU	Electronic Control Unit
EGR	Exhaust Gas Recirculation
ELS	Electronic Load Sensing
EPA	Environmental Protection Agency
ESM	Emulated Series-Production Machine
ETAC	Electronic Transmission Automotive Control
ETC	Electronic Torque Control
EV	Electric Vehicle
GNSS	Global Navigation Satellite System
GPS	Global Positioning System
HC	Hydrocarbon
HIL	Hardware in the Loop
HSD	Hydrostatic Drive
ICE	Internal Combustion Engine
I/O	Input/Output
IVT	Infinitely Variable Transmission
LNT	Lean NOx trap
LS	Load Sensing

LTC	Low Temperature Combustion
MIL	Model in the Loop
MinRpm	Minimum rpm Approach with Power Management
NCS	Networked Control System
NOx	Nitrogen Oxides
PC	Personal Computer
PLC	Programmable Control Units
PM	Particulate Matter
RPM	Revolutions per Minute
SCR	Selective Catalytic Reduction
SIL	Software in the Loop

1 INTRODUCTION

Agricultural tractors, mining machines, construction machines and other types of non-road working machines carry out various operations that depend on the application and work tasks. From these operations, typical work cycles can be defined for each machine type and for different tasks, which can later be used when analyzing the performance of machines or operators.

Controllability and safety are always aspects that should be considered when these machines are studied. In terms of fuel economy and machine performance, control should be carried out with a system architecture that supports improvements to both the operability and performance of the machine. A non-road working machine consists of systems with multiple actuators and subsystems that are coupled together with inputs or outputs. The main subsystems in terms of fuel economy are the primary power source, drivetrain, steering and boom, and gripper or manipulator. These systems contain different kinds of actuators, such as hydraulic valves, hydraulic pumps and motors, or electric motors. Furthermore, the control system might have connections to the driving lights, dashboard meters, ignition system, relays, and other devices.

The electrification and automated functionalities of non-road working machines are constantly increasing, which, in turn, enables multiple approaches to improving controllability, energy efficiency or decreasing total emissions during the work tasks. The challenge involves how to design a control system that can optimize and realize multiple requirements. Some of these objectives can be mutually inconsistent – for example, decreasing fuel consumption can increase NOx emissions due higher temperature of the combustion. Furthermore, productivity and performance can entail various objectives that can be different to those set while improving fuel economy or decreasing emissions. The control systems of non-road working machines should therefore provide an architecture that supports the development of control methods and functions that achieve multiple objectives.

1.1 Motivation and background

A briefing paper from the Transport and Environment Association indicates that forecasts for a market share of electric vehicles (EV) will average 20% in the year 2025, but vary widely between five to over 50 [1]. However, the market share of non-road working machines is unlikely to change that fast. One of the main issues is the low energy density of batteries (1-4 MJ/kg) compared with fossil fuels (42-44 MJ/kg) [2, 3]. The chemical energy consumed in the powertrain (tank-to-wheel) in an electric vehicle is one-third of that in a gasoline vehicle [3]. The energy density is more significant in off-road vehicles, because charging is not always possible due to long operating times and limited charging possibilities when operating far from the electric infrastructure. Therefore, internal combustion engines will still have a significant role in non-road working machines in future decades.

Furthermore, the cost of fuel and tightened emission legislations and standards highlight the need to develop new methods for the reduction of both emissions and fuel consumption. There are multiple approaches for reducing fuel consumption by improving individual components or subsystems, such as pump efficiency [4], drivelines [5], implemented hydraulics [6, 7] or steering systems [8]. Another active area is hybrid and electric machines, where research is currently focusing on system configurations and optimizing total energy consumption [9-11] or extending the optimization to the work process [12].

Without new components or system configurations, fuel economy can be improved by optimizing the path and trajectories of the machines during work cycles [13, 14] or considering new control strategies for their actuators and subsystems, such as controlling a diesel engine [15] or driveline [11]. Optimizing the control of subsystems does not result in the overall optimized operation of the machine components. Instead, overall optimization can lead to a significant saving in fuel consumption by using predictive methods and known work cycles [16, 17] or by trying to optimize the operation point in current conditions [18-20].

As non-road working machines contain multiple subsystems that are controlled in parallel, a system architecture that allows the independent control of subsystems but supports co-coordinated control is required. A top-rated approach to manage the various functions that can control multiple components is distributed control system architecture, where control is distributed in different tasks. There are multiple

examples of how the control system can be distributed in tractors, harvesters or mining machines [18, 21-24]. Typically, this system is close to networked control systems (NCSs). NCSs apply a shared communication network, whereby distributed controllers operate at the intersection of control and communication theories [25].

1.2 Scope of the thesis

The objective of this thesis is to define a system architecture and algorithms that support improvements in the automation level and fuel economy of non-road working machines by increasing the efficient use of the components and subsystems. The results of the study apply to non-hybrid machines and autonomous machines. Improving fuel consumption should take into consideration the properties of non-road working machines, including rapidly changing power demands, various operation conditions and work cycles, controllability, and multiple actuators and subsystems. The system architecture considers a machine with alternative control methods and control modes, such as a manual, teleoperated and autonomous. The study is realised with a municipal wheel loader that represents a typical non-road working machine.

From these objectives, the following research questions were derived:

RQ1: *How can the system architecture support the development of automation and fuel economy of a non-road working machine?*

Since the objective is to improve the fuel economy and automation level by researching alternative control methods of the entire machine, the following questions arise: How can the system architecture support the communication between different subsystems? How can control methods be developed that allow a comparison of improvements in fuel economy? How can the system architecture support the development of alternative control methods and how can the operating modes from a manual, semi-autonomous to autonomous operation be changed? What are the requirements for the architecture, and how can these be fulfilled in comparison with alternative architectures? Furthermore, typical non-road machines consist of several subsystems that might be developed by different teams or subcontractors; therefore, how can modularity be supported in the architecture so that the different subsystems work together?

RQ2: *How can the control methods be realised in the architecture and what are the improvements that can be achieved in a wheel loader with hydrostatic drive?*

When the objective is to develop control algorithms that improve fuel economy or introduce new control methods, how can these be realised in the system architecture? What are the improvements that can be achieved in fuel economy without modifying the components (such as hybrids or new components), and how do different control methods affect the fuel economy? How much potential is there for fuel savings in a real machine with realistic work cycles as the control should guarantee the operational performance?

RQ3: *How are typical functionalities of the wheel loader realised in the designed architecture?*

Various functionalities, such as anti-stalling of the engine, engine braking or torque control, are needed; thus, how can these be realised in the selected architecture? What limitations are there, and how are these related to the alternative control modes? What limitations are related to the control methods that improve fuel economy?

1.3 Methodology

This study concentrates on the development of a system architecture and control method for fuel efficient non-road machines. The research process had the following steps: (1) analysis and identification of requirements, (2) design, development and evaluation of a system architecture, (3) design and implementation of control methods, and (4) evaluation and analysis of the results. In practice, the process comprised several iterative steps to reach the final results.

The system development was based on the theoretical background of control architectures and was applied in the field of non-road machines, which sets the requirements for the design. The designate architecture was evaluated against alternative approaches. The design and implementation of a control method realised with the architecture was based on the studied efficiencies and preliminary analysis of the fuel economy.

The preliminary fuel economy analysis of the experimental machine was carried out in the simulation study with steady-state conditions. The efficiencies of the

subsystems were defined from the measured data points and were analysed with Matlab/Simulink. Further, the steady-state model of the municipal wheel loader was defined to support the analysis of different control methods. The parameters of the machine were based on the experimental measurements. The alternative solution for the steady-state simulations would be the dynamic model of the experimental machine and analyzing a full work cycle that contains transient operation conditions.

Nevertheless, one challenge of the dynamic models and simulations was the non-linear behavior of the components that requires detailed data about the components and system parameters. In particular, an accurate simulation of fuel consumption is challenging in dynamic operation conditions as the fuel consumption of the internal combustion engine has significant difference from the steady-state points. Due to these challenges, the simulation study was limited to steady-state conditions.

After design and implementation of the developed control method, experimental evaluation was used to prove the achieved improvements in the fuel economy. The experimental test cases were defined from the literature and earlier studies, including the experience that was gained from the studied machine. Therefore, the used test cases are assumed to represent typical work cycles for the studied machine. Further, the experimental tests were analyzed in detail in terms of performance and fuel economy in different operation conditions.

Further, Matlab/Simulink with code generation tools was applied for the implementation of the control methods. That shortened the implementation phase as the same realisation of the control method was used both in the simulations and executed in the target system of the experimental machine.

1.4 Boundaries

This work proposes system architecture that is suitable for research of alternative control methods and can be operated in different operation modes. Further, the purpose is to provide a control architecture that improves fuel economy and can handle the constraints of non-road working machines that are related to unknown work cycles and required performance. Control methods and signals should be easy to modify, without significant change in the system architecture.

As long as the next work actions cannot be predicted with certainty, there should be enough reserved power for further actions. The proposed control method is designed for conventional machines, not hybrids, so there is no other energy storage except the diesel engine that provides the mechanical energy.

Further, the assumption here is that the actuators can be decoupled from the engine, with a continuously variable gear ratio for a drive that can be realized with hydrostatic transmission or with another system that provides continuously variable transmission for implements that are typically realized with throttle controlled valves. In this study, the control with these boundaries is defined for the municipal wheel loader used in the experimental tests.

Due to these boundaries, the used control method does not ensure the optimal operation point for the machine in all possible operation conditions. The improvements in fuel economy were demonstrated in the typical work cycles of the municipal wheel loader. These work cycles were analyzed in detail to show the functions that produce fuel savings. This information could be applied in other types of machines and work cycles. Furthermore, the fuel economy of the proposed approach was compared with the emulated series-production machine to illustrate the potential of fuel improvements in commonly used machines.

1.5 Contribution

The contributions of this thesis are related to previous research on non-road working machines. The branches of science to which this research applies are software (modularity and communication interfaces), control (feedback loops and low level control), system design (system architecture and distribution), hydraulics and automation (simulation and control of hydraulic components).

1.5.1 Scientific contribution

The main contributions of this thesis are the following:

C1: *Design and realisation of system architecture and a modular power management system that is compliant with alternative control methods and multiple operation modes*

The proposed system architecture and modular power management architecture is presented in Chapters 5 and 6. The system architecture is analyzed by comparing the system characteristics with alternative approaches in Chapter 5. The machine specific functionalities are implemented in the modular power management in Chapter 7. That shows how the system constraints can be handled with the module level functions. Chapter 8 shows that the architecture and functions are capable of performing similarly in the municipal wheel loader compared with the series-production machine. This demonstrates the capability of the system architecture to adapt to alternative control flows and modes.

C2: *Comparison of fuel economy in municipal wheel loader with hydrostatic drive between a minimizing engine rotational speed approach and a conventional control method*

The fuel economy of the municipal wheel loader is analyzed by the simulation research in Chapter 4, which compares the traditional control method of hydrostatic drive with the optimal approach. Based on the simulation study and earlier studies, an alternative control method with a designed system architecture is tested in real-world work cycles, and is shown in Chapter 8. The test results are analyzed with a comparison of control methods and demonstrating where fuel economy is improved. Further, Chapter 8 shows that the machine can maintain performance in comparison with the conventional control method.

C3: *Experimentally validated functionalities in machine specific work cycles*

The machine specific functionalities are implemented in the modular power management in Chapter 7. The robustness of modular power management is shown with experimental tests in Chapter 8. The chapter demonstrates improvements in fuel economy and shows how different functionalities of the modules operate. The fuel economy of the developed machine is compared with an emulated series-production machine. This demonstrates not only improvements in fuel economy but additionally the capability of system architecture to comply with alternative control flows and methods.

1.5.2 The author's contribution

The experimental wheel loader used in this study was designed and built by teamwork at the Laboratory of Automation and Hydraulics (AUT, formerly IHA).

The machine has been used as the research platform for several studies in the field of design, energy efficient components, fuel economy, emissions, surround sensing and autonomous operation. In this study, the author contributed the research in the fields of fuel economy, system design and control design.

For the preliminary analysis of fuel economy, the author developed the model of machine and component efficiencies based on the available data from an earlier study. The models and parameters are adapted and updated to this study. The author used these models for simulations of the fuel economy of different control methods. Further, the control methods of the reference systems were adapted from the literature and implemented in Simulink by the author.

The author defines the architecture and control method that results in improved fuel economy in comparison with the series-production machine. The design was based on information gathered in the research of non-road working machines carried out in the laboratory facilities. Further, based on that information, the required system features and characteristics were defined for evaluation of the system architectures. The realisation the control algorithms of the drive and engine control in the machine was done by using Matlab/Simulink and code generation tools for C-code by the author. However, the design and realisation of the low-level control functions of the implements (tilt and lift) was not performed by the author. These low-level functionalities include the control of the proportional valves and the load sensing control of the implemented pump and power restriction. Nevertheless, the author modified the realisation so that it is integrated into the power management architecture of the machine.

Finally, the author defined the test procedure and test cycles for the experimental tests. Additionally the data collection and analysis of the measurement presented in this study was performed by the author.

1.5.3 Publications

The publications that this thesis is based on are as follows:

Publication I M. Ahopelto, J. Backas, K. Huhtala, Power Management in a Mobile Work machine: Reduced Diesel RPM for Better Energy Efficiency, Proceedings of the 7th FPNI PhD Symposium on Fluid Power,

Reggio Emilia, Italy, June 27-30, 2012, University of Modena and Reggio Emilia., Reggio Emilia, Italy, pp. 133-148.

Publication II M. Ahopelto, J. Backas, R. Ghabcheloo, K. Huhtala, Improved Energy Efficiency and Controllability of Mobile Work Machines by Reduced Engine Rotational Speed, Proceedings of the ASME 2013 International Mechanical Engineering Congress and Exposition, IMECE2013, San Diego, California, USA, November 15–21, 2013, ASME, pp. 1-8.

Publication III M. Ahopelto, K. Huhtala, Prediction of Drive Torque in Hydraulic Wheel Loader, Bath, United Kingdom, September 10–12, 2014, The American Society of Mechanical Engineers ASME, pp. 1-8.

Publications that are related to this thesis:

Publication IV M. Huova, M. Ahopelto, M. Ketonen, V. Ahola, M. Linjama, K. Huhtala, Characteristics of Digital Hydraulics with Commercial Controllers, The Seventh Workshop on Digital Fluid Power, Linz, Austria, February 26 - 27, 2015, Linz Center of Mechatronics. pp. 114-128.

Publication V M. Ahopelto, T. Krogerus, K. Huhtala, Vehicle Mass Estimation for Hydraulic Drive System using Longitudinal Motion Model, The Fourteenth Scandinavian International Conference on Fluid Power, SICFP15, Tampere, Finland, May 20-22, 2015, pp.433-442.

Declaration of author's contribution to the publications:

Publication I presented a preliminary version of the power management architecture and experimental comparison measurements of the fuel consumption. The study was realized in a wheel loader with hub motors, which was different than that used in this thesis. The author designed the architecture and implemented the controller in the machine. Joni Backas helped with the comparison measurements of fuel economy and wrote the paper with the author. Professor Kalevi Huhtala reviewed the paper.

Publication II showed how the control architecture with minimized rpm approach was implemented in the studied machine. The author implemented the algorithms in the commercial PLC controller using the programming languages defined in the IEC 61131-3. Joni Backas helped with the measurements and wrote the paper with the author. Professor Reza Ghabcheloo helped in the writing and reviewed the paper with Professor Kalevi Huhtala.

Publication III defined a longitudinal drive model for the studied machine with defined parameters. This model was applied in the steady-state simulation of the machine in this thesis. The author wrote the paper, developed the model and made the experimental measurements. Professor Kalevi Huhtala reviewed the paper.

Publication IV presented how the code of the digital hydraulic controller can be generated from Simulink to the PLC code. In this thesis, a similar code generation approach is used to generate executable code for the controllers of the machine. Mikko Huova developed the controller, made the coding in Simulink, and was responsible for the writing of the paper. The author made the code generation, integration and scheduling of the controller in the PLC code and wrote the sections related to the hardware independent development process, code generation and scheduling. Miikka Ketonen, Ville Ahola, Matti Linjama and Kalevi Huhtala reviewed the paper.

Publication V presented the use of the longitudinal drive model for estimation of the mass of the machine. The same model is applied in this thesis in the steady-state simulations. The paper showed that the model was accurate enough to estimate vehicle mass in predefined conditions. The author defined the model, performed the experimental measurements and wrote the paper. Doctor Tomi Krogerus and Professor Kalevi Huhtala reviewed the paper.

1.6 Outline of the thesis

This thesis comprises nine chapters, each of which contributes to the topics of improving fuel economy and modular power management architecture. Chapter 1 begins with the introduction, motivation and background for this work. Further, Chapter 1 presents the research methodology used, the boundaries to and contributions of the research.

Chapter 2 introduces the state of the art of energy efficiency in non-road working machines, consisting of a short summary of the energy efficiency of components, suitable systems and control architectures for non-road working machines, the current approaches to the power management of non-road working machines, and the challenges posed by the standard work cycles.

Chapter 3 presents the experimental wheel loader used in this study. Further, the chapter defines the model for the machine and its subsystems. The model was used to study the efficiency of the machine and its subsystems in different steady-state operation conditions. This analysis is presented in Chapter 4, which shows the potential for fuel economy in the driving and compares the efficiencies of different control methods.

Chapter 5 presents the system architecture and evaluation with alternative architectures by using trade-off analysis with defined scoring functions. Chapter 6 shows the modular power management approach that separates control to the subsystems. Further, the architecture allows the integration of autonomous functions with machine-level control. The primary requirements and control design for the different modules of the system are also presented in Chapter 6.

Chapter 7 discusses the constraints related to drive performance and system dynamics and how these can be handled with modular power management. The constraints are derived from both the required drive functions and the required performance of the machine. Further, the modules of the power management architecture are interconnected systems that require control to prevent oscillations and ensure robust operation in unpredicted operation conditions. The functionalities that can handle these requirements are presented in Chapter 7.

Chapter 8 illustrates experimental tests from real-world drive and work cycles. The performance of the presented approach is compared with an emulated control of the series-production machine in terms of fuel economy and performance. The test cases represent typical cycles for the applied machine.

Chapter 9 discusses the presented results and answers to the research questions outlined in Chapter 1.2. Finally, Chapter 10 concludes by summarizing the thesis contributions and suggestions for future research.

2 STATE OF THE ART OF ENERGY EFFICIENT NON-ROAD WORKING MACHINES

This chapter describes the state of the art of energy efficient non-road working machines, how and where energy losses originate, the typical efficiencies of subsystems (Chapter 2.1), the kind of system and control architecture required for working machines (Chapter 2.2), the control approaches needed for improving energy efficiency and power management (Chapter 2.3), and how the energy efficiency of a variety of machines can be tested in realistic work cycles (Chapter 2.4).

2.1 Energy efficiency and fuel consumption

Energy losses are highly dependent on the work cycle [26], machine type [27-30] or operator actions [31-33]. The generalization of energy losses in actual fuel consumption is always challenging because of the involvement of many variables and cycles. Sometimes, even a small change in efficiency can have a dramatic effect on fuel consumption. In the simulated load cycles of the displacement-controlled actuator system, comparing the performance of two axial piston-type pumps with a difference of maximum total efficiency of only 3% results in 20% less energy consumption [26]. Based on these studies, it is important to research efficiency over a full work cycle, not only at a single efficiency point.

Figure 1 shows the power demand of an excavator, agricultural tractor, wheel loader and backhoe loader during the typical work cycle of each machine. The transient power with high peaks is typical for the power demand of non-road working machines. For conventional machines without external energy storage and powered by diesel engines, high peaks mean that the engine must always have reserve power for the peaks. Accordingly, this makes the optimization of fuel consumption challenging for these machines.

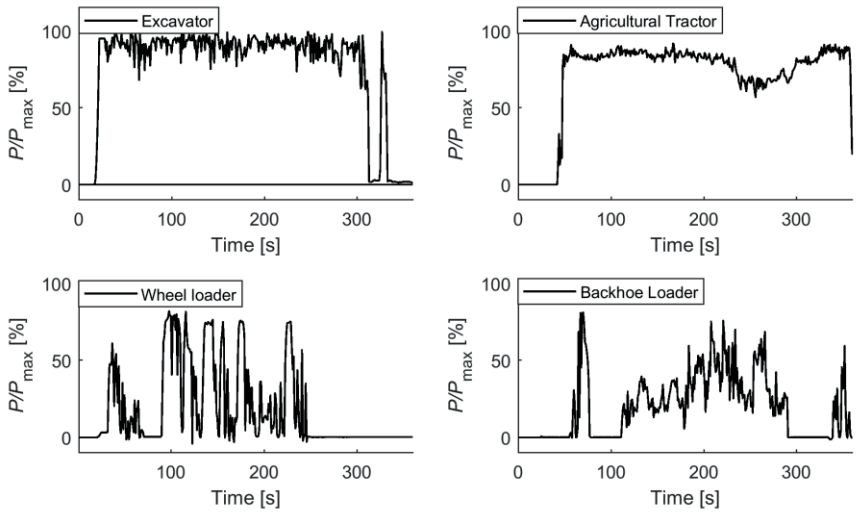

Figure 1. Typical power consumption from four different types of machine: data gathered in the field for EPA non-regulatory non-road duty cycles. [34]

Further, in many work tasks, idle time has a relatively high share. Therefore, reducing idling losses, for example with a start-stop system, can lower fuel consumption significantly.

2.1.1 Energy efficiency of machines

When the target is to improve fuel economy in a non-road working machine, it is essential to demonstrate savings in fuel consumption, not only power savings in the subsystems. Therefore, the energy distribution should be observed from the fuel chemical energy to the energy used for actual work from tank-to-wheel, or, in non-road working machines, from tank-to-work.

Typically, the highest loss from single components is caused by diesel engines. In the simulation study, a wheel loader working in the typical work cycle with four stages (filling the bucket, going to the unloading point, unloading the bucket, returning to the initial point) has 63% losses in the diesel engine, as shown in Figure 2. There, 78% of fuel energy is lost, and only 22% goes to the wheels, steering and implements (boom and bucket) [35]. The simulation study makes assumptions that the engine

efficiency, auxiliary load and efficiency of the pumps are constant. Therefore, the total losses could be different if measured in real-world driving.

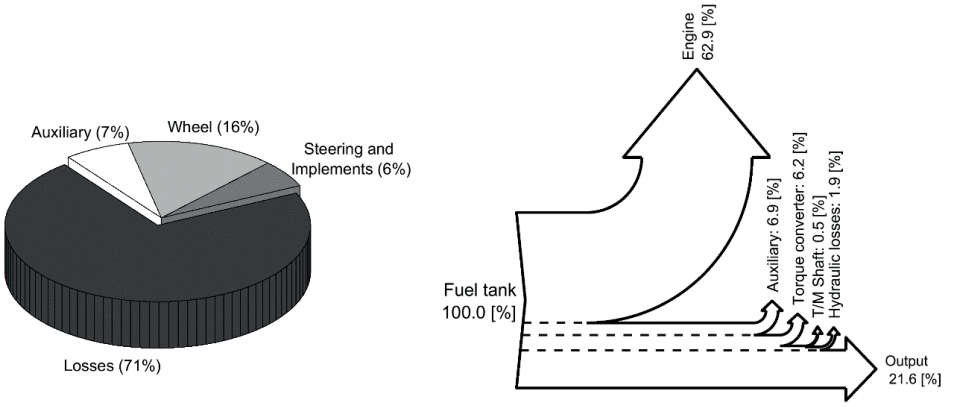

Figure 2. Only 22% of the fuel energy goes to the actual work; the remaining energy is lost or is used for the auxiliary. The figure is modified from [35].

Further, the idling time and performance of the work cycle have significant effects on the fuel consumption and energy share. The energy distribution of a working machine that repeats the work cycle without a long idling time is measured in the real machine and is shown in Figure 3.

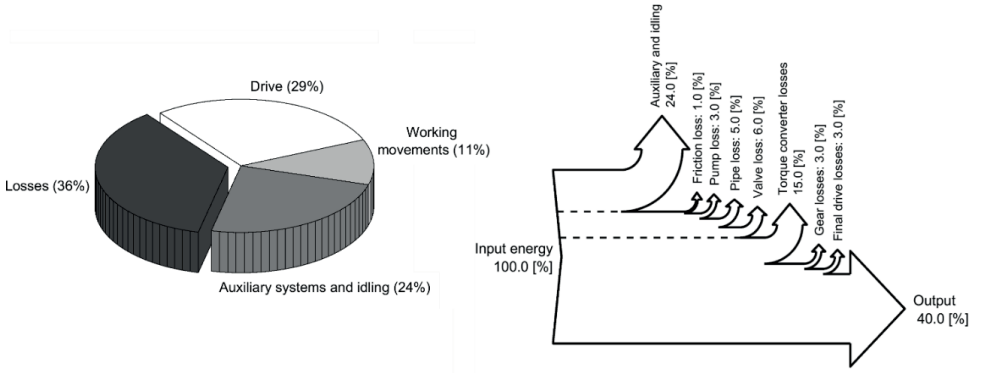

Figure 3. The average energy flow of a mobile working machine under a work cycle with 5% idling, where the input energy is the mechanical energy of the diesel engine. The figure is modified from [36].

The input energy is the mechanical energy of the diesel engine, and therefore the losses are 60% from that energy. In the study, the energy efficiency of the diesel engine was about 30% resulting in only 12% of the fuel energy for the actual work. From the output energy, 11% goes to the work movements, and 29% goes to the drive. The highest losses come from the auxiliary and from idling, followed by the torque converter [36].

Typically, energy consumption can be divided into main systems that are required for functions such as driving, steering or lifting, and auxiliary or external systems. The energy consumption of the main systems depends on the work cycle and operation point of the system, whereas the energy consumption of auxiliary systems is more dependent on other factors. For example, the usage and energy consumption of the oil coolers depend on the outdoor temperature, or energy consumption of the alternator depends on the electrical usage of the machine. Therefore, in some cases, the power consumption or torque consumption of the auxiliary systems can be assumed to be fixed.

2.1.2 Fuel economy and emissions of diesel engines

The maximum efficiency of an off-road machine diesel engine is typically close to 40%. For example, the highest thermal efficiency of the four-cylinder diesel engine of an agricultural tractor is 38% [37] or the average peak efficiency of a heavy-duty diesel engine is 39% [38]. The average energy efficiency is typically much lower when the loading of the diesel engine is not optimal. For example, the average efficiency for a diesel engine in motion applications (truck, car, ship, train and generator) is 22% [39]. The reason for this low average efficiency is the low efficiency of the diesel engine during low loading, as shown in Figure 4. Therefore, optimal use of the diesel engine could have a significant effect on the fuel economy of the machines.

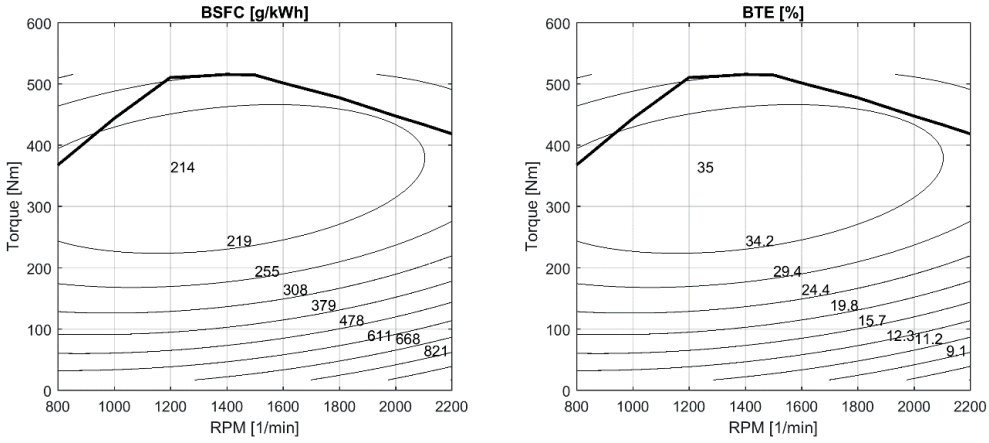

Figure 4. Calculated brake-specific fuel consumption (BSFC) and brake thermal efficiency (BTE) of a 95 kW four-cylinder diesel engine.

The development strategies for a high efficiency diesel engine typically conflict with emission reduction strategies and make efficiency improvements challenging. For example, exhaust gas recirculation (EGR) decreases nitrogen oxides (NOx), but with aggressive use, results in a significant increase in fuel consumption. Low temperature combustion (LTC) may improve fuel consumption, while at the same time reducing NOx and soot by separating the diesel injection from the combustion event. Limited load range and lack of control over ignition timing due to the properties of neat diesel fluid are still challenging for LTC strategies. The common NOx after-treatment systems are selective catalytic reduction (SCR) that requires the continuous injection of urea into the exhaust system, or a lean NOx trap (LNT) that requires external fuel, late-post injection or periodic rich combustion. These systems can decrease emissions but increase fuel consumption or costs [40]. Furthermore, diesel particulate filters (DPF) that remove soot or particulate matter require periodic regeneration that causes fuel penalties, decreasing fuel economy [41].

The used fuel has a significant effect on the combustion properties of engines, and engine operation could be optimized for different kinds of fuel [37, 40, 42]. Therefore, to achieve high fuel economy and low diesel engine emissions, the optimization should consider both the combustion system properties and fuel properties.

The average fuel consumption and emission maps of diesel engines are inconsistent with the optimal operation point. This is because of the shape of the fuel consumption and emission maps differing as a function of power and rotational speed. Therefore, each optimizing function is different, and optimizing only one variable can cause a penalty in another. Due to these reasons, it is not seen as a significant improvement to diesel efficiency in the near future; instead, higher improvement in machine efficiency could be achieved by optimizing the use of diesel engines.

Typically, in non-road working machines, the operation point of the diesel engine is always changed, as the work cycles of the machines include idling, high torque peaks, regenerated power, and varying torque and speed demands. Therefore, the operation of the diesel engine is highly dynamic, especially in conventional machines. In hybrid machines, the operation point of the diesel engine could be more stationary, as peak energy could be taken from the external energy source.

Lindgren showed that transient conditions affect the fuel consumption and emissions of diesel engines [43]. Several factors have been identified as to why fuel consumption and emissions differ between steady-state conditions and transient conditions. The inertia of the turbocharger has a time lag of several seconds during variations in engine load and speed. The response time for a mechanical governor and fuel pump rack position affects the time when the engine reaches a steady-state position [43]. It has been shown that transient conditions reduce fuel economy significantly compared with steady-state operation [44, 45].

As there are many factors that affect the emissions and fuel economy of diesel engines, accurate modeling is challenging, especially if the transient behavior of the engine is taken into account. Therefore, for reliable results regarding fuel economy, real-world fuel consumption measurements are used usually needed to proof the real fuel consumption.

2.1.3 Efficiency of subsystems

Mechanical energy from the engine is used for work actions, traction or auxiliary systems. The demand for high forces by work functions is typically facilitated with hydraulics that provide a high power density. The efficiencies of components vary as a function of the operation point; for example, the efficiency of a hydraulic pump

varies as a function of rotational speed, displacement ratio and pressure difference [26, 46, 47]. Efficiency can be separated into volumetric and hydro-mechanical efficiency; conversely, total efficiency is a combination of these. The best total efficiency is achieved with a high displacement ratio and relatively high pressure. Fluid properties, such as viscosity, can also change hydraulic efficiency and will thus be taken into consideration. Hydraulic motors have a similar efficiency behavior to pumps [47].

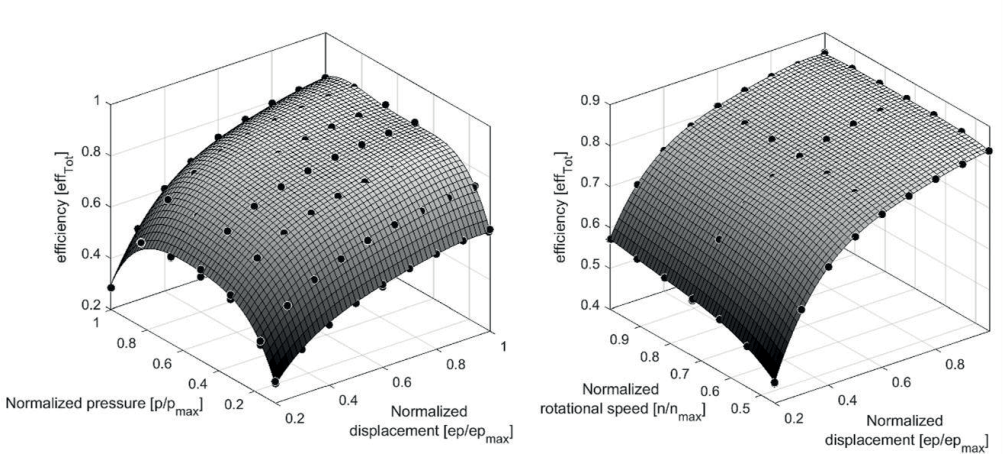

Figure 5. Total efficiency of a pump as a function of normalised pressure and displacement (left), and total efficiency of the pump as a function of normalized speed and displacement (right). The points were measured in laboratory conditions with a constant temperature.

Hydraulic-driven work actions are typically throttle-controlled with a pressure-compensated load-sensing system (LS) [48], or the cylinders are directly pump-controlled [49]. In load-sensing systems, the highest load (the highest pressure) sets the demand for the pump, and the flow is controlled by proportional valves. Conventional throttle control is not very energy efficient when there is a high difference in actuator loads, because the pressure drop over proportional valves is converted to heat. Therefore, efficiency improvements in load-sensing systems have been studied by using flow control [50] or digital hydraulic valve control [51].

Traction systems define how engine power is delivered to the wheels. The typically used systems for small- to medium-sized machines are hydrostatic transmissions with a coupled system comprising a hydraulic pump and motor, and a belt-driven

[52] or hydrostatic continuously variable transmission (CVT) [5]. For heavy machines, torque converters are commonly used. Furthermore, mechanical transmission with a gearbox can be used, but it does not provide continuously variable transmission. The efficiency of these systems varies as a function of rotational speed, torque and gear ratio. Hydrostatic transmission efficiency depends on the efficiency of the hydraulic pump and motor, as presented in Figure 5. The efficiency of a torque converter depends on the properties of the turbine. CVT has high efficiency in operation points where torque is transmitted mechanically. The mechanical drivetrain reaches high efficiency but does not provide a continuously variable transmission.

As the kinematic structure of non-road working machines varies widely, various steering types are implanted, such as wheel steering, axle steering, articulated frame steering (AFS), skid steering or track steering. Due to the diversity of steering mechanisms, the energy required for steering is not always easy to fractionate from the traction systems or auxiliary systems. In skid and track steering systems, the steering energy is a portion of the driving energy, as steering is controlled by changing the velocity of each side of the machine separately. AFS systems are often implemented with an independent hydraulic pump that generates power for the steering cylinders. Differential steering systems might have power-assisted steering that reduces the steering effort required from the driver. The overall operating efficiency of conventional valve-controlled AFS systems ranges between 0% and 67% depending on operation conditions and these have an effect on the total fuel consumption of the machine [8].

In addition to major energy consumers (work actions, traction and steering), non-road working machines have several auxiliary systems that consume energy, such as boost pumps, battery chargers, oil coolers and fans. The energy consumption of these systems is relative to operation time and operation conditions. Many of these systems, such as fixed displacement pumps and fans, cause an approximately constant torque on the engine, but power consumption is relative to the rotational speed of the engine. The energy consumption of alternators and actively controlled oil coolers is not that reliant on the engine's operation conditions, as their power consumption can be demand-controlled. In general, the energy consumption of auxiliary systems is significant in non-road working machines [35, 36].

To enable independence for the control of the engine and subsystems (work actions, steering and traction), power transmission between the engine and final actuator should be continuously variable. When the power transmission is discrete with a gear system or a fixed ratio, such as a fixed displacement pump, then the freedom of control degrees is limited. Furthermore, electric transmission provides continuously variable power transmission between the engine and actuators and can be used as continuously variable power transmission.

2.2 System and control architectures

The integration and implementation process of software and control hardware in non-road working machines are somewhat unique, yet do contain some common factors. The systems are real-time mechatronic applications, where the applications set requirements on how the control hardware is connected to the actuators and sensors and determine the required functionality, performance and safety levels of the hardware and software. Due to the variation of these requirements and the low production volumes of non-road working machines compared with the automotive industry, the realized systems and control architectures diverge widely. Furthermore, the long life cycle of non-road working machines, which can exceed 30 years, poses manageability challenges for the electronics and software [53].

2.2.1 Design and development architecture

A system design, implementation and verification process is described in Figure 6 according to the V-model [54], which represents a development process with the relationships between development phases and testing phases. The V-model integrates system testing for each development phase to validate the system against the specifications and design. Introducing a simulation into that process speeds up the process and facilitates the testing phases at an earlier stage. In the early phase, when the actual control system is not ready, a model in the loop (MIL) simulation is used for testing the control algorithms and system functionalities. When the control hardware is not available but the software is in development, software in the loop (SIL) simulation runs a compiled source code in development PC with a simulation environment. This in turn enables testing of the control software with interaction from a complex system. Hardware in the loop (HIL) simulation is useful when the

actual system is not ready or when testing will be done in a controlled environment or conditions. HIL simulations can vary from simulations with control electronics to complete hardware running on the laboratory test bench.

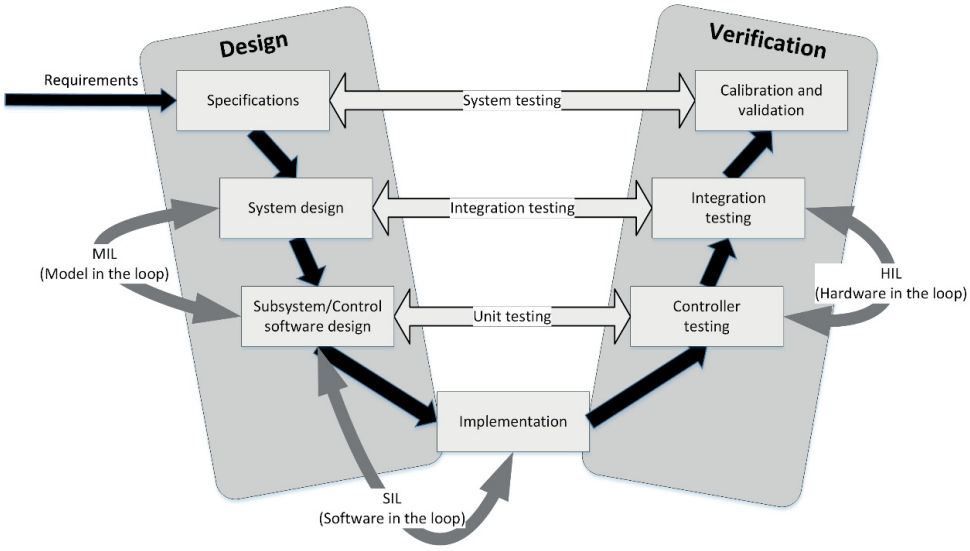

Figure 6. V-model for the design process of controllers which integrates a model-based development process.

The development process is rarely as straightforward as described in Figure 6; instead, it can involve several iterative steps, where the available simulation environments are adapted to the current development phase. Integrating simulations in the design process has been successfully demonstrated with several applications, such as engine control systems [55, 56], control of hybrid energy systems [57, 58] or automotive control systems [59-61]. The benefit of simulations is that they speed up the development process and facilitate testing earlier in the design process.

Conventionally, the automation software of non-road working machines is developed and tested with programmable logic controllers or dedicated microcontrollers. The preliminary design and prototype testing is accomplished with a dedicated test platforms like dSpace [62] or LabVIEW [63], or with offline simulation platforms like Matlab/Simulink [64] or LMS Amesim Platform [65]. To combine the development phase and production phase, code generation tools are available: for instance, Matlab/Simulink provides an Embedded coder [66] that

generates optimized C and C++ code for specific processors, while Simulink PLC coder [67] generates hardware-independent IEC 61131-3 structured text from the Simulink models.

The implementation and verification of a production phase controller from prototype systems is time-consuming and complex due to the multiple iterations during software and hardware development. Code generation reduces the development phases between prototype and production controllers when both adapt the same source code and development environment. Nevertheless, automatic code generation for different platforms has some restrictions: for example, sampling, quantization, ECU scaling, fixed-point arithmetic, saturation and operating system adjustments can cause mismatches between the functionality of different controllers [55].

2.2.2 Software architecture and modularity

The control systems of modern non-road working machines consist of several controllers, and the software is distributed in these controllers. Therefore, the system architecture should support the modularity of software development that increases the importance of clearly defined interfaces. Furthermore, interfaces with real-world actuators and mechatronic systems sensors limit how the modularity can be implemented. When the number of sensors and autonomous functions increases in non-road working machines, the control architecture will be highly related to mobile robotics.

For many years in robotic control architectures, sense-plan-act was a dominant approach [68]. Later on, it was noticed that, in many cases, planning took an excessively long time, and robots acting out a plan without environmental interruptions can lead to hazard situations. To resolve this, behavior-based reactive planning and a layered control architecture were developed to execute several actions so that the higher level could take control from the lower level when required [69]. With behavior-based architectures, the optimization of operations and long-range goals is hard to achieve. For this, the agent-based approach integrates reactive and deliberative control [70]. Table 1 presents some noteworthy architectures in robotics.

Table 1. Control architecture solutions that have been developed for mobile robots in previous years.

Name	Description	Authors	Year	Ref.
An Architecture for Sensor Fusion	Sequential sense-plan-act approach	S. Shafer, A. Stentz, C. Thorpe	1986	[68]
A Robust Layered Control System	Control system is decomposed into task-achieving behaviors	R.A. Brooks	1986	[69]
ATLANTIS (A Three-Layer Architecture for Navigating through Intricate Situations)	Heterogeneous and asynchronous architecture for controlling	E. Gat	1992	[71]
A Three-layer Architecture with Reactive Agents	Experiences with an architecture for intelligent, reactive agents	R. Peter Bonasso et al.	1997	[70]
Functionally Distributed Control Architecture	Architecture is based on distributed and parallel control of functional modules	T. Taira, N. Yamasaki.	2003	[72]
Agent-based Distributed Architecture for Mobile Robot Control	Distributed control system architecture based on reactive and deliberative levels	J. L. Posadas et al.	2008	[73]

An Intelligent Agent for a Vacuum Cleaner	Agent-based approach for controlling	A.R. Khan, D.M. Asghar.	2009	[74]
RoboEarth Architecture	Three-layered architecture: server layer, generic hardware-independent layer, robot-specific layer.	M. Waibel et al.	2011	[75]

Because of a wide variety of non-road working machines, the configurations of machine-specific hardware and components are somewhat unique, although in part the same components are involved. Therefore, the software architecture of non-road working machines should allow a machine-specific control layer where the low-level system is integrated. This layer would provide an interface for the higher level that could take control of the whole system without knowing the details of the low-level control. The challenge of the layered approach is that subsystems cannot be fully isolated. For example, in the automatic wheel loader, control of the bucket system must be coordinated with the vehicle propulsion system [76].

2.2.3 Communication architecture

With several independent modules, data availability and routing is challenging because all modules must have the required information so that interconnected actuator systems can operate inherently. For this, networked control systems (NCSs) have contributed many advantages for managing information. As traditional control theory addresses the behavior of dynamical systems, NCSs include communication theory when information is not flowing through ideal channels because of linkages between different systems. The difference between conventional control system architecture and NCS architecture is shown in Figure 7. In NCSs, control is distributed with multiple devices that communicate with a shared network. This poses different challenges in terms of control, communication and design.

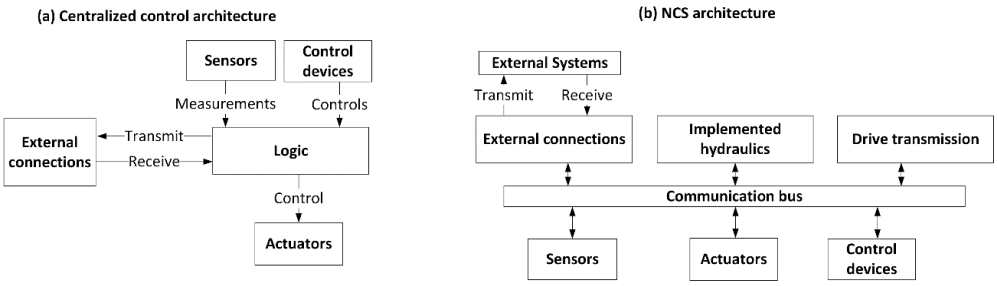

Figure 7. In centralised control architecture, (a), all information flow is managed through one channel. In NSC architecture, (b), the information is applied in multiple control devices with a shared network.

In the automotive industry, off-road vehicles and non-road working machines have adopted the NCSs and distributed systems [21-23, 77, 78]. One reason for this is the increased amount of information and number of controllers. For example, Volvo XC90, BMW 7 Series and VW Passat have increased the number of networked ECUs from five to over 30 during the last decades [78]. The benefit of using a shared network is that all information is always available and the control system can be designed in a modular way. In practice, the control systems are not always purely centralized or distributed, such as with NCS. Non-road working machines include several subsystems that are not always standardized and can have different real-time and connection requirements. Furthermore, applied communication technology with data transfer capacity and safety requirements are limiting factors for purely NCS implementations. Therefore, the automotive architecture is typically distributed with several networks, each of which have different functionalities (typically, powertrain and chassis, body electronics and infotainment). Furthermore, the control system might have connections to the driving lights, meters, ignition system, relays and other devices.

In the modern vehicle industry, CAN-based communication networks are widely adapted for the interactions of subsystems and controllers [77]. The network architectures of non-road working machines are similar to those in the automotive industry. The systems are distributed via several busses designed for different purposes and functionalities [18, 21, 22]. The subsystems have low-level communication channels, analog and digital connections to the sensors, and actuators that induce variations compared with systems designed purely with NCS architecture.

2.2.4 System architectures of autonomous non-road working machines

The system architecture of autonomous non-road machines can abstract the lowest level hardware and software from higher level systems [18, 79-82], or all the sensors and actuators can be mapped to the higher level systems [21, 76, 83, 84]. The remote control, autonomous functions and mission control are typically realized in higher level systems or in the external systems.

To combine low-level control with higher level control, a four-layer design framework for autonomous machines is suggested with technical layers comprising (1) machine architecture, (2) machine awareness, (3) machine control, and (4) machine behavior. At the lowest level, the machine is composed of hardware and software components required for the machine level functions [79]. The system architecture of an autonomous tractor is developed to allow behavior control. The system is based on the object oriented and message passing approach with the agents of identified instances: Coordinator, Supervisor, Mode Changer, Route Plan Generator, Detailed Route Plan Generator, Multiple Object Tracking, Object Classifier and Hardware Abstraction Layer. The Hardware Abstraction Layer hides the close kinematic model and close loop control from the other agents. The Mode Changer can command other agents to switch to a particular mode. Other agents respond if the mode change is possible or not. The complexity of the system is huge, as it tries to handle the complexity of the real world and avoid simplifying the problems. [80]

Two alternative designs based on the layered framework are analyzed in terms of the safety, flexibility and use of a product platform. The typical scenario for the articulated hauler was defined as a use case of an autonomous construction vehicle. The low- level signals of the sensors and actuators were mapped to the higher level that allows the reorganization of primitive level control. The design with the first hypothesis (H1) has an own node for each subsystem such as propulsion or bucket motion control. The second hypothesis (H2) combines the coordination between vehicle propulsion and bucket motion on the subsystem level. H1 was more appropriate for structuring the system into a platform, so the low-level control could easily be changed. Secondly, the coordination between bucket control and motion control at a low-level in the hierarchy was smoother in H2. The subsystems that share the same actuators on the primitive level were identified to increase risks as the control of the actuator was not coordinated. The comparison reveals that the

low-level hierarchy and how the software is organized are important when autonomous systems are designed. [76]

2.3 Power management of non-road working machines

The driving, steering, implement and external systems are parallel controlled subsystems of non-road working machines that take power from a combustion engine or battery. The control of the energy flows or power in the machines is managed in several ways: from straightforward ones, where an operator prepares enough energy for maximum loading, to complex systems that automatically manage dynamic power transitions with accurate control of each subsystem. The minimum requirements for any power management system for non-road working machines are:

- The engine does not stall while performing a typical work cycle
- Overspeed condition in the engine is not allowed
- All subsystems meet the power requirements set by power management
- The power limits of the actuators are not exceeded

These requirements are valid for both hybrid and non-hybrid machines, but hybrid machines also have requirements related to secondary power sources [85]. Figure 8 presents the typical control elements of a hydraulic-operated non-road working machine: a diesel engine, drive pump, drive motor, implement pump and implement valves. The actual configuration can vary, but the subsystem is coupled with the rotational speed of the diesel engine.

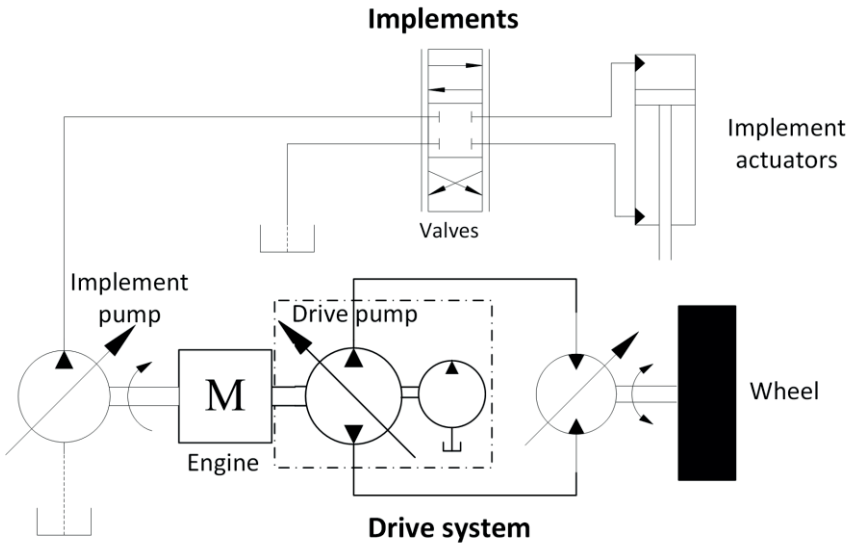

Figure 8. The hydraulic control schematics of a typical non-road working machine include a drive system and implement hydraulic system which are coupled with the engine.

This chapter reviews commercial and academic approaches to the power management of machines with one power source and, lastly, shows some hybrid solutions where control approaches can be adapted for non-hybrid machines.

2.3.1 Applications of control featuring power constraints

The power management of hydraulic-operated non-road working machines is carried out with hydro-mechanical approaches or with electronic controls. One of the simplest ways for power management is the control method, where the valves are directly controlled by the joystick and the transmission ratio of the drive (for example, displacement of the drive pump) is controlled directly from the accelerator pedal. The power level of the engine is then based on a predefined set point of the rotational speed that can be set automatically or by an operator. The control concept is called here direct control and is shown in Figure 8a, where the engine control is independent from the control of the actuators. Direct control is typical in excavators and smaller loaders, such as Bobcat 853 skid-steer loader [86], Avant 635 loader [87] or Volvo EW210C excavator [88].

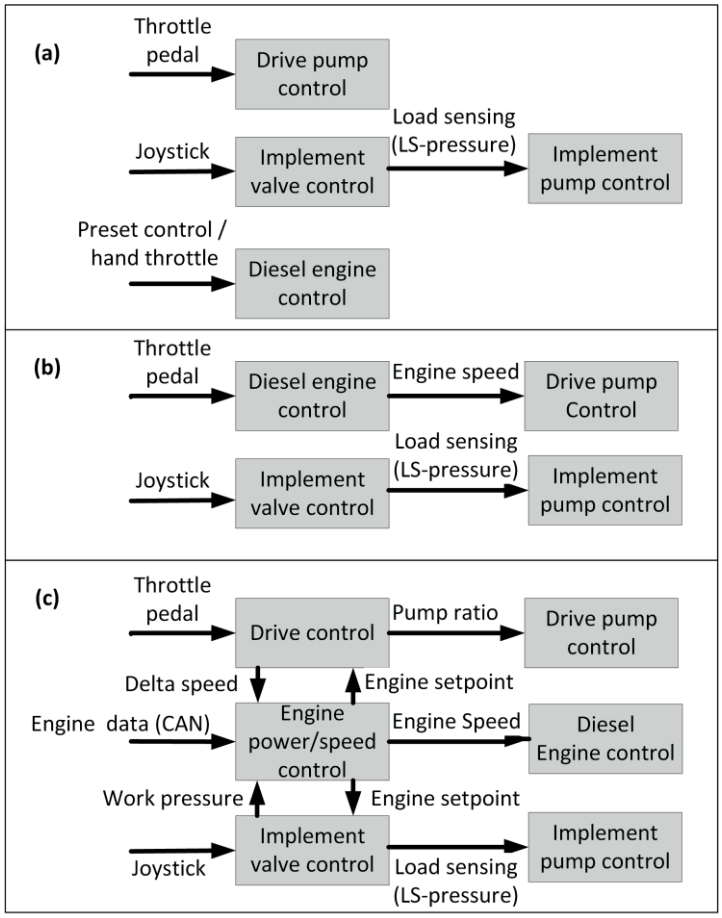

Figure 9. Control flow of power management for non-road working machines: (a) Direct control, (b) Drive and Anti-stall control (DA) and Electronic Transmission Automotive Control (ETAC), (c) Best Point Control (BPC) and Electronic Torque Control (ETC).

When the rotational speed of the engine is set by an operator or based on a predefined setpoint, then the operation point is often selected based on the maximum load to ensure operability in all conditions. Furthermore, the attention of the operator is on the performed work tasks, not on subsidiary control of the engine, resulting in a non-optimal operation point of the engine. To achieve better fuel economy, a lower noise level and higher performance, automatic control of the engine rpm was developed.

Drive and Anti-stall control (DA) from Bosch Rexroth is a hydro-mechanic approach that realizes automatic transmission and anti-stall control for hydrostatic driving [89]. A human operator controls the speed of the engine with the accelerator pedal, and the travel speed of the machine is a function of engine speed and traction force. Figure 9 describes the control flow, where the engine and drive system are coupled and the control of implemented hydraulics is independent of the engine [89]. As DA is a comfortable, robust and reliable solution, it has a very high presence in the market for non-road working machines, especially machines below seven tons. The disadvantage of DA is increased fuel consumption in drive operation, as the implementation of fuel economy algorithms is not possible without electronics.

DA-control is also available in an electrified version with an eDA package (electronic DA) [90]. The advantage of electronic control is the possibility to implement alternative algorithms and the expandability of software functionalities. The diesel speed can be separated from the output torque, which allows application-specific operation modes. For example, the ECO mode reduces consumption and noise by dynamically adapting the engine speed.

Electronic Transmission Automotive Control (ETAC) from Eaton allows hydrostatic transmission operation in a way very similar to a standard automotive with an automatic transmission. Anti-stall, hydrostatic braking and inching control are multifunctional operations of hydrostatic drives [91]. The functionality of the system is comparable to that of DA-control.

Electrified control of hydraulic components is enabling technology for software-based control. Best point control (BPC) from Danfoss is a drive application software that adjusts the engine speed with power management functionalities. The power management function is based on the required power, including an electronic pressure limiter and anti-stall control of the engine. Engine control is based on the power request from the control of drive and implement as described in Figure 9 [92]. Integrated with the work function control, BPC covers the control system of the whole machine. Danfoss claimed significant fuel savings in comparison to classical control approaches [93].

Electronic torque control (ETC) from Bosch Rexroth is an actuation concept that decouples the wheel torque from the diesel speed and sets a new layer for the hydraulic functions. The control functions are separated into machine subsystems and controlled systems that define a matrix structure. All power related

communication is handled with an isolated power manager that coordinates the energy flows of the power sources and consumers. The basic idea is that power consumed by the system is exactly the same as the power made available to the system. In the driving, the human operator sets the desired tractive effort instead of controlling engine speed through a gas pedal. This in turn enables, for example, faster lifting when the engine power is decoupled from driving [94].

Linde Hydraulics has an Engine-Speed-Dependent driving control that is comparable with DA or ETAC. There, the engine speed and high pressure of the system defines the final velocity of the machine [95]. Further, LinDrive from Linde hydraulics is a propel drive solution that seeks to increase the efficiency and usage of the installed power [96]. LinDrive is comparable with BPC and ETC.

2.3.2 Research of control featuring power constraints

Traditionally, two control sequences are suggested for hydrostatic drive in the academic research: a nominal speed approach [47], or an approach where engine speed is increased at the beginning [97, 98]. The control sequences are shown in Figure 10. These do not have any functions of power management or anti-stall functions of the engine. Therefore, the control sequences are typically designed so that the engine always operates with enough power (for example, setting the nominal speed of the engine relatively high). To include power management functionality in the control, the control sequence can be based on the actual rotational speed of the engine such as the DA-control. An alternative approach is to use the power management algorithm that overrides the control sequence if higher power from the engine is needed, or limiting the input power for the hydrostatic transmission.

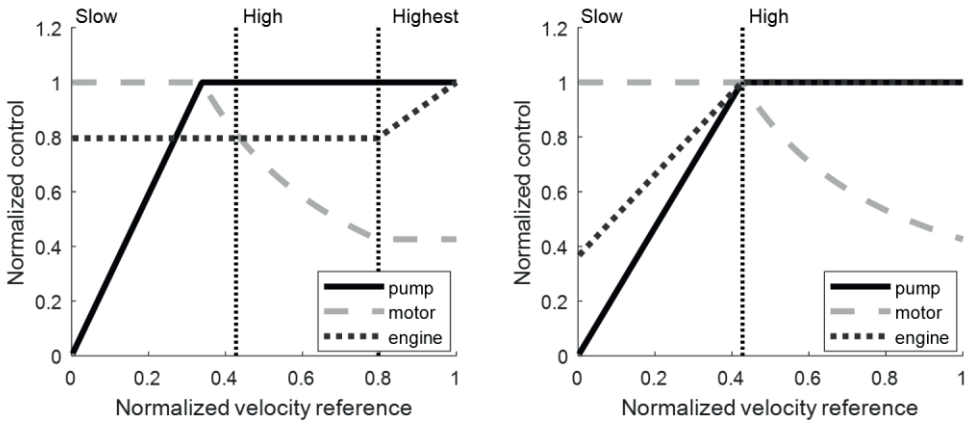

Figure 10. Traditionally, two control sequences are determined for hydrostatic transmission: first, where the engine speed is set at its nominal speed until the highest speed region; and second, where the engine speed is increased from idling to the maximum in the first speed region.

In driving, Continuously Variable Transmission (CVT) or Infinitely Variable Transmission (IVT) offer the potential to optimize fuel efficiency by shifting engine operation points to fuel optimal points. Compared with manual and automatic transmissions, wheel speed is independent of the engine speed up to the maximum ratio of CVT. Based on the given freedom, fuel economy is improved by optimizing and controlling the operation point of the engine and transmission [20, 99-102]. For example, Pfiffner and Guzzella showed 4 to 6% fuel economy improvements through optimal control [99]. Nevertheless, these studies were limited to the control and optimizing of the drive system, although non-road working machines include implements and other systems that influence control and fuel economy. Therefore, an approach to overall control and optimization of the system is required.

Optimization of the efficiency of hydrostatic drives showed that operating the ICE as long as possible in the minimum specific consumption zone reduces fuel consumption significantly. The comparison was done with standard speed control, where a constant nominal speed of ICE was used until the hydrostatic drive reached the maximum. Therefore, the assumption was that there a constant nominal speed providing enough power. [47] Further, the optimization procedure for driveline control showed 13% [103] or 14% [104] reduction in fuel consumption. Nevertheless, the fuel consumptions were optimized with known work cycles, so power management was not needed for unpredicted operation conditions. Further,

secondary control is one way to improve the energy efficiency of hydraulic systems. Advanced control can handle the power restriction functions that are needed for the power management [105, 106].

General power management with available and consumed power and flow rate was developed in a telehandler, showing that it is capable of functionalities such as anti-stall, flow-sharing, pressure control and prioritization of the steering. The hydraulic load-sensing system (LS) was upgraded to electronic load-sensing (ELS) to allow the use of various control algorithms. Developed power management with a flow feed-forward from the joystick to the pump enhances dynamic performance and lowers the LS-margin down to 7 bar to improve efficiency. [107]

To minimize the rate of fuel consumption for a multi-actuator non-road machine, a static optimisation algorithm with power management was demonstrated in a mini excavator. The optimization shows 69% fuel savings compared to the standard LS-excavator, and 56% compared to constant engine speed algorithms. A relatively large solution space for the optimization, and the number of inputs and frequently changing speed and load make the optimization challenging in non-road working machines. Furthermore, stability and performance should be guaranteed in the control of hydraulic systems [108].

With dynamic optimization, fuel consumption can be minimized by determining the optimal speed trajectories for the engine in vehicle accelerations. The optimization is based on a simple model of the engine, drivetrain and vehicle. The control input to the optimization is the throttle valve angle. The experiments show that a linear engine speed trajectory consumes 13% more fuel compared with the trajectory generated with dynamic optimization [109].

2.3.3 Control of hybrid vehicles

Manufacturers have introduced hybrid wheel loaders, such as Hitachi ZW220HYB-5B that reduces fuel consumption by up to 31% [110] or Volvo CE LX1 that reduces fuel consumption by up to 35% [111].With additional energy storage, hybrid wheel loaders can gain 10-45% fuel saving in some work cycles compared with traditional wheel loaders [112]. The market share of hybrid loaders is still small, as the new technology involves complex control, complicated construction, additional manufacturing cost, and reliability and operability challenges [112, 113]. Despite

these, hybrid machines are still an interesting research area due their potential for energy saving and productivity improvements.

Additional energy storage and powertrain complexity require energy management strategies that maximize fuel economy and preserve handling performance. Energy management strategies can be divided into global optimization strategies that optimize energy consumption in the work cycle [16, 114] and real-time optimization that optimizes fuel consumption instantaneously [9, 115, 116]. Compared with conventional non-road working machines, the control of hybrid machines mainly concentrates on energy management due to the need for additional energy storage, and not on the input–output power matching required in non-hybrid machines. Despite differences in the freedom of control and control constraints, some control elements and configurations from hybrid machines can be adapted in the power management of non-hybrid machines.

The modularized and distributed control architecture of the demonstration vehicle 'Green Wheel Loader' shows an operating strategy whereby the operator does not directly influence the engine speed. Instead, the operator commands are demands for the implement functions and for the drive system. Therefore, the control system can minimize the engine speed and ensure enough power for the engine that is supported dynamically by the hybrid module. Fuel savings of 10–15% are achieved in comparison with the presented series-production machine in a short loading cycle [18].

Power management for a hydraulic hybrid multi-actuator machine entails a supervisory system that handles energy generation, conversion, storage and transmission between the different energy sources and consumers. The primary goal of power management is to study and validate near-optimal strategies for fuel consumption. The secondary goal is to meet performance requirements, and finally, meet both requirements in the optimal way. The study demonstrates two power management strategies: a novel rule-based strategy that, based on the optimal results obtained from dynamic programming, minimizes the speed of the engine; and an instantaneous approach, called the equivalent consumption minimization strategy, which uses stationary optimization at every time instant while meeting performance constraints. Both strategies show circa 20% fuel improvements compared with non-hybrid machines [85].

Based on the power matching and supervisory control of the subsystems, Caterpillar has patented a system which includes a controller for controlling the power signals. The controller provides signals either to receive power from the engine or to supply power to the engine based on the engine properties. Further, the signals for the speed and output of the engine are supported in the controller. Therefore, at least one device results in engine operation to the requested operation point. [117]

Volvo has patented a method for a working machine with a power source and a plurality of power consumer systems. The method balances provided power with demanded power according to the prediction model in which different power consuming systems are operated simultaneously, such as in a wheel loader. A torque control unit, or a similar one, is arranged between the transmission line, the internal combustion engine and the hydraulic system to control the power/torque exchanged between the power sources and consumers. An auxiliary power source such as an electric motor or generator can be used to assist the combustion engine to reach the required rotational speed. This guarantees the performance of the machine, as the torque control unit can add torque from the auxiliary source to reduce the load on the combustion engine [118].

Due to the additional energy storage, the constraints and control degree of hybrid machines are different than in non-hybrid machines. This is because in non-hybrid machines the engine should have a power reserve for changing the operation point of the engine and for unpredicted power peaks that cannot be compensated for from the additional energy source. Therefore, the requirements for the control and power management architecture are different in hybrid and non-hybrid machines.

2.4 Test cycles of non-road working machines

For passenger cars, multiple standardized test cycles represent typical driving conditions in cities and highways, and include supplemental tests that combine the city and highway test cycles. In the official statistics for drive cycles and real-world driving, fuel consumption and emissions still diverge dramatically. For example, the gap between real-world and official CO2 emissions increased from approximately 8% in 2001 to 40% in 2014 [119]. The challenges in standardized real-world test cycles are variations in driving conditions, the behavior of drivers, and vehicle types. In comparison with passenger cars and heavy-duty vehicles, representative test cycles

are more challenging due to the wide variation in the size and payload of heavy-duty vehicles.

Non-road working machines are, typically, applications where the duty cycle consists of both driving and working actions. As there are a wide variety of machine types, sizes, work tasks and conditions, representative test cycles are hard to determine. The United States Environmental Protection Agency (EPA) has collected engine data for reproducing the real-world activity of various non-road vehicles. Samples of that data are shown in Figure 11 for excavators, skid steer loaders and wheel loaders.

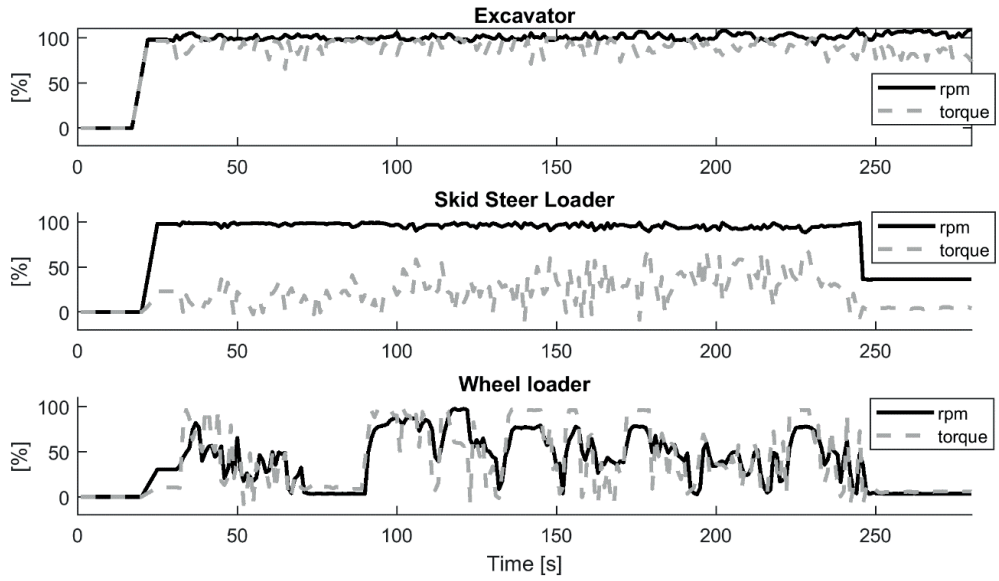

Figure 11. EPA non-regulatory, non-road duty cycles for excavators, skid steer loaders and wheel loaders as a function of normalized rotational speed and torque of the engine [34].

The collected data contain the normalized rotational speed and torque of the engine. The excavator operates with the maximum rotational speed and relatively high torque, whereas the skid steer loader and wheel loader cycles contain variations in operation conditions. Further, it can be noted that the torque of the loaders can be slightly negative due to the engine braking. The presented duty cycles are not relevant to hybrid machines or machines with advanced control, as the operation points of the engine are different than in the predefined duty cycle. Furthermore, the power

required from the engine or power source is more relevant, but does not fully cover the different mechanical and control configurations of the machines.

The real-world test cycles of non-road working machines are not only highly machine-type-dependent, but also depend on the size of the machine, the configuration of the machine and driver behavior. Further, the energy distribution of the machine has wide variations between the work cycles and drivers [32]. Due to these variations and dependencies, overly simplified test cycles can produce non-representative results [120].

For wheel loaders, multiple cycles are defined, but loading within the y-cycle (180-degree cycle) and x-cycle (360-degree cycle) is most often used. Both cycles are shown in Figure 12, which contains the same phases: towards bank, retardation at bank, bucket filling, leaving bank, retardation, reversing, towards load receiver, bucket emptying, leaving load receiver, retardation and reversing.

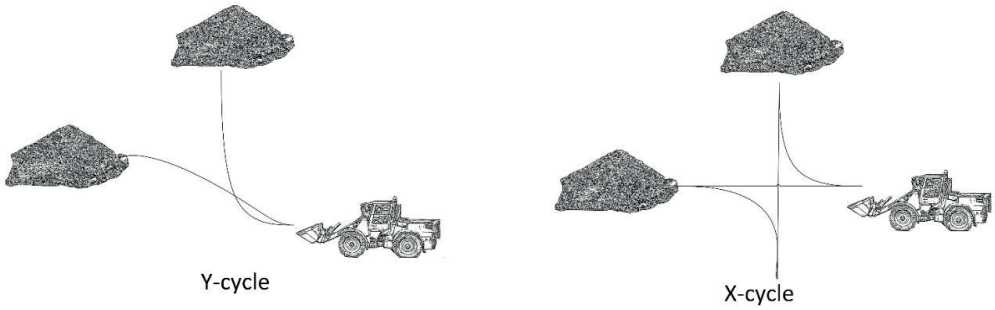

Figure 12. Short loading cycle: y-cycle and x-cycle are commonly used for testing wheel loaders.

The trajectories of the loading can be optimized with different target functions, such as driving distance, driving time, productivity, fuel consumption or operator workload [121]. The fuel consumption of wheel loaders is mostly dependent on the driving distance in the cycle, the acceleration rate and, to some extent, gravel interaction with the bucket [122]. The driving distance or the amount of moved material cannot be generalized, because the machines are designed for different purposes and their sizes are different.

The work tasks of non-road working machines are not homogenous, and only one work cycle could cover the full operation of a machine. Therefore, the EPA has

measured multiple duty cycles for wheel loaders with variations in the torque and speed profiles of the engine [34]. Furthermore, the duty cycles contain idling times for the machines corresponding to breaks in operation – for example, when the load receiver is changing. The work sites of a machine change from time to time, and when the distance between the sites is relatively short, the machine is driven to the new work site. Therefore, it makes sense to also include travel driving in the test cycles.

3 MODELING OF THE WHEEL LOADER AND ENERGY EFFICIENCY

A mathematical model and the parameters for driving are required for comparing different control scenarios, especially if the results are to be compared with optimal operation points in terms of fuel consumption. Additionally, the efficiency models of the diesel engine and subsystems, such as driving and implements, are required. For that purpose, an experimental non-road working machine was defined and applied in the preliminary study of fuel consumption.

A municipal wheel loader, shown in Figure 13, was selected to represent a typical construction machine, and it was used to analyze the fuel consumption of different control methods. The machine was rebuilt and electrified for research purposes using the factory-made series-production machine as a starting point. The machine is hydraulically operated, with three main hydraulic systems: a hydrostatic drive, implemented hydraulics and an external hydraulic circuit for steering and braking. The hydrostatic drive circuit (HSD) is a coupled system with a variable displacement pump and a variable displacement motor. The drive motor is connected to a gear box which defines a final gear ratio between the tires and engine.

Figure 13. This experimental wheel loader was applied in the analysis and research of fuel economy.

The implements (lifting and tilting) are both implemented with two parallel cylinders. For research purposes, there are two options for controlling the cylinders: a digital valve system (DVS) [6], and a conventional proportional valve system. The systems cannot be used in parallel, so only one of the systems can be active at a time. In both cases, the supply pressure is generated from the electronic load-sensing pump (ELS), where the load-sensing signal can be transmitted via CAN-bus. With digital valve control, one DVS is for the lift and the other is for the tilt. In the DVS system, the flow rate is controlled with four digital flow control units (DFCU), each consisting of six ON/OFF-valves of different nominal sizes [6]. The proportional valve system is implemented with two standard valves: one for the tilt and one for the lift. In this study, only the approach with the proportional valves was used.

The external hydraulic circuit powers the steering, braking and external hydraulic components that can be attached to the machine. The circuit has a fixed displacement pump and an unloading circuit with a pressure relief valve. The function of the steering system is guaranteed with a prioritisation valve and controlled with an orbitrol. In cases such as teleoperation or automated driving, the orbitrol can be overdriven with a proportional valve.

The purpose of the modeling is to provide required information on the machine for a feasibility study to simulate the fuel efficiency of different control methods for the driving. Further, the information from the modeling and simulation results is applied for constructing the controllers of the machine that are realised for the experimental tests. Therefore, the modeling is simplified, and some assumptions might not be valid for all work cycles, such as considering only for the longitudinal forces of driving.

The total energy loss of the machine depends on the efficiency of the subsystems, their components and respective control. To analyze energy loss in different operation points, efficiency models for the components were required.

3.1 Efficiency of diesel engine

The diesel engine of the experimental machine is a 96-kW diesel engine from Caterpillar featuring Common Rail technology and a turbocharger. The manufacturer provides only maximum torque and power curves as a function of the

rotational speed of the engine and fuel consumption in these points. To define fuel consumption in other operation points, a Brake Specific Fuel Consumption map (BSFC-map) is needed. As these data were not available for the engine, the data points for fuel consumption were derived from the literature for the same type of engine [123].There, the BSFC data points were measured as a function of the engine speed and torque. To calculate the fuel efficiency of the engine, the formula of BSFC was used:

$$BSFC = \frac{r_{\text{fuel}}}{P_{\text{out}}} \tag{3.1}$$

where r_{fuel} is the fuel consumption rate and P_{out} is the power produced by the engine. The main parameters from the engine of the experimental machine and the respective engine are listed in Table 2. The most significant differences are the type of turbocharger, the compression rate and different maximum rotational speed of the engine.

Table 2. General parameters of the C4.4 engines from the experimental machine and from the respective engine [123].

	Engine of the experimental machine	**Respective engine [123]**
Engine Model	C4.4	C4.4
Fuel	Diesel	Diesel
Turbocharger model	Borg Warner B1 with wastegate	Cat GT22 56/50mm
Intercooler type	Air to Air	Air to Air
Compression rate	16.2 : 1	16.5 : 1
Common rail	Yes	Yes
Displacement	4.4 liters	4.4 liters
Stroke	4 Stroke	4 Stroke
Engine low idle & high idle	800 ... 2200 rpm	800, 1950 rpm
Bore & Stroke	105 mm, 127 mm	105 mm, 127 mm

Despite the differences in the engines, it is assumed that the BSFC of the experimental machine is close to that of the respective machine. Therefore, the data points from the respective engine were used to generate the BSFC map. The

maximum torque curve was adapted from the calibration measurements done with the diesel engine of the experimental machine. For generating the map, the data points were fitted in the polynomial functions using the fit function from Matlab. The BSFC maps with maximum torque and data points used are shown in Figure 14.

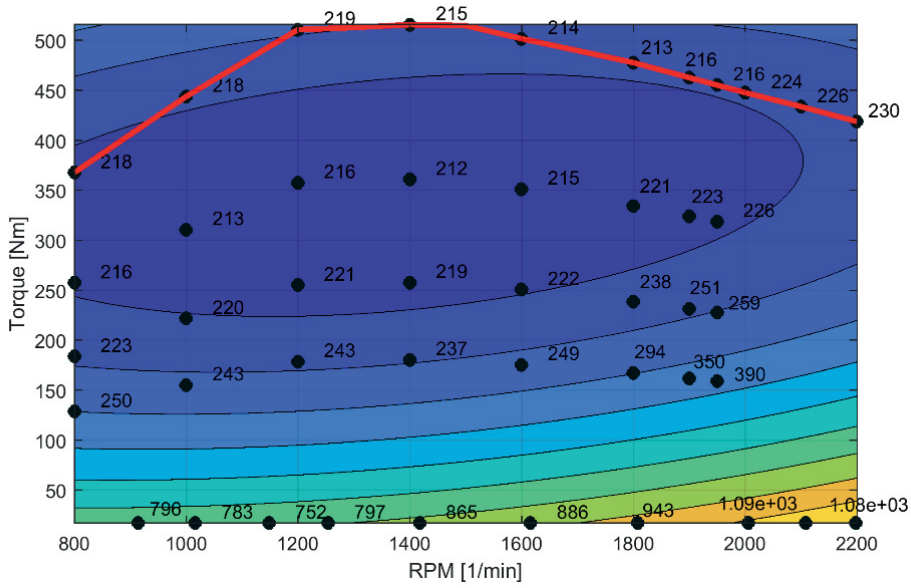

Figure 14. Brake-specific fuel consumption map of the engine CAT C4.4.

The data points from 1950 to 2200 were extrapolated from the respective engine so that the values of the BSFC were available at the full speed range of the diesel engine. Furthermore, the fuel consumption points for low torque were added from the experimental machine to restrict the BSFC from zero. In the modeling, the fuel rate map was used instead of the BSFC to avoid the data points tending towards infinity with a low torque condition. The modeled fuel rate map with derived data points from the BSFC map is shown in Figure 15.

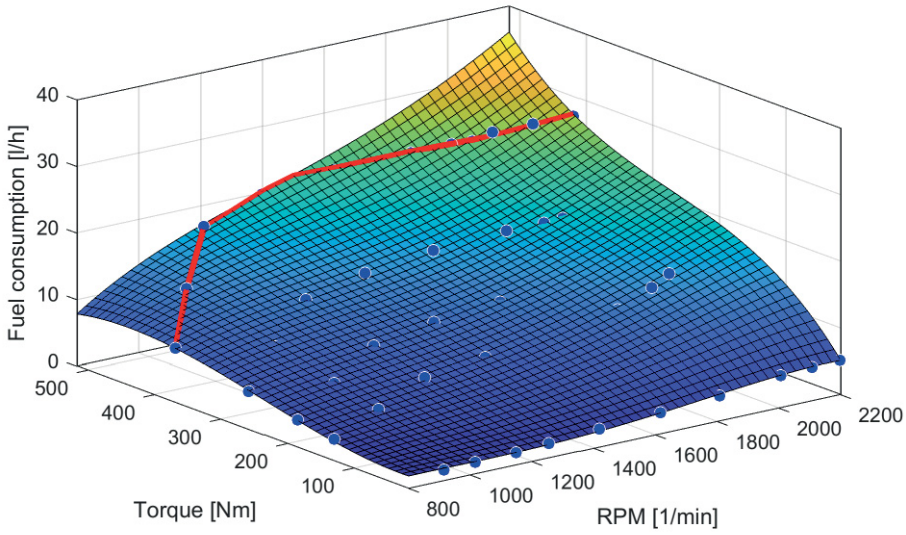

Figure 15. The fuel rate of the engine CAT C4.4 was modeled as a function of the rotational speed and output torque. The red line represents the maximum torque of the engine.

3.2 Efficiency of driving

The efficiency of driving is derived from the resistance of driving conditions and from internal resistances. For simplicity, the modeling assumes only a straight driving condition. This sets the lateral forces to zero, and the road forces are assumed to spread evenly on the right and left wheels, so that only longitudinal tractive forces are affected. In reality, the tire slip and steering have a significant effect on the resistance force of the tires. The total tractive effort of the wheels is therefore the summation of the tractive forces of each tire:

$$F_{\mathrm{acc}} = m\dot{v} = F_{\mathrm{FR}} + F_{\mathrm{FL}} + F_{\mathrm{RR}} + F_{\mathrm{RL}} - F_{\mathrm{roll}} - F_{\mathrm{air}} - F_{\mathrm{slope}} \qquad (3.2)$$

where, F_{acc} is the acceleration force, m is the mass, $\dot{v}$ is the acceleration, F_{FR}, F_{FL}, F_{RR} and F_{RL} are the forces of the tires, and F_{roll}, F_{air} and F_{slope} are the forces caused by the rolling resistance, air drag and road grade. These forces are derived from [124]:

$$F_{\text{roll}} = f_{\text{roll}} mg \cos(\theta) \tag{3.3a}$$

$$F_{\text{air}} = 0.5 \rho_{\text{air}} C_{\text{air}} A (v + v_{\text{w}})^2 \tag{3.3b}$$

$$F_{\text{slope}} = mg \sin(\theta) \tag{3.3b}$$

where f_{roll} is the tire rolling resistance coefficient, g is the gravity, θ is the angle of inclination to the horizontal (slope grade), ρ_{air} is the air density, C_{air} is the aerodynamic drag coefficient, and v_{w} is the head-wind velocity. The directions of the force vectors are shown in Figure 16, where positive directions of forces are observed against the direction of the movement.

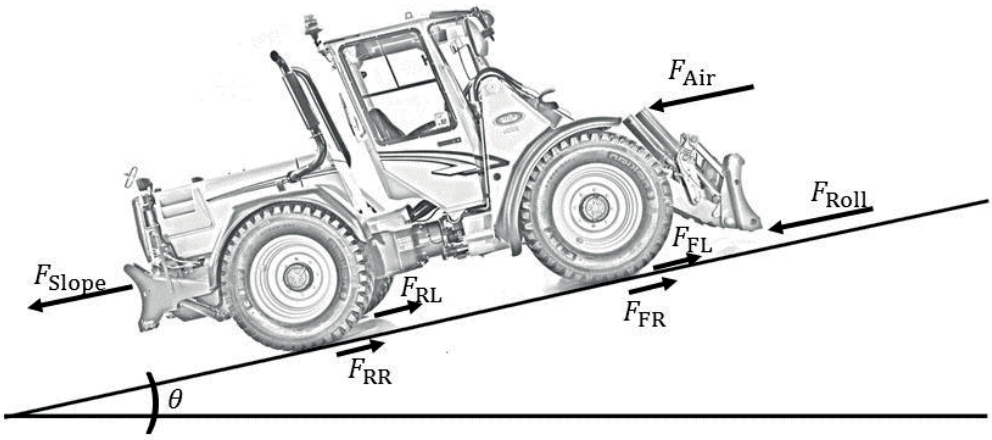

Figure 16. Direction of longitudinal forces observed against the direction of the movement.

Tire slip is ignored in the model, so all tractive forces of the wheels are affecting the road. Furthermore, the vehicle is considered as one mass point, and forces are assumed to be distributed evenly between the tires.

3.2.1 Efficiency of driveline

The efficiency of the driveline depends on the efficiency of the hydraulic pump and hydraulic motor of the drive system, losses in the hoses, and the friction in the driveline. The losses of the boost pump are defined with supporting systems and

therefore are not included for the driveline. The driveline of the experimental wheel loader is a coupled system with a variable displacement hydraulic pump and motor connected to a gear box, as shown in Figure 17. The gear box has two different gear ratios for high and low speed driving. Further, the front and rear shafts are connected to gear boxes that have a fixed gear ratio.

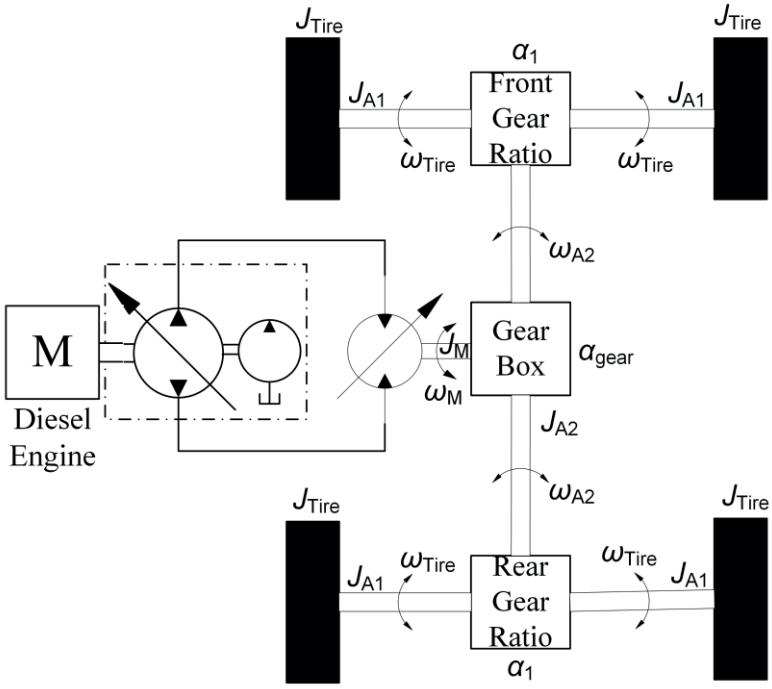

Figure 17. The driveline of the experimental wheel loader is a coupled system of a hydraulic pump and motor connected to a gear box.

During the acceleration or deceleration phase, the effective mass of the vehicle is not only the non-rotating mass. The tires, shafts and other rotating mechanisms of the mechanical drivetrain affect the overall torque of the drive system required from the hydraulic motor. The effective mass can be separated into the rotational mass and non-rotating mass of the vehicle as:

$$F_{\text{acc}} = m_{\text{eff}}\dot{v} = \left(m + \frac{J_{\text{eff}}}{r_{\text{Tire}}^2}\right)\dot{v} \tag{3.4}$$

where is m_{eff} is the effective mass of the vehicle, J_{eff} is the effective rotational inertia containing all rotational inertia from the hydraulic motor to the tires and is relative to the rotational speeds of the tires, and r_{Tire} is the effective radius of the tire. During acceleration, the force is positive; in deceleration, the force is negative.

The mechanical drivetrain of the wheel loader has several rotating inertias at different rotational speeds, as shown in Figure 17. These generate internal torque while accelerating and decelerating the vehicle. The effective inertia as proportional to the tire speed is combined from the partially defined inertias and speeds:

$$J_{\mathrm{eff}} = 4J_{\mathrm{tire}} + J_{\mathrm{A1}} + J_{\mathrm{A2}}\alpha_1^2 + J_{\mathrm{M}}(\alpha_1\alpha_{\mathrm{gear}})^2 \tag{3.5}$$

where, $J_{\mathrm{tire}}, J_{\mathrm{A1}}, J_{\mathrm{A2}}$ and J_{M} are the inertia of the tire, shafts and hydraulic motor, α_1 is the gear ratio of the front and rear gear box, and α_{gear} is the gear ratio of the gear box connected to the hydraulic motor.

The efficiency of the mechanical drivetrain is dependent on the torque loss between the tires and the hydraulic motor, which is a result of losses in the gear boxes and the friction of the rotating shafts. With the simplified model, the total torque losses are modeled with the influence of viscous and coulomb friction [125, 126] and formulated as a function of machine velocity:

$$F_{\mathrm{drivetrain}} = F_{\mathrm{c}}\mathrm{sgn}(v) + b_{\mathrm{v}}v \tag{3.6}$$

where v is the velocity of the machine, F_{c} is the coulomb friction force and b_{v} is the viscous friction coefficient. For zero velocity, the sign function is defined so that it returns zero. From the driveline resistances and longitudinal forces, the torque of the hydraulic motor is derived:

$$T_{\mathrm{m}} = \alpha_{\mathrm{final}} r_{\mathrm{tire}}(F_{\mathrm{acc}} + F_{\mathrm{roll}} + F_{\mathrm{air}} + F_{\mathrm{slope}} + F_{\mathrm{drivetrain}}) \tag{3.7}$$

where α_{final} is the final gear ratio between the tire and the hydraulic motor (here: $\alpha_{\mathrm{final}} = \alpha_1\alpha_{\mathrm{gear}}$).

The torque of the hydraulic motor is produced hydrostatically with a standard close-circuit system of the pump and motor, as shown in Figure 18. The close-circuit hydraulic pump contains the boost pump to ensure the cooling, pilot pressure and

the back pressure level for the low pressure side. The energy loss of the boost pump is taken into account with the supporting subsystems of the machine.

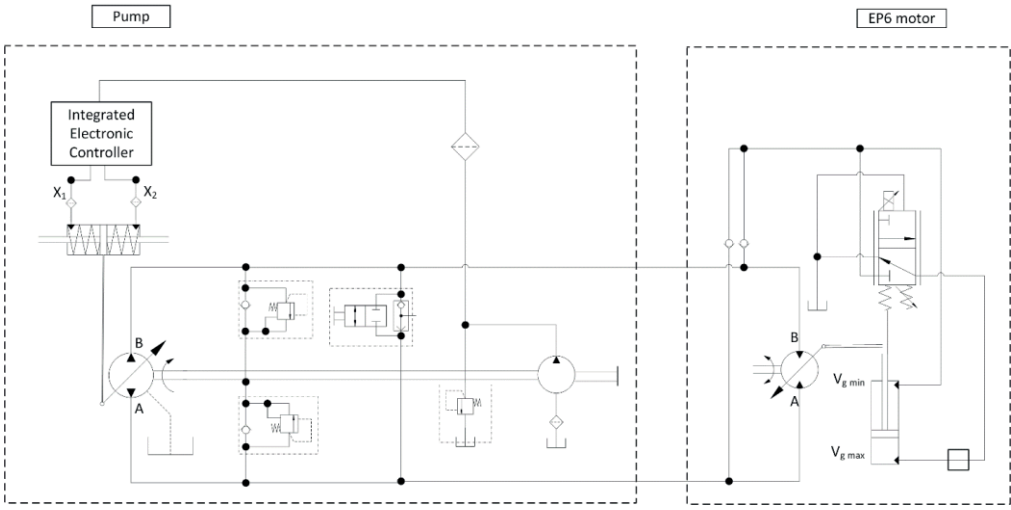

Figure 18. The hydraulic drive system of the wheel loader is a closed circuit of the hydraulic pump and motor [127, 128].

The hydraulic pump and motor are electrically controlled, which enables software-based control for hydrostatic driving. The pump has an integrated electronic controller commanded via CAN-messages, and the motor is controlled by changing the current of the solenoid.

Due to the hydrostatic drivetrain, the torque of the hydraulic motor defined in Equation (3.7) is produced hydraulically and corresponds to the torque caused by longitudinal motion. Further, the flow rate, torque and power of the hydraulic motor are defined as follows:

$$Q_{\mathrm{m}} = \frac{\omega_{\mathrm{m}} \varepsilon_{\mathrm{m}} V_{\mathrm{m}}}{2\pi \eta_{\mathrm{vol,m}}} \tag{3.8a}$$

$$T_{\mathrm{m}} = \frac{\varepsilon_{\mathrm{m}} V_{\mathrm{m}} \eta_{\mathrm{hm,m}}}{2\pi} \Delta p \tag{3.8b}$$

$$P_{\mathrm{m}} = T_{\mathrm{m}} \omega_{\mathrm{m}} = Q_{\mathrm{m}} \eta_{\mathrm{tot,m}} \Delta p \tag{3.8c}$$

where ω_{m} is the angular velocity of the hydraulic motor, ε_{m} is the displacement ratio of the hydraulic motor, V_{m} is the maximum displacement of the hydraulic motor (maximum capacity per revolution), Δp is differential pressure over the motor, and $\eta_{\mathrm{vol,m}}$, $\eta_{\mathrm{hm,m}}$ and $\eta_{\mathrm{tot,m}}$ are the volumetric, hydro-mechanical and total efficiency of the motor. The hydraulic motor is connected to the drive pump, where the flow rate, torque and power of the pump are defined as follows:

$$Q_{\mathrm{p}} = \frac{\omega_{\mathrm{p}} \varepsilon_{\mathrm{p}} V_{\mathrm{p}} \eta_{\mathrm{vol,p}}}{2\pi} \tag{3.9a}$$

$$T_{\mathrm{p}} = \frac{\varepsilon_{\mathrm{p}} V_{\mathrm{p}}}{2\pi \eta_{\mathrm{hm,p}}} \Delta p \tag{3.9b}$$

$$P_{\mathrm{p}} = T_{\mathrm{p}} \omega_{\mathrm{p}} = \frac{Q_{\mathrm{p}}}{\eta_{\mathrm{tot,p}}} \Delta p \tag{3.9c}$$

where ω_{p} is the angular velocity of the hydraulic pump, ε_{p} is the displacement ratio of the hydraulic pump, V_{p} is the maximum displacement of the hydraulic pump and $\eta_{\mathrm{vol,p}}$, $\eta_{\mathrm{hm,p}}$ and $\eta_{\mathrm{tot,p}}$ are the volumetric, hydro-mechanical and total efficiency of the pump. Here, the hoses between the hydraulic pump and motor are ignored. Therefore, the pump and motor have the same differential pressure (Δp) and flow rate ($Q_{\mathrm{p}} = Q_{\mathrm{m}}$). Further, the output torque of the engine for the drive system and the rotational speed of the engine are the same as the input torque of the pump and the rotational speed of the pump.

The final velocity of the machine is a function of the coupled system of hydraulic pump and motor, which is not rigid. Therefore, the hydraulic efficiencies also affect the final speed of the vehicle:

$$v = 2\pi r_{\mathrm{tire}} n_{\mathrm{tire}} = \frac{r_{\mathrm{tire}} \omega_{\mathrm{m}}}{\alpha_{\mathrm{final}}} = \frac{r_{\mathrm{tire}}}{\alpha_{\mathrm{final}}} \frac{\omega_{\mathrm{p}} \varepsilon_{\mathrm{p}} V_{\mathrm{p}} \eta_{\mathrm{vol,p}} \eta_{\mathrm{vol,m}}}{\varepsilon_{\mathrm{m}} V_{\mathrm{m}}} \tag{3.10}$$

With the defined driveline model, the velocity of the machine is based on the operation points of the engine, hydraulic pump and motor. Further, the efficiencies of the components define the losses that produce the load for the engine with drive resistance.

3.2.2 Drive parameters of experimental machine

To model the driveline efficiency, the hydro-mechanical and volumetric efficiency of the hydraulic motor and pump were measured in the laboratory. The efficiencies were defined in steady-state operation points as a function of the displacement ratio, rotational speed and differential pressure. The efficiencies were defined separately as the ratio of the outputs and inputs:

$$\eta_{\mathrm{vol}} = \frac{Q_{\mathrm{out}}}{Q_{\mathrm{in}}} \tag{3.11a}$$

$$\eta_{\mathrm{hm}} = \frac{T_{\mathrm{out}}}{T_{\mathrm{in}}} \tag{3.11b}$$

$$\eta_{\mathrm{tot}} = \eta_{\mathrm{hm}}\eta_{\mathrm{vol}} = \frac{P_{\mathrm{out}}}{P_{\mathrm{in}}} \tag{3.11b}$$

where η_{vol}, η_{hm} and η_{tot} are the volumetric, hydro-mechanical and total efficiency, Q is the flow rate, T is the torque and P is the power. The measured data points of the efficiencies were fitted to the polynomial functions so that efficiency could be resolved in any given rotational speed, torque and pressure: $\eta = f(\varepsilon, \omega, \Delta p)$. For the modeling, the loss functions were used instead of the efficiencies to prevent the efficiencies from approaching zero in the low displacement ratios.

To apply the longitudinal motion model, the parameters defined from literal study and experimental measurements were assumed to be constant during the simulations: these parameters were defined in an earlier study [129]. Table 3 shows the parameters of the wheel loader.

Table 3. Longitudinal motion parameters of the wheel loader were defined from literal study and experimental measurements in an earlier study [129].

Variable	Symbol	Value
Rolling resistance coefficient	f_{roll}	0.025
Air drag coefficient	C_{air}	2.0
Density of air at sea level 15C°	ρ_{air}	1.225 kg/m3
Mass of the vehicle	m	5435 kg
Gravity	g	9.81 m/s2

Frontal area of vehicle	A	4.0 m2
Effective rotational inertia	J_{eff}	144 kgm2
Coulomb friction	F_{c}	950 N
Viscous friction coefficient	b_{v}	10 kg/s
Tire radius	r_{Tire}	0.55 m
Maximum displacement of the pump	V_{p}	85e-6 m3
Maximum displacement of the motor	V_{m}	85e-6 m3
Final gear ratio (slow / fast)	α_{final}	0.3636 / 0.7273

As some parameters were not defined with experimental measurements, the value was estimated based on the literal study. For example, the air drag coefficient (C_{air}) was assumed to be a flat plate which could yield a pessimistic estimation. The defined drive parameters can later be used for simulations of the experimental wheel loader and for defining the efficiency of the drive system in the predefined operation points.

3.3 Efficiency of implements

The implements (lift and tilt) of the experimental wheel loader were built with parallel connected cylinders, which are controlled in this case with proportional valves. The loader has a hydro-mechanical self-level stabilization feature which maintains the angle of the bucket almost constant compared to the frame of the machine (other option would be mechanical linkage). Figure 19 shows the hydraulic schematics of the implement.

The hydraulic pump is an open circuit pump with control elements that allow the motoring mode with negative swash plate angles. In this study, the motoring mode of the pump was not used. The valves are standard proportional valves with a pressure compensation function. The power, force and velocity of the cylinders are calculated with:

$$F_{\text{cyl}} = (p_{\text{A}} A_{\text{A}} - p_{\text{B}} A_{\text{B}})\, \eta_{\text{HM}} \tag{3.12a}$$

$$v_{\text{cyl}} = \frac{Q_{\text{A}} \eta_{\text{Vol}}}{A_{\text{A}}} = \frac{Q_{\text{B}} \eta_{\text{Vol}}}{A_{\text{B}}} \tag{3.12b}$$

$$P_{\mathrm{cyl}} = v_{\mathrm{cyl}}(p_{\mathrm{A}}A_{\mathrm{A}} - p_{\mathrm{B}}A_{\mathrm{B}})\eta_{\mathrm{HM}} \tag{3.12c}$$

where p_{A} and p_{B} are the pressures of A and B-chambers, $A_{\mathrm{A}}$and A_{B} are the area of chambers, Q_{A} and Q_{B} are the input flow rates in the chambers, η_{HM} is the hydro-mechanical efficiency, η_{Vol} is the volumetric efficiency. Here, the leakage of the cylinders is assumed to be insignificant and therefore $\eta_{\mathrm{Vol}} \approx 1$.

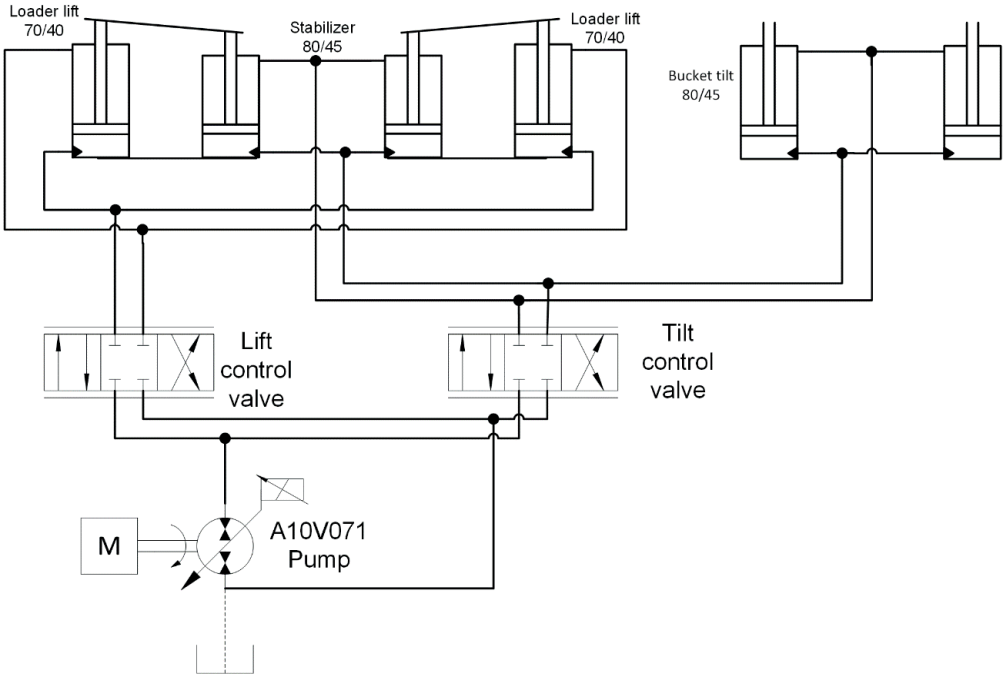

Figure 19. The hydraulic schematics of the implements have a hydraulic self-level feature for the bucket.

Further, the volumetric efficiency of the valves is assumed to be one ($\eta_{\mathrm{Vol}} \approx 1$). Therefore, the efficiency of the valves is dependent only on the pressure loss in the valve. Similarly, the pressure loss of the connectors, pipes and hoses defines the power loss:

$$P_{\mathrm{loss}} = p_{\mathrm{loss}}Q_{\mathrm{in}} \tag{3.13}$$

where p_{loss} is the pressure loss of the component, and Q_{in} is the flow rate through the component.

The efficiencies of the pump can be derived from function $\eta = f(\varepsilon, \omega, \Delta p)$. This is defined from the measured data points similarly to the efficiencies of the drive pump. The input power from the engine to the implements is transferred hydraulically from the pump to the cylinders:

$$P_{\mathrm{in}} = \frac{Q_{\mathrm{p}} \Delta p_{\mathrm{p}}}{\eta_{\mathrm{tot,p}}(\omega, T, \Delta p)} = \sum \left(v_{\mathrm{cyl}} (p_{\mathrm{A}} A_{\mathrm{A}} - p_{\mathrm{B}} A_{\mathrm{B}}) \right) + \sum (P_{\mathrm{loss}}) \qquad (3.14)$$

where Q_{p} is flow rate of the pump, and the summation $\sum (P_{\mathrm{loss}})$ is the loss of hydraulic lines containing the losses in the valves, connectors, pipes and hoses. The hydraulic system is controlled as a standard ELS system, where the highest actuator pressure defines the LS pressure. The LS pressure with a pressure margin defines the reference for the pump control.

3.4 Efficiency of supporting subsystems

The auxiliary systems defined here contain the boost pump of the drive, auxiliary pump, chargers, oil coolers and fans. The boost pump (19cc) and auxiliary pump (25cc) are both fixed displacement gear-type pumps. The boost pump provides pressure to the displacement control mechanism of the drive pump and substitute flow rate to the low-pressure side of the drive pump. Therefore, the boost pump has the same pressure level as the low pressure of the drive circuit, assumed to be 23 bar in all operation conditions.

The auxiliary pump provides power for the steering, brakes and external hydraulics. In the steering circuit, the priority valve is connected to the orbitrol, ensuring proper operation of the steering. Moreover, the flow rate of the auxiliary pump is used for charging the braking circuit and powering attachments if needed. A supplementary flow rate of the auxiliary pump goes to the tank over a freewheeling valve. The pressure loss of the pump is at least 13 bar even when the whole flow rate is going through the freewheeling valve.

The efficiencies of the boost pump and auxiliary pump are assumed to be constant and relatively high values as the exact efficiencies are not known. The volumetric

and hydro-mechanical efficiency are assumed to be 0.95, resulting in total efficiency of 0.9025. Furthermore, the oil cooler, alternator, and fans cause additional torque for the engine. The torque of the supporting subsystems is assumed to be 13 Nm (including the torque of the auxiliary and boost pump) and speed-independent due the simplicity of simulations and modeling. Nevertheless, the power usage depends on the rotational speed of the engine when the torque is constant.

4 SIMULATION STUDY OF FUEL ECONOMY IN STEADY-STATE DRIVING

The objective of this chapter is to support controller design by performing a feasibility study of fuel economy of the different control methods. That information was used for the controller design when the control strategy of the machine was defined. Especially, defining how much potential there is for fuel saving in the different operation points of the driving reveals the benefit that can be gained from the control strategy. Here, the different control methods for driving were compared with the optimal operation points in steady-state driving conditions.

The resistance forces of a vehicle are air resistance, rolling resistance and slope resistance. Figure 20 shows the forces for the experimental wheel loader and demonstrates how the forces increase as a function of slope and velocity. The forces are simulated with Equations (3.3a, 3.3b and 3.3c) in steady state when the machine is driving straight on a dry asphalt road and the wind velocity is assumed to zero.

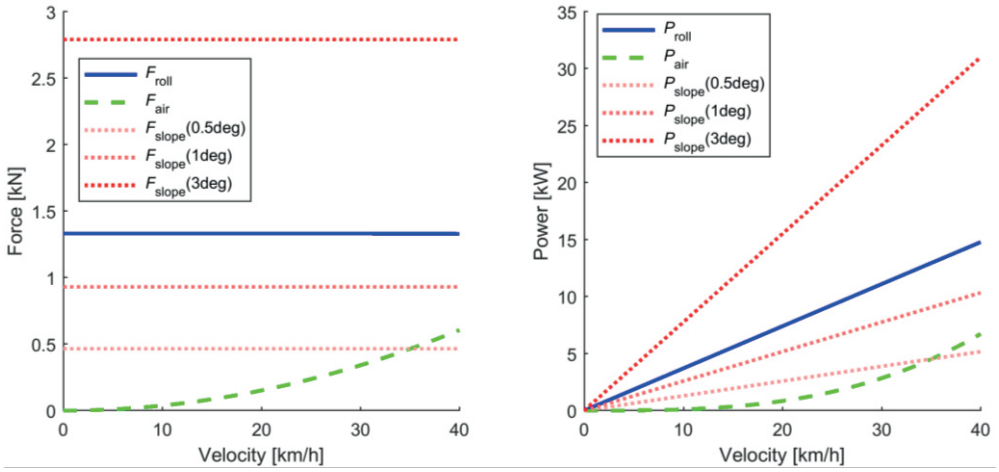

Figure 20. Resistance forces of the slope, air drag and rolling as a function of the velocity when the vehicle is driving on asphalt.

In the result, it can be observed that the slope resistance is higher than the rolling resistance after a 1.5 degree slope (≈2.6%). When the velocities are below 40 km/h, the air drag is less than the rolling resistance. Further, it can be seen that even a small change in the slope angle has a considerable effect on power consumption, especially at higher velocities.

To compare the fuel consumption of different control methods, three different control methods were selected: pump displacement control, automatic speed-related control and minimised rpm control. The pump displacement control and automatic speed-related control methods are currently used for the control of hydrostatic transmission in the wheel loaders as discussed in Chapter 2.3.1. The minimized rpm control results in the engine operating at lower rotational speeds and a better fuel efficiency zone, which is assumed to improve fuel economy [47]. The control methods were compared with the optimal operation points, defined in steady-state conditions. The simulation results are based on the modeling of the machine presented in Chapter 3.

4.1 Optimal operation points in steady-state driving conditions

To compare the fuel consumption of different control methods, and especially to determine the optimal control point for each velocity, the matrices were defined in steady-state driving conditions. This enabled the search for the optimal operation point of the fuel consumption or defining the fuel consumption at the given operation point. Defining the fuel consumption in dynamic operation conditions such as acceleration or deceleration would require modeling the transient fuel consumption of the engine. That requires a transient fuel consumption model of the engine that can differ from the steady-state operation points that are given for the engine. Further, the optimization problem would be different as also time

A $121 \times 101 \times 301$ matrix $\boldsymbol{A}(n, \varepsilon_{\mathrm{p}}, \Delta p)$ was defined as a function of the rotational speed of the engine, the displacement ratio of the pump and the differential pressure of the pump. A 401×101 matrix $\boldsymbol{B}(v, \varepsilon_{\mathrm{m}})$ was defined as the function of the velocity of the machine and the displacement ratio of the motor. The range and intervals of the operation points in the matrices are shown in Table 4.

Table 4. To define fuel consumption in steady-state operation conditions, predefined control values were used.

Matrix	Variable	Range	Interval	Dimension
$\boldsymbol{A(n, \varepsilon_p, \Delta p)}$	Engine speed	1000…2200 rev/min	10 rev/min	121
	Pump displacement ratio	0..1	1%	101
	Pressure difference	0...300 bar	1 bar	301
$\boldsymbol{B(v, \varepsilon_m)}$	Motor displacement ratio	Vmax…Vmin (1…0.42)	1%	101
	Velocity of the machine	0…40 km/h	0.1 km/h	401

In the predefined operation points, the resulting matrices were calculated for the flow rate and torque of the pump, the fuel consumption of the engine, the flow rate, differential pressure and the output torque of the motor. The resulting matrices are shown in Table 5.

The single values of the matrices were calculated by using the fuel efficiency function of the diesel engine and the loss functions of the hydraulic pump and hydraulic motor, as described in Chapter 3. With a given velocity, the rotational speed and output torque of the hydraulic motor were defined from the gear ratio between the tires and hydraulic motor and from the resistance forces with Equation (3.7).

Table 5. Pre-calculated values in the matrices were used to determine the fuel consumption and power loss of the subsystems for an optimal approach compared to control methods.

Variable	Matrix	Equation	Unit	Dimension
Input torque of the pump	$\boldsymbol{A}_T(n, \varepsilon_p, \Delta p)$	Eq. (3.9b)	Nm	$121 \times 101 \times 301$
Flow rate of the pump	$\boldsymbol{A}_q(n, \varepsilon_p, \Delta p)$	Eq. (3.9a)	l/min	$121 \times 101 \times 301$
Fuel consumption	$\boldsymbol{A}_{FC}(n, \varepsilon_p, \Delta p)$	BSFC-map	l/h	$121 \times 101 \times 301$
Output torque of the motor	$\boldsymbol{B}_T(v, \varepsilon_m)$	Eq. (3.7)	Nm	401×101

Flow rate of the motor	$\boldsymbol{B}_{\mathrm{q}}(v, \varepsilon_{\mathrm{m}})$	Eq. (3.8a)	l/min	401×101
Pressure difference of the motor	$\boldsymbol{B}_{\Delta \mathrm{p}}(v, \varepsilon_{\mathrm{m}})$	Eq. (3.8b)	bar	401×101

To define the fuel optimal operation points for the wheel loader, the matrices $\boldsymbol{A}(n, \varepsilon_{\mathrm{p}}, \Delta p)$ and $\boldsymbol{B}(v, \varepsilon_{\mathrm{m}})$ were used. The optimal control values were searched for each velocity (401 points) separately. At first, all velocities that were close to the searched velocity from matrix $\boldsymbol{B}_{\mathrm{v}}$ were selected. For each operation point, the corresponding pressure and flow rate of the hydraulic motor were defined from matrices $\boldsymbol{B}_{\Delta \mathrm{p}}$ and $\boldsymbol{B}_{\mathrm{q}}$.

As the pressure loss in the hoses between the hydraulic pump and motor were ignored, the flow rate and differential pressure of the hydraulic motor should have matched the flow rate and pressure of the pump. Therefore, a corresponding pair of pressure and flow rate could be searched from matrices $\boldsymbol{A}_{\Delta \mathrm{p}}$ and $\boldsymbol{A}_{\mathrm{q}}$. Here, all pairs of indexes (a_i, b_i) that were close enough to the searched conditions were defined:

$$\begin{aligned} &\forall a_i \in \boldsymbol{A}, \forall b_i \in \boldsymbol{B}: \left|\boldsymbol{B}_v(b_i) - v_{\mathrm{src}}\right| \leq i_{\mathrm{v}} \wedge \\ &\left(\left|1 - \boldsymbol{B}_{\mathrm{q}}(b_i)/\boldsymbol{A}_{\mathrm{q}}(a_i)\right| \leq i_{\mathrm{q}} \wedge \left|\boldsymbol{B}_{\Delta \mathrm{p}}(b_i) - \boldsymbol{A}_{\Delta \mathrm{p}}(a_i)\right| \leq i_{\Delta \mathrm{p}}\right) \end{aligned} \tag{4.1}$$

where v_{src} is the searched velocity, $i_{\mathrm{v}} = 0$ is the accepted error of velocity, $i_{\mathrm{q}} = 0.01$ is the accepted error of flow rate and $i_{\Delta \mathrm{p}} = 0.55$ bar is the accepted error of differential pressure, and the pair (a_i, b_i) are members of the matrices that fulfil the results. When all combinations were found that fulfilled the search criteria, the optimal fuel economy was in the operation condition where the fuel economy function received the smallest value:

$$\begin{aligned} \exists a_{\mathrm{opt}} \in \boldsymbol{A}, b_{\mathrm{opt}} \in \boldsymbol{B}: \forall a_i \in \boldsymbol{A}, b_i \in \boldsymbol{B}: & \frac{\boldsymbol{A}_{\mathrm{FC}}(a_{\mathrm{opt}})}{\boldsymbol{B}_{\mathrm{v}}(b_{\mathrm{opt}})} \\ & \leq \frac{\boldsymbol{A}_{\mathrm{FC}}(a_i)}{\boldsymbol{B}_{\mathrm{v}}(b_i)} \end{aligned} \tag{4.2}$$

where pair $(a_{\mathrm{opt}}, b_{\mathrm{opt}})$ represents the optimal operation condition that defines the minimum fuel economy for the given velocity. Further, the pairs (a_i, b_i) are all the indexes that fulfilled a condition defined in Equation (4.1).

The optimal fuel economy and operation conditions were defined for all velocities between 0 to 40 km/h with an interval of 0.1 km/h. The normalized control values and the power loss of the subsystems are shown as a function of the velocity in the optimal operation conditions in Figure 21.

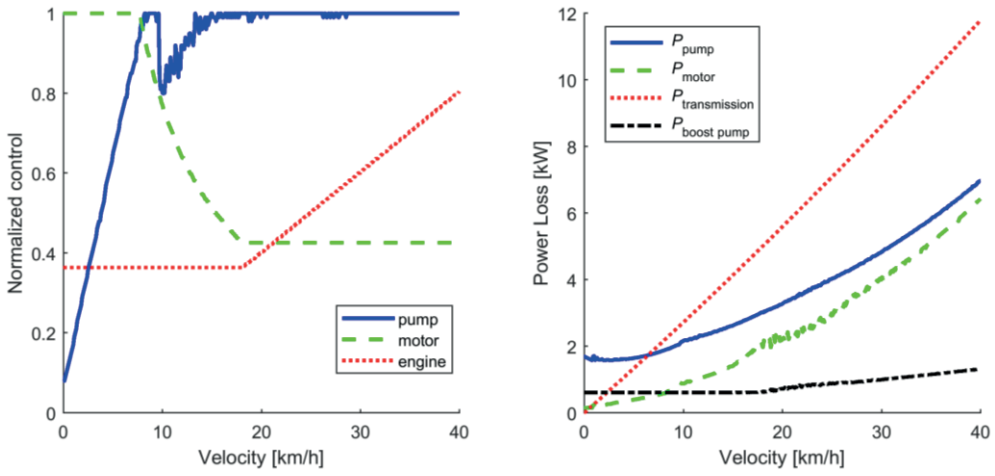

Figure 21. Normalized control signals of the components and power loss of the vehicle in the fuel optimal operation points when driving in steady-state operation conditions are defined in 401 different velocities.

From the results, it can be noted that the optimal approach increases the displacement ratio of the pump first; second, the displacement ratio of the motor is reduced; and finally, the rotational speed of the engine is increased to reach the highest velocity. In velocity between 10 and 15 km/h, the motor displacement ratio decreases rapidly and is compensated for by decreasing the displacement ratio of the pump. It seems that optimization determines the higher efficiency of the driveline when the differential pressure is increased at these velocities.

Further, the control sequence has small variations in the control values when the rotational speed of the engine is still at the minimum (in velocities below 22 km/h). There, the operation point of the pump and motor do not have a dramatic effect on fuel consumption. Besides, inaccuracies in the optimization might affect the results when the difference in fuel consumption is not high. These inaccuracies are mainly induced from matching the flow rate and differential pressure of the pump and motor. As these values are defined in different matrices, an error of 0.55 bar in pressure and 1% in the flow rate are accepted.

4.2 Control methods

To compare the fuel consumption of different control methods, the control sequence as a function of the velocity was defined for displacement control, DA-control and minimised rpm control. For the applied machine, 40 km/h was the maximum allowed velocity set by the local legislation. Therefore, the maximum velocity of each control method was tuned to that limit, although the maximum velocity of the machine is theoretically about 50km/h.

The control sequence was predefined for each control strategy separately. When the control sequence was defined, the matrices $\boldsymbol{A}(n, \varepsilon_{\mathrm{p}}, \Delta p)$ and $\boldsymbol{B}(v, \varepsilon_{\mathrm{m}})$ were used to define the power loss of the subsystems and the fuel consumption. The predefined control sequence defined the operation point for the machine, which was searched from the matrices separately at different velocity points (401 points).

4.2.1 Pump displacement control

In the pump displacement control method, the rotational speed of the engine and displacement ratio of the hydraulic motor were fixed. The displacement ratio of the hydraulic motor was set at the minimum to provide a maximum hydrostatic gear ratio. The rotational speed of the engine was set at the level where the machine reached a velocity of 40 km/h at a maximum gear ratio and maximum displacement ratio of the pump. The velocity of the machine was then controlled by changing the displacement ratio of the hydraulic pump.

Displacement control does not produce maximum tractive force if the hydraulic motor is not actively controlled. In the simulations, the machine was driving in a steady-state velocity on flat terrain. Therefore, control of the hydraulic motor did not restrict the performance, as the drive torque was sufficiently even with the minimum displacement ratio. The displacement control is used in excavators and smaller machines. In these machines, the size of the hydraulic motor is typically designed so that the vehicle can fulfil the required performance.

Figure 22 shows the control sequence of displacement control on the left and the power loss of the subsystems on the right. Based on the control sequence, the power losses of the subsystems were defined by using the matrices $\boldsymbol{A}(n, \varepsilon_{\mathrm{p}}, \Delta p)$ and $\boldsymbol{B}(v, \varepsilon_{\mathrm{m}})$ as described earlier.

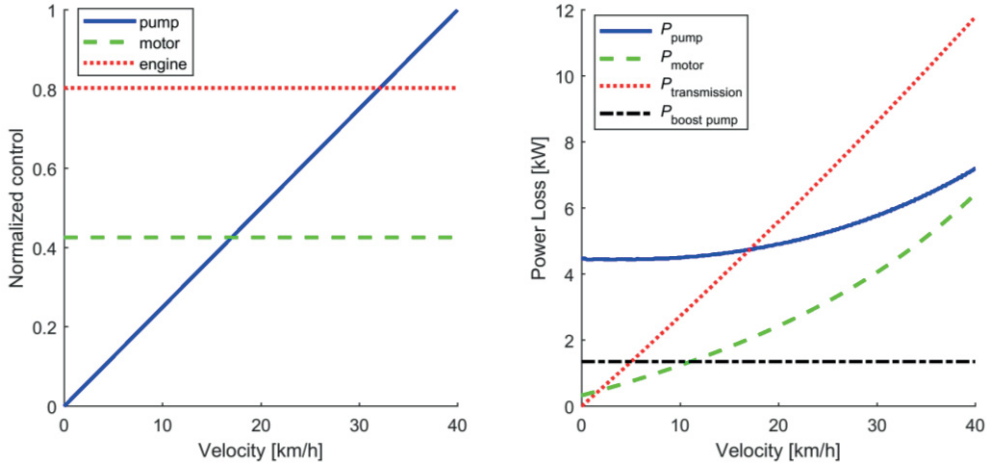

Figure 22. A normalised control signal of the components and power loss of the vehicle as a function of the velocity with displacement control.

The power loss of the boost pump was constant, as it is a fixed displacement pump, and the rotational speed is constant with the displacement control. The power loss of the transmission resulted from friction in the gears and increased as a function of the drive speed. Further, the power loss of the hydraulic pump and motor increased as a function of the velocity. Compared with the optimal approach, the power loss of the drive pump and boost pump were higher due to the higher rotational speed of the engine.

4.2.2 Automatic speed-related control

There are alternative commercial approaches to controlling hydraulic transmission based on the rotational speed of the engine and load conditions. The original series-production machine manufactured by Vilakone uses automatic speed-related control (hydro-mechanical DA-control) from Bosch Rexroth and is therefore presented here. The hydraulic pump and motor of the original machine were not equipped with displacement sensors, and therefore could not be measured straight from the machine. Further, the hydrostatic pump and motor were sized differently compared with the studied machine. Therefore, the DA-control is emulated here and the same emulation model is used in the comparison measurement of the real machine later on.

In DA-control, the accelerator pedal directly sets the rotational speed reference for the engine. The displacement ratio of the hydraulic pump and motor are proportional to the rotational speed of the engine, resulting in an increased hydrostatic gear ratio when the rotational speed of the engine increases. The control principle of hydro-mechanical DA-control is shown in Figure 23.

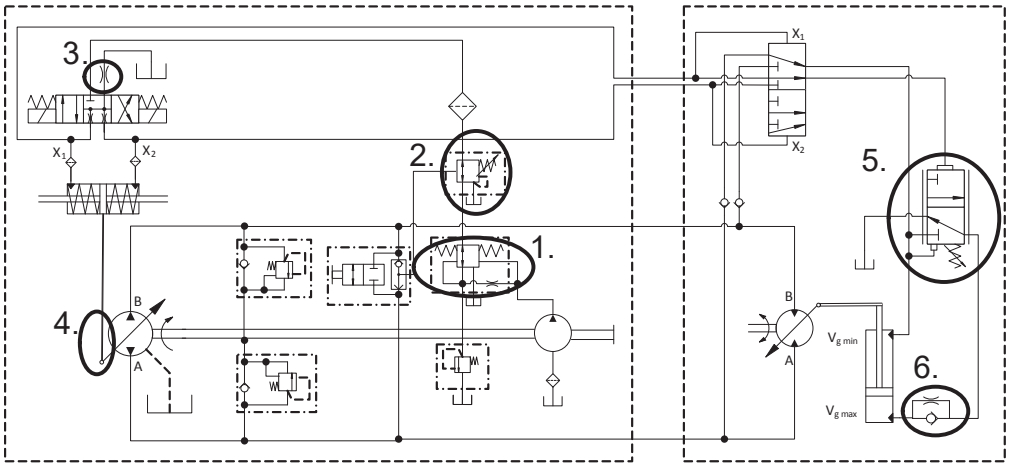

Figure 23. Hydraulic diagram of DA-control with control elements [127, 128].

The hydraulic pump and motor are the same as in the wheel loader used in this study, only the control device is electrified instead of the hydro-mechanical DA-control. Therefore, DA-control can be emulated with the current system only by changing the software of the control system. The most significant elements of hydro-mechanical DA-control are shown in Figure 23:

1. DA-valve that generates a pilot pressure for the control valve and cylinder of the pump (the same pressure is affecting the motor, depending on the drive direction selected by the control valve of the pump). The pressure depends on the flow rate of the boost pump, which is proportional to the rotational speed of the engine.

2. The pressure relief valve for a pressure cut-off reduces pilot pressure when the drive pressure nears the maximum pressure level of the system.

3. The orifice of the control valve ensures smooth directional change and sometimes restricts the increasing speed of the pump.

4. The control mechanism of the pump takes into account the load conditions as increased pressure reduces the pump displacement.

5. The setpoint of the pilot pressure controls the displacement of the hydraulic motor depending on the operating conditions.

6. The orifice of the hydraulic motor restricts the increasing speed of the displacement ratio.

For DA-emulation, the components (engine, hydraulic pump and motor) should be controlled independently, which is possible in the experimental machine. The Simulink model of the DA-emulation is shown in Figure 24. The foremost functionalities are emphasized with numbers and correspond to the elements in the hydraulic diagram of the DA-control. The rotational speed of the diesel engine is directly proportional to the position of an accelerator pedal. Therefore, the control of the engine is not shown here.

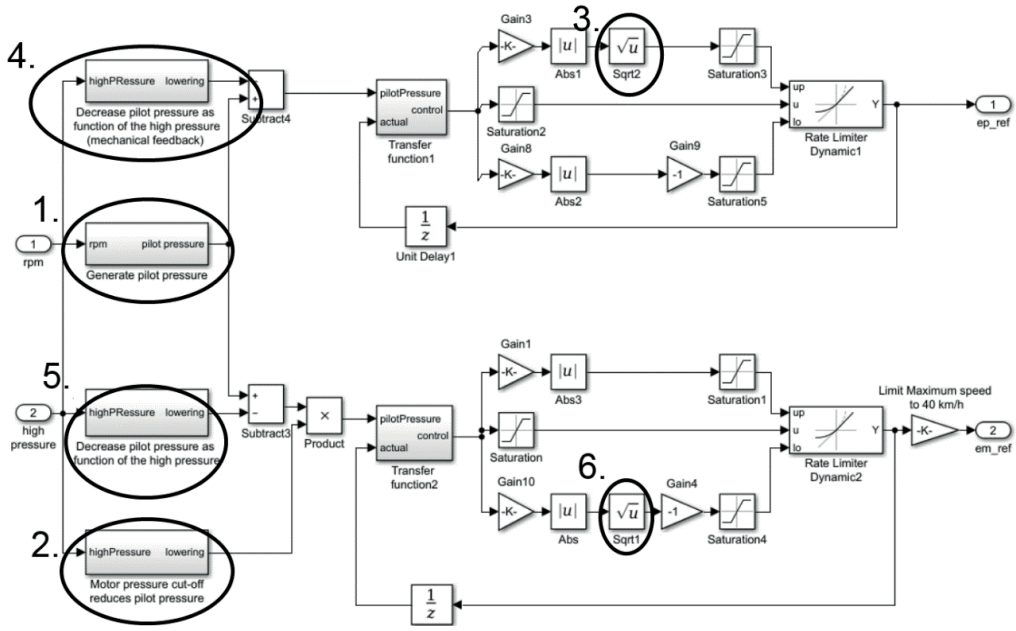

Figure 24. Simulink model for the emulation of the DA-control is based on the modelling of the control elements of the hydro-mechanical DA-control.

The pilot pressure is generated from the measured rotational speed of the engine (input 1). The high side pressure of the pump (input 2) reduces the pilot pressure for the pump and motor. Further, when the high side pressure is close to the maximum, the cut-off function starts to decrease the pilot pressure for the motor, resulting in

the maximum torque for the hydraulic motor. The cut-off functionality of the pump is integrated into the controller of the pump and is therefore not emulated.

The flow rates through the orifices are emulated with the square root functions that represent dependence of flow rate and pressure. The dynamics of the control cylinders are then limited to that rate with the rate limiters, as shown in Figure 24. Further, the maximum velocity of the machine can be tuned with a gain that defines the smallest displacement ratio of the hydraulic motor. The outputs of the DA-emulation are displacement ratio references for the pump and motor.

The control sequence of the DA-control was obtained by simulating the DA-emulation in the steady-state driving. Originally, the accelerator pedal was directly controlling the rotational speed of the diesel engine and was therefore simulated by changing the rotational speed linearly. The load conditions (the high side pressure) and the rotational speed of the engine defined the final control values of the pump and motor. The high side pressure was obtained from the differential pressure by adding the low pressure setting of the pump. The differential pressure and the velocity of the machine were derived from the machine model defined in Chapter 3. Figure 25 shows the control sequence of the DA-control and the power loss of the subsystems defined from matrices $\boldsymbol{A}(n, \varepsilon_{\mathrm{p}}, \Delta p)$ and $\boldsymbol{B}(v, \varepsilon_{\mathrm{m}})$ when the control sequence was known.

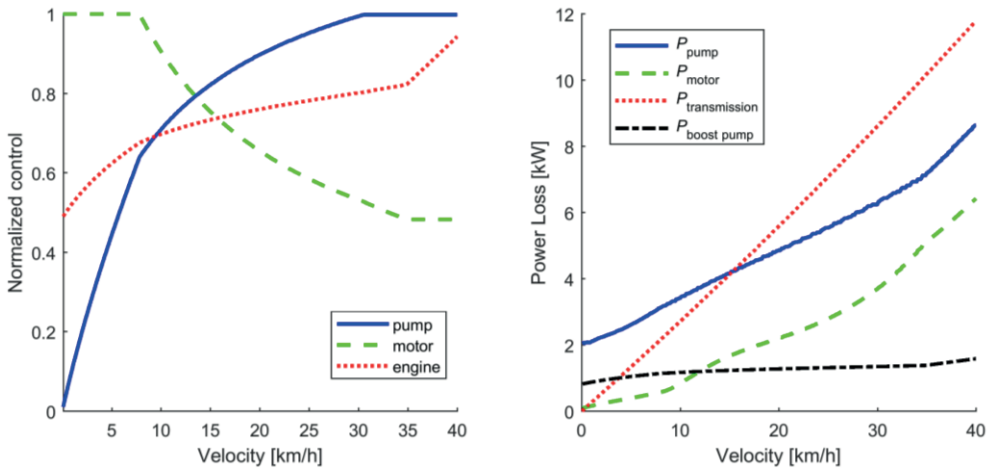

Figure 25. A control sequence and power loss of the vehicle with DA-control.

At high velocities, only the rotational speed of the engine was increased, as the hydrostatic transmission reached the maximum gear ratio earlier when driving on flat terrain. This resulted in an increased rate of power loss of the boost pump and hydrostatic pump, which can be seen at velocities higher than 35 km/h in Figure 25.

The original DA-control mechanism has several machine-specific parameters that can be tuned, such as the size of orifices and the pre-tension of the springs, which have an effect on the properties of the drive function. To ensure reasonable settings for the DA-emulation, the emulation was compared and verified with the series-production machine equipped with a DA-control. The verification measurements were done with both gear ratios (turtle and rabbit) and with different slopes of the road. The measurement defines the starting point of the machine and steady-state velocity at the different load conditions and operation points of the engine. Further, the acceleration and deceleration of the series-production machine were measured by testing the step responses. Based on the verification measurements, the parameters of the DA-emulation were tuned so that the drive functionality corresponded to the series-production machine. That was tested by running the DA-emulation in the control system of the studied machine in the same drive conditions as the series-production machine.

Nevertheless, the displacements of the hydraulic pump and motor could not be measured from the series-production machine. Therefore, the starting point of the hydraulic motor may be different in comparison with the original series-production machine.

4.2.3 Minimized rpm control

Minimised rpm control is a control method that minimizes the rotational speed of the diesel engine. With minimized rotational speed, the engine operates at higher partial loads because the required power is the same but the maximum power capacity of the engine is lower. Therefore, the engine operates in a higher fuel efficiency region. Further, the subsystems operating nearly constant torque have smaller power consumption when operating with reduced rotational speed. Therefore, the minimized rpm approach has the potential to improve fuel economy.

This control method is similar to the standard speed control presented in the optimization study of hydrostatic drives, except that the minimum rotational speed

of the engine used here is the idle speed, not the nominal speed. The nominal speed is typically higher than the idle speed due to the power requirements. Further, the study shows that fuel consumption is reduced when the nominal speed of the engine is lower, which supports the assumption that lower rotational speed can improve the fuel economy. [47]

A control sequence of the minimized rpm and the power loss of the subsystems are shown in Figure 26. The control is separated into three speed regions: in the first speed region, the displacement ratio of the pump is increased; in the second speed region, the displacement ratio of the hydraulic motor is reduced; and in the third speed region, the rotational speed of the diesel engine is increased.

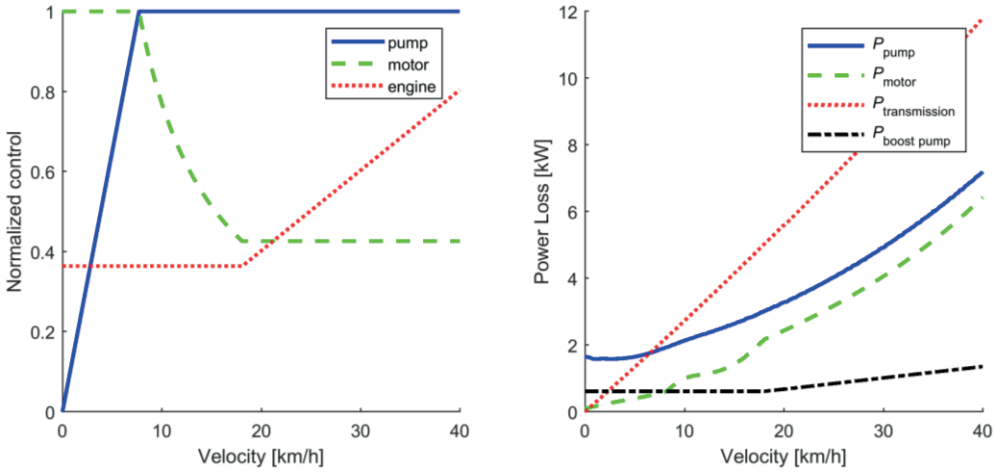

Figure 26. A control sequence and power loss of the vehicle with minimized rpm control, where the control signals are normalized between 0 and 1.

The power losses of the subsystems were defined from matrices $\boldsymbol{A}(n, \varepsilon_{\mathrm{p}}, \Delta p)$ and $\boldsymbol{B}(v, \varepsilon_{\mathrm{m}})$. The power loss of the boost pump started to increase when the rotational speed of engine was increased. Further, the power losses were close to the optimal approach.

In steady-state driving, the power of the engine was not restrictive, as the experimental machine was equipped with a relatively large engine. Nevertheless, in real-world drive and work cycles, the minimum rpm did not provide enough power in all operation conditions. Therefore, the minimum rpm approach requires that the

power management algorithm ensures enough power to fulfil the power demand in different operation conditions and to prevent engine stall.

4.3 Comparison of control methods for minimum fuel consumption in steady-state driving

The fuel consumption and power consumption of the presented control methods were defined and compared with the optimal approach as a function of the velocity. The fuel consumption was analyzed in steady-state conditions by using the predefined matrices as described earlier. Figure 27 compares the power loss of the drive system at different control methods with the optimal approach. The total power loss of the drive is a summation of the power losses in the transmission, boost pump, hydraulic motor and hydraulic pump.

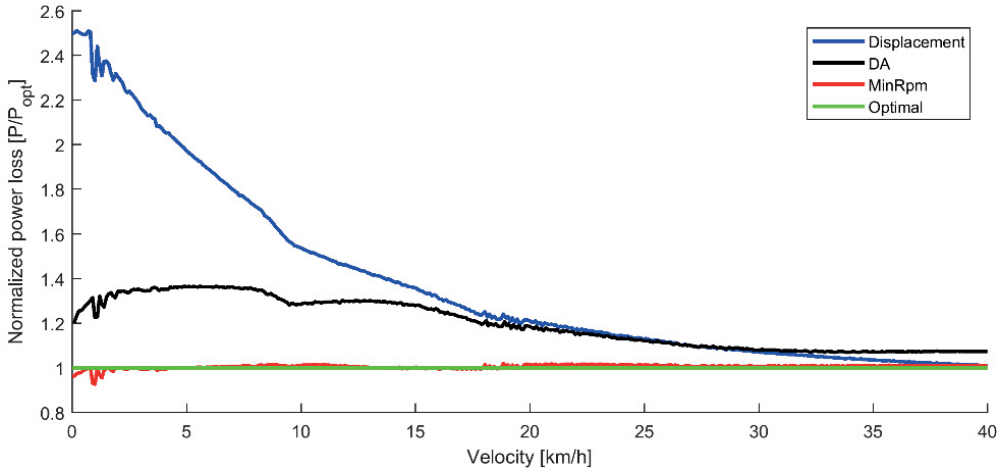

Figure 27. Simulated power loss of the drive system with displacement control, DA-control and minimized rpm control compared with the optimal approach.

At low velocities, the selected control method affects the power loss more than at higher velocities. The power loss of the pumps is proportional to the rotational speed of the engine, and therefore the control methods that operate with higher engine speeds produce higher power losses. Further, due to the inaccuracy of the matrices used, some oscillation in the results occurred, and the MinRpm approach appears to have a slightly lower power loss than the optimal in some operation points.

When the torque and rotational speed of the engine are known, the fuel consumption is defined by using the BSFC-map of the diesel engine. The fuel consumptions of different control methods are compared in Figure 28. The fuel consumption of the minimum rpm approach is close to the optimal, as the control sequence of the engine is similar to the optimal operation points. In the DA-control, the velocity limitations to 40 km/h are done by limiting the minimum displacement of the motor. Therefore, at the highest velocities, the rotational speed and fuel consumption of the engine are higher than with other control methods.

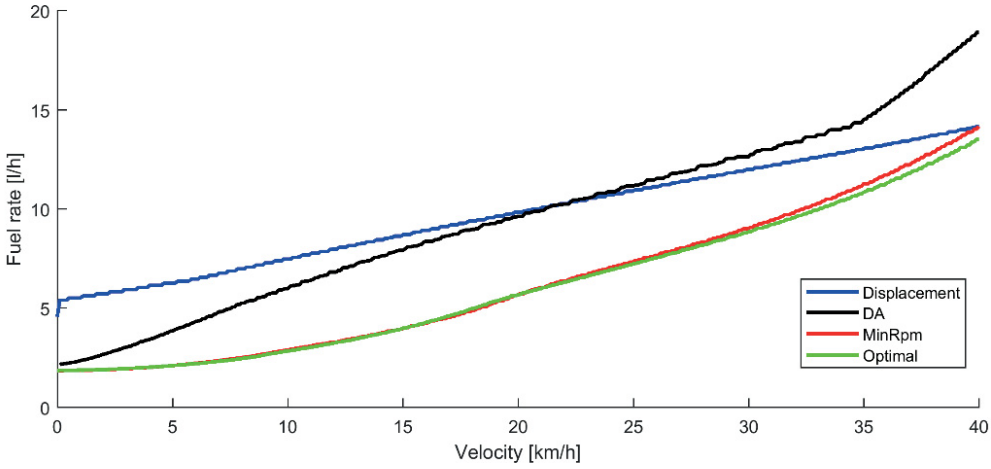

Figure 28. Simulated fuel rate of the engine with displacement control, DA-control and minimized rpm control compared with the optimal approach.

The fuel economy of the minimized rpm control is very close to the optimal, as shown in Figure 29. At low velocities, the displacement control consumes over two times as much fuel as the optimal approach. The best fuel economy, 26.4 litres per 100 kilometres, is achieved with the optimal operation points at a velocity of 15 km/h: that is, operation points where the hydrostatic transmission ratio is at the maximum but the rotational speed of the engine is not increased from the minimum yet.

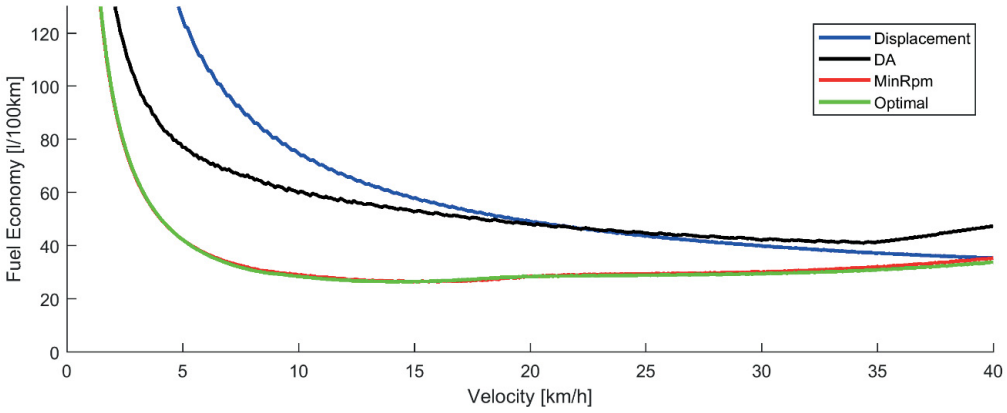

Figure 29. Simulated fuel economy of displacement control, DA-control and minimized rpm control compared with the optimal approach.

Figure 30 shows the fuel economy with four different velocities. The difference in the fuel economy of the DA-control compared with the optimal is the highest at velocities between 15 and 25 km/h. At high velocities, the difference in the fuel economy is lower because all control methods are operating close to the maximum hydrostatic transmission ratio.

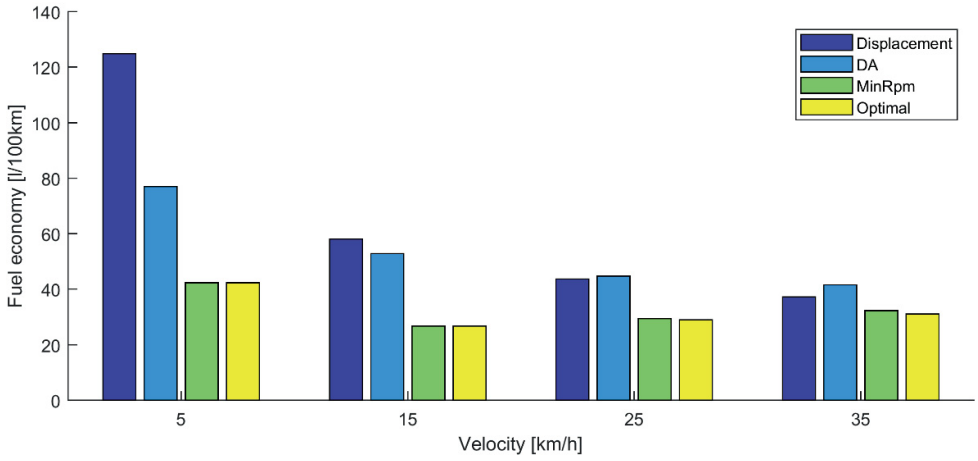

Figure 30. The fuel economy of different control methods is compared with velocities 5, 15, 25 and 35 km/h.

Simulated fuel economy in steady-state driving conditions reveals that the selected control method has a significant effect on the fuel consumption. Further, the minimized rpm approach achieves a fuel economy close to the optimal. The accuracy of the predefined matrices and tuning the parameters of the control methods can have an effect on the results. Nevertheless, reducing the rotational speed of the diesel engine tends to increase the fuel economy of the machine.

In steady-state driving conditions on flat terrain, the power of the engine is not a limiting factor. However, in real driving conditions with dynamic operations, the power capacity of the engine limits the control freedom of the drive system. Further, the work functionalities, steering and other machine-related functions have an effect on the fuel consumption and control of the system. Therefore, the full-scale control system should be able to operate with these constraints without stalling the engine or limiting the performance of the machine.

5 DESIGN OF MODULAR CONTROL ARCHITECTURE

Research and prototyping require a rapid development environment that allows the extension of the functionalities and hardware of the system to meet unforeseeable requirements in the future. Therefore, a hierarchical hardware abstraction with a modular approach was selected as the design principle for the control system architecture of the experimental wheel loader. The control hardware was distributed into three functional layers, as shown in Figure 31.

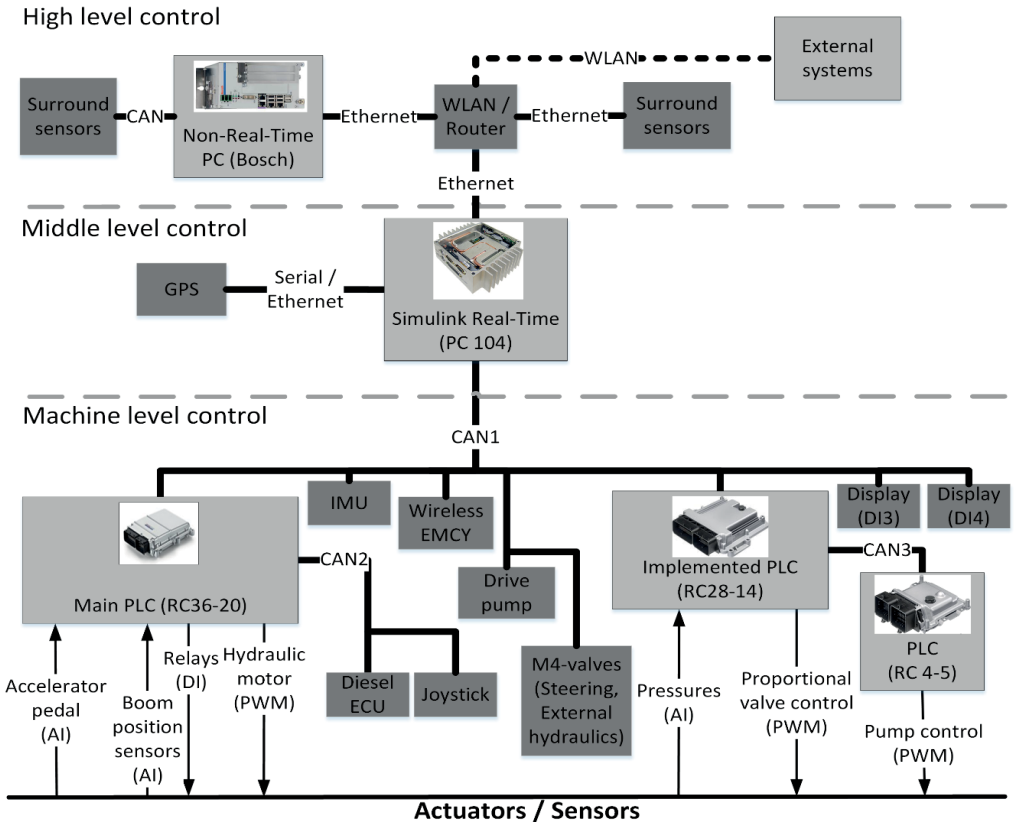

Figure 31. Control hardware of the experimental wheel loader is distributed into three functional layers: machine level, middle level and high level.

The control layer of the machine level is responsible for the basic functionalities of the machine, managing all actuators and sensors at the machine level. The machine level control layer provides safety functions, control mode selection and control interfaces for the higher levels. The middle level is implemented with Simulink Real-Time to ensure the real-time control of autonomous driving, remote control and data collection. Therefore, a Global Positioning System (GPS) is realized at this level to ensure real-time navigation and path following.

The control layer at the high level is for non-real-time functionalities, such as path planning, process control of the machine or environment mapping and object recognition, which cannot be run with hard real-time requirements. Further, the high level control layer makes it possible to integrate the machine with external systems, such as remote control or process control of the worksite.

The software at the machine level is designed over the hardware boundaries with a modular abstraction layer approach, as shown in Figure 32. The submodules are always implemented in one controller, but the upper level module can be composed of multiple submodules implemented with different controllers. The modularity of the systems is based on the logical entities that implement certain functionalities, such as steering, drive, implements, or how the control inputs are selected.

At the machine level, the main modules are supervisory control, which handles the safety and consistency of the control; input handler, which defines an active control interface to the machine; and power management, which ensures responses to the required control commands. The input handler module provides different control inputs for the manual control, remote control and autonomous control by wrapping the actual control interface required for the power management module. Therefore, the drive, steering and implement modules can be independent from the actual commands.

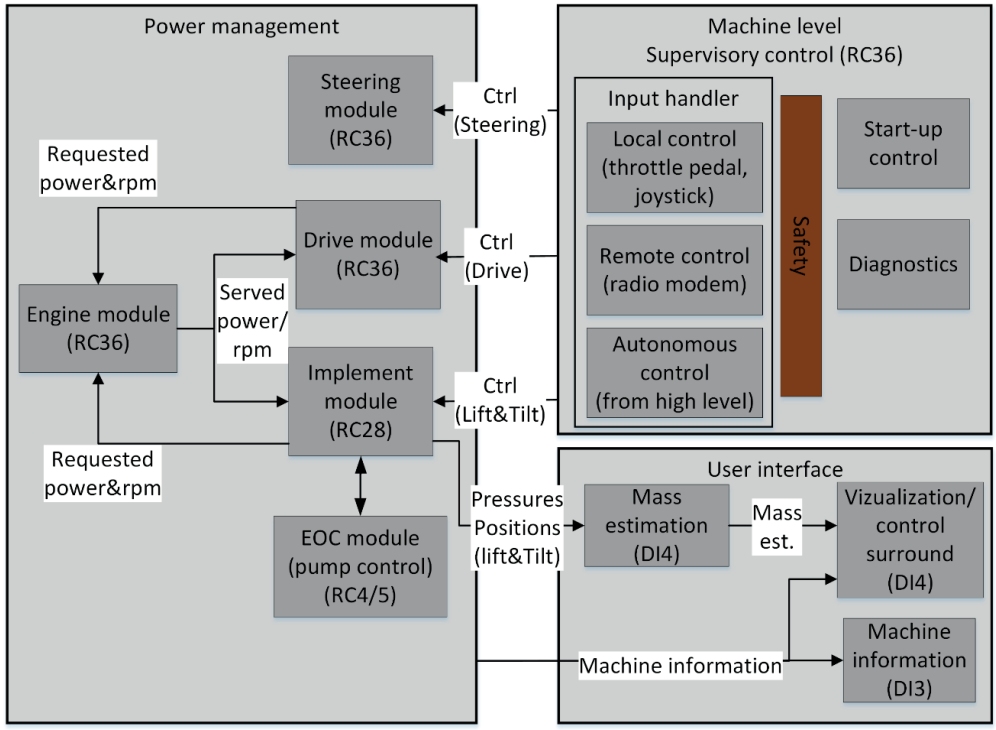

Figure 32. The modular abstraction layer approach for control architecture of the experimental wheel loader is implemented with several controllers at the machine level.

In the modular approach, the interfaces between the modules are critical for ensuring the consistent and safe operation of the machine. Further, as the machine is designed for research purposes, the raw data of the sensors and actuators are usually delivered with communication interfaces. Therefore, the raw data are available for data logging or developing new functionalities. Nevertheless, the transfer capacity of the CAN-bus limits the frequency and the amount of raw data. Thus, the subsidiary data are discarded.

5.1 Alternative approaches for machine level control

Two alternative architectures are described as exemplary systems to provide comparison and analyses with the modular abstraction layer architecture. The first system is realised with centralised computation that was developed for a skid-steered wheel loader [130-132]. The second system is a functionally distributed system that

was developed for a small articulated-frame-steered wheel loader originally by the author in his master's thesis [133]. All the loaders are fully electrified and capable of autonomous operation by connecting the machine level control system to the autonomy system in the higher control layer.

Figure 33 shows a system layout of the skid-steered loader that represents centralized system architecture. The display module, DM586 is a centralized computing unit that is connected to the sensors, actuators and control devices via CAN-bus connected I/O modules. The display operates as a master of CAN bus, executes the high level tasks, communicates with a remote control user interface, or is connected with higher level control systems. I/O modules function as signal converters and do not perform any control loops. [132] The centralized approach has similarities to the alternative control approaches of non-road working machines that are described in the literature [21, 84].

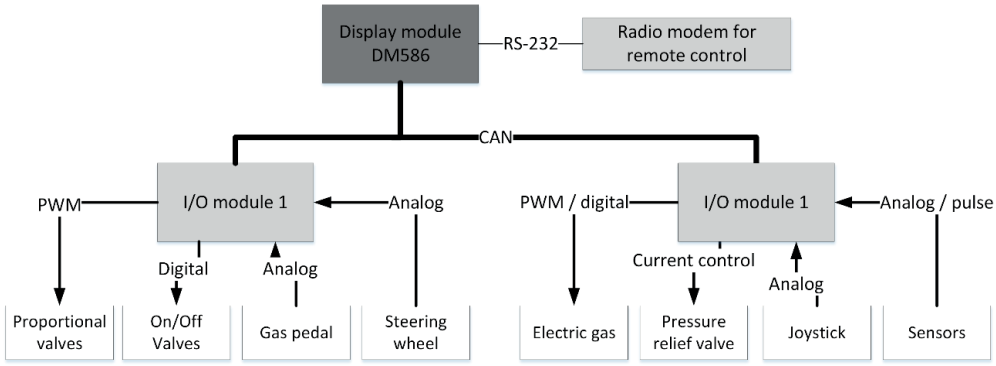

Figure 33. Centralized control system of the skid-steered loader modified from [132].

A second approach is a functionally distributed control system that was developed for the small articulated-frame-steered wheel loader shown in Figure 34. The system architecture is comparable with other architectures that are functionally distributed [18, 22, 23].

All modules realize one or several functionalities, so that functionality and hardware are combined together. For example, a gas pedal, reversing device, and drive pump solenoids are connected to the same module that takes care of the control of the drive system. To ensure consistency and safety, the master module is responsible for control modes and error handling. To manage the mode change from the close loop

to open loop control, the master module commands the mode change. Similarly, the master module commands other modules to manual, remote or autonomous mode when the operation mode is changed. All other modules respond with the status of code that indicates if the mode change was successful or indicates a failure.

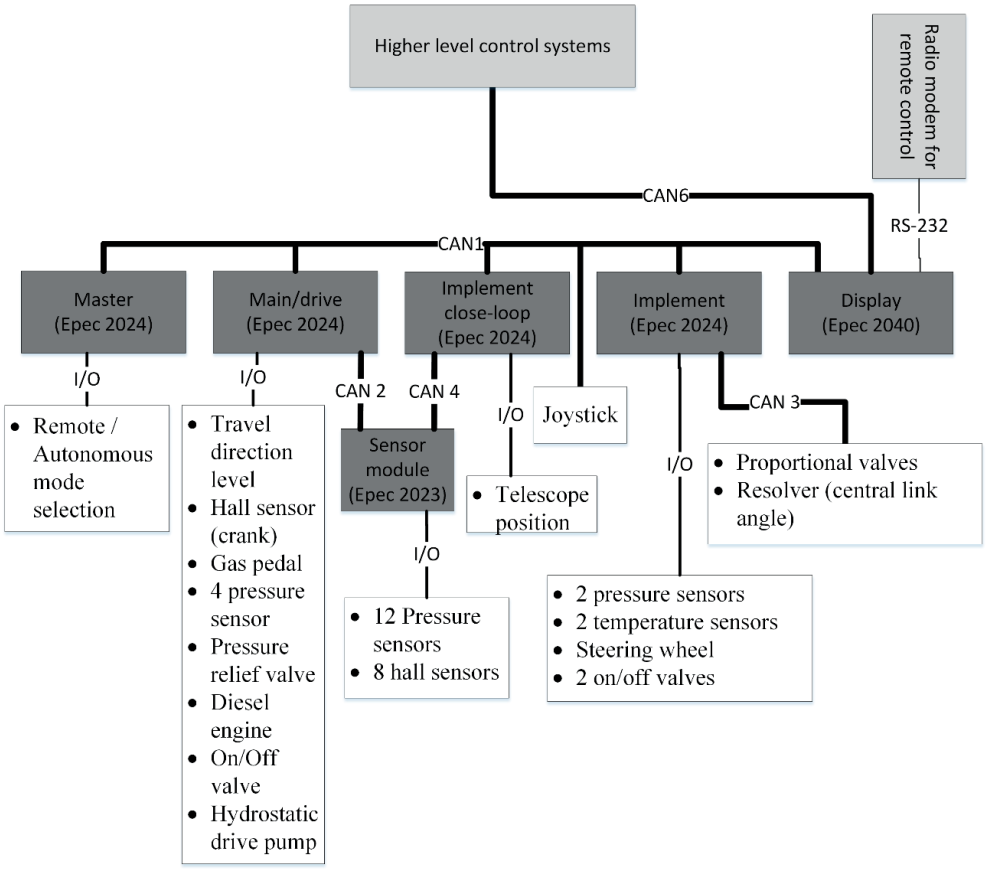

Figure 34. Functionally distributed control system of the articulated-frame-steered wheel loader.

Both low level system architectures, centralized and functionally distributed systems are realized with prototype machines and are shown to be capable of operating in the manual, remote or autonomous mode. Based on the information gained during the usage and development of these systems, the characteristics and features of the architectures can be analyzed. Further, both systems are capable of the functions of the reference architectures needed for the autonomous machines. For example, in 4D/SRC architecture, the presented architectures represent Servo and Primitive levels in the 4D/SRC hierarchy [83].

5.2 Trade-off analysis of machine level architectures

Three system architectures of the wheel loaders are compared from the system designer's point of view. The objectives of the architectures are flexibility and capability to adapt in different operation modes such as manual operation, teleoperation or autonomous operation. Further, the systems should be capable of research of alternative control methods for hydrostatic drive and implement systems.

The comparison is based on the author's observation during the development process or usage of the systems. The centralized and functionally distributed control system are compared earlier with some of the key characteristics [132]. The information gained from that analysis is updated and extended so that characteristics can be scored. Further, the scoring and analysis are extended to cover the modular abstraction layer approach presented in Chapter 5.1. The characteristics are defined so that each system can be scored on a scale from one to three points. The maximum is three points and the minimum one point. Table 6 shows the scoring of each characteristic and describes how the scoring is defined for the selected architecture. It should be noted that the architectures of the control systems are developed and compared based on the components that are generally available for working machines. These controllers have a compact assembly and are designed for use in harsh environment.

Table 6. Scoring is defined for each characteristic so that different architectures can be compared.

	Centralized computation	**Distributed computation in functional modules**	**Modular abstraction layer**
Characteristic	**System 1**	**System 2**	**System 3**
Avoids complexity in hardware design *1: Increases complexity* *2: Introduces some complexity* *3: Avoids complexity*	*Score: 3* Simple hardware architecture as all the signals are connected with I/O modules and control is realized in the master module.	*Score: 1* Complex hardware architecture requires good design so that functionalities are logical in different operation modes.	*Score: 2* Complex hardware architecture and abstraction layers allow the reorganisation of functionalities.

Possibility to optimize capacity of controllers and cable routing *1: Possibility of optimization is limited* *2: Some limitations for optimization* *3: Supports optimization*	*Score: 2* Master device is required with powerful real-time computation, slave modules can be optimized with sufficient I/O interfaces.	*Score: 1* Functionalities require several devices, where the requirement of I/Os varies. Therefore, high usage of I/O is hard to reach.	*Score: 3* Devices can be optimized based on the distribution of the functions.
Hardware expandability afterwards *1: Limited expandability* *2: Some limitations to expandability* *3: Expandability is not limited*	*Score: 1* New I/O-modules can be added to the system. One computation module and capacity of communication limits the expandability.	*Score: 2* New hardware can be added for new functionalities or I/O-modules can be expanded. Selected distribution architecture of functions limits expandability.	*Score: 3* Functions are realized with higher abstraction level, so the hardware can be expanded if communication bus capacity is not limiting functionality.
Exploitable computing capacity *1: Computing capacity is not fully exploitable* *2: Some limitations to exploitability* *3: Computing capacity can be exploited*	*Score: 3* With pre-emptive scheduling, the computing capacity can be exploited.	*Score: 1* The computing requirements of the functions are not evenly distributed, so the load of the computing devices varies.	*Score: 2* Execution of the function can be optimized based on the computing capacity, although communication capacity limits the optimization.

Routing and modification of signals and execution path of control loops *1: Rerouting is limited* *2: Some limitations to rerouting* *3: Rerouting is supported*	*Score: 2* All signals are handled in one computing unit, so the modification of control loops does not require rerouting of the signals. Required I/O modules and communication paths can induce delays.	*Score: 1* If sensors and actuators are connected to the same control unit, then unnecessary delays can be avoided. Otherwise, new functions introduce delays or require a reconfiguration of the hardware.	*Score: 2* No unnecessary delays if functions are executed close to the sensors and actuators. Functions can be reorganized based on the required signals.
Easiness of software management *1: Software management is fragmented* *2: Some limitations to software management* *3: Software management is easy*	*Score: 3* All information (program code) exists in one module. So architecture does not limit software management.	*Score: 1* If part of the system needs to be modified, usually several modules need to be updated.	*Score 2:* If part of the system needs to be modified, usually the functionalities can be reorganized.
Consistency and simplicity of safety features and supervisory functionalities *1: Management of consistency and safety is challenging* *2: Management of consistency or safety has some challenges*	*Score: 2* All the diagnostics and supervisory are realized in the same module. Safety is hard to isolate from the non-safety functions (especially in the hardware level).	*Score: 2* All modules have internal diagnostics and safety can be isolated. Supervisory is needed and carefully designed to ensure consistency for system failures and operation mode handling.	*Score: 3* All the functions and supervisory can be realized with abstraction layers. The safety can be isolated from the non-safety functionalities.

3: Safety and consistency are easy to realize			
Support for availability, fault recovery and isolation *1: Isolation is hard to realize* *2: Some functions can be isolated* *3: Most of the functions can be isolated*	*Score: 1* If hardware fails, it usually affects the entire machine as computation is realized in one module.	*Score: 3* If hardware fails, the failed module can be isolated and other modules can operate independently in the climbing mode.	*Score: 2* If hardware fails, the failure has an effect on all the functions that are executed in the same module. Other functions can be operated independently.

The result of the system architecture comparison is shown in Table 7, including the scoring and weighting factors of the characteristics. The scoring functions give one to three points for each characteristic. The characteristics are weighted from zero to five, defining their significance: (0: not important, 1: nice to have, 2: good to have, 3: notable, 4: important, 5: very important).

The scoring function is based on the properties defined in Table 6. The weight factor defines how important the characteristic is for the research machine. The weights are defined from the use cases of the research machine and from the expected development need for the future research. The weighted score is the weight factor multiplied with the unweighted score. The total unweighted score is the sum of the score and the total weighted score is the sum of the weighted score. Further, the normalized unweighted and weighted score are calculated to stress the differences of the architectures.

The modular abstraction layer approach, system 3, gets the highest unweighted score, followed by the centralized approach, system 1 (8% difference in score), and the functionally distributed, system 2 approach is last (with 29% of difference in

score). Considering the weighted scores, the systems have the same order, but with higher differences. The centralized approach results in a 13% difference in the weighted score and the functionally distributed approach in a 31% difference in the weighted score.

Table 7. Trade-off analysis of system characteristics required for the control system.

Characteristic	Weight	System 1	System 2	System 3
Avoids complexity in hardware design	**3**	3	1	2
Possibility to optimize capacity of controllers and cable routing	**4**	2	1	3
Hardware expandability afterwards	**4**	1	2	3
Exploitable computing capacity	**2**	3	1	2
Routing and modification of signals and execution path of control loops	**4**	2	1	2
Easiness of software management	**4**	3	1	2
Consistency and simplicity of safety features and supervisory functionalities	**5**	2	2	3
Support for availability, fault recovery and isolation	**3**	1	3	2
Total unweighted score		**17**	**12**	**19**
Total weighted score		**48**	**40**	**63**
Normalized unweighted score		**71 %**	**50 %**	**79 %**
Normalized weighted score		**69 %**	**51 %**	**82 %**

Based on the results of the trade-off analysis, the control system with modular abstraction layers is selected to be the most suitable. It should be noted that especially the definition of the weight factors is application-specific and should be re-evaluated for each application. Therefore, the weights of the characteristics cannot be generalized without known use cases. Here, the assumed use cases were different operation modes (manual, remote, autonomous), the research of alternative control methods, and the possibility to make measurements.

Furthermore, the trade-off analysis was based on components that are designed to be used in rugged conditions, such as in wet, dirty or dusty working environments. If the components from factory automation with higher computation and fieldbus capacity could be used, then the scoring and the trade-off analysis must be re-evaluated.

6 DESIGN OF MODULAR POWER MANAGEMENT INTEGRATED INTO SYSTEM ARCHITECTURE

Modular power management is designed to provide the required power for the actuators and to prevent overloading of the engine in dynamic work cycles. The objective of the modular power management architecture is to divide the power sources and consumers into independent modules that are connected with predefined interfaces. Here, power management consists of three independent modules:

- Engine module
- Drive module
- Implement module

The interfaces between modules, inputs and outputs are described in Figure 35. The inputs of the system are velocity command of the machine and velocity command for the tilt and lift (entering from the left). The outputs are the reference of the actuators (existing from the power management module). Further, the feedback signals coming from the machine are required for the control of the power management modules.

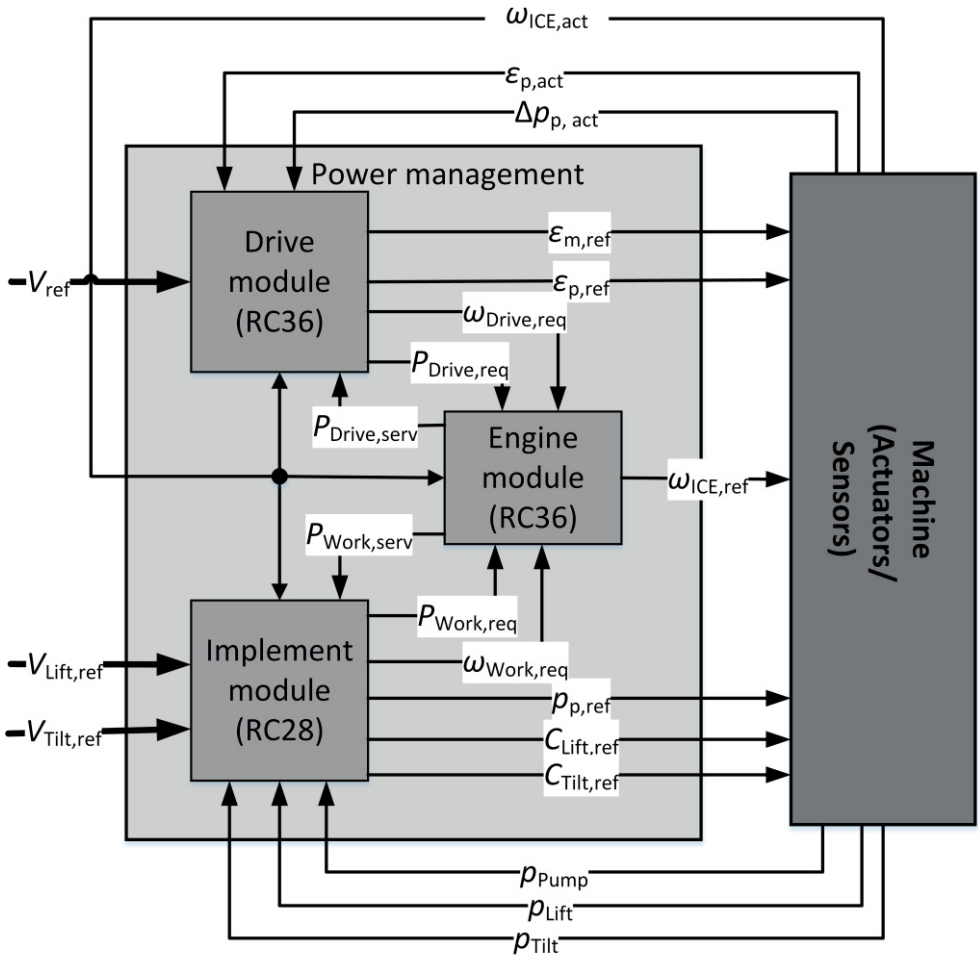

Figure 35. Power management is distributed into three independent modules.

Power consumers (drive and implement modules) request both power and rotational speed from the engine module. Based on the control of the engine module in the current operation conditions, the engine module serves the available power to the consumers. Each module is responsible for operating with the given power constraints. Further, the power consumers request the minimum rotational speed from the engine module. The minimum rotational speed is defined in the consumer modules so that the modules can fulfil the operator commands (for example, required drive velocity or required cylinder velocity). Here, the limiting factor is the

maximum hydrostatic gear ratio between the engine and the actuator that defines the minimum rotational speed.

The interfaces of the modular power management architecture were originally introduced in a municipal wheel loader realized with hydrostatic hub motors and digital hydraulic valves by the author [134]. Later on, with the machine used in this study, power management was introduced with digital hydraulic valves in the implements, showing significant savings in the fuel consumption while driving [135].

6.1 Power producer: Engine module

The engine module handles the control of the internal combustion engine (ICE), attempting to fulfil the requirements set by the power consuming modules. The requests from the consumers correspond to the power and the minimum required rotational speed of the engine. The overall power request of the engine is defined as the summation of the power consumers:

$$P_{\mathrm{ICE,req}} = P_{\mathrm{Drive,req}} + P_{\mathrm{Implement,req}} + P_{\mathrm{Extra,req}} \tag{6.1}$$

where $P_{\mathrm{Drive,req}}$ and $P_{\mathrm{Implement,req}}$ are the power request of the drive and implement module. $P_{\mathrm{Extra,req}}$ contains the power requested for the steering system and external systems, and the power reserved for the acceleration of the engine:

$$P_{\mathrm{Extra,req}} = (J_{\mathrm{ICE+aux}}\dot{\omega}_{\mathrm{ICE}} + T_{\mathrm{External}})\omega_{\mathrm{ICE}} \tag{6.2}$$

where $J_{\mathrm{ICE+aux}}\dot{\omega}_{\mathrm{ICE}}$ is the torque reserved for the acceleration of the engine inertia and its subsystems, the torque required for steering and external systems is lumped into T_{External}, J_{ICE} is the moment of inertia of the engine, $\dot{\omega}_{\mathrm{ICE}}$ is the angular acceleration of the engine, and ω_{ICE} is the rotational speed of the engine. The angular acceleration of the engine is defined from the gap between the actual and reference rotational speeds of the engine, which reserves a predefined time slot for acceleration of the engine. For the steering and brake system, a fixed amount of torque is reserved, as that system has the highest prioritization and the torque of the fixed displacement pump cannot be controlled.

The hydraulic systems of the machine realize the continuously variable gear ratios between the engine and actuator. Therefore, to fulfil the desired velocity of the actuator, the maximum gear ratio defines the minimum for the rotational speed of the engine. From the requested rotational speeds, the greatest value defines the minimum for the rotational speed of the engine:

$$\omega_{\mathrm{ICE,req}} = \max(\omega_{\mathrm{idle}}, \omega_{\mathrm{Drive,req}}, \omega_{\mathrm{Implement,req}}) \tag{6.3}$$

where ω_{idle} is the idle speed of the engine, $\omega_{\mathrm{Drive,req}}$ and $\omega_{\mathrm{Implement,req}}$ are the requested rotational angular velocities of the drive module and implement module. To define the final rotational speed reference for the engine, the power request and rotational speed request from Equations (6.1, 6.2 and 6.3) are applied:

$$\omega_{\mathrm{ICE,ref}} = \max(\omega_{\mathrm{ICE,req}}, \omega_{\mathrm{PowerCurve}}(P_{\mathrm{ICE,req}})) \tag{6.4}$$

where $\omega_{\mathrm{PowerCurve}}(P_{\mathrm{ICE,req}}))$ defines the lowest rotational speed from the maximum power curve of the engine, where the engine power is higher than the requested power. If the requested power is higher than the maximum power, then the power curve function returns the maximum rotational speed.

To ensure enough power for steering and braking and to prevent an engine stall, the served power to the drive and implement module is restricted. Further, due to the highest priority of steering and braking and to ensure some power for accelerating the engine, that power is always reserved. The residual power is divided into the power consumers in the ratio of the requests:

$$P_{\mathrm{Drive,serv}} = \frac{P_{\mathrm{ICE}}(\omega_{\mathrm{ICE}}) - P_{\mathrm{Extra,req}}}{P_{\mathrm{Drive,req}} + P_{\mathrm{Implement,req}}} P_{\mathrm{Drive,req}} \tag{6.5a}$$

$$P_{\mathrm{Implement,serv}} = \frac{P_{\mathrm{ICE}}(\omega_{\mathrm{ICE}}) - P_{\mathrm{Extra,req}}}{P_{\mathrm{Implement,req}} + P_{\mathrm{Drive,req}}} P_{\mathrm{Implement,req}} \tag{6.5b}$$

where $P_{\mathrm{ICE}}(\omega_{\mathrm{ICE}})$ returns the available power of the engine at current rotational speed, and $P_{\mathrm{Drive,req}}$ and $P_{\mathrm{Implement,req}}$ are defined in the drive and implement modules.

6.2 Power consumer: Drive module

The drive module realizes the interfaces of the power consumer from the modular power management architecture. Further, the module realizes the control of the drive system, where the input signal is the velocity command from the operator. The velocity command defines the target velocity for the machine, which is reached by controlling the displacement ratios of the pump and motor and requesting rotational speed from the engine module.

The control principle of the drive systems follows the predefined control sequence from the minimised rpm approach, as shown in Figure 36. The control sequence is separated into three velocity regions: a low velocity region, where the displacement ratio of the pump is increased; a high velocity region, where the displacement ratio of the engine is decreased; and the highest velocity region, where the rotational speed of the engine is increased to reach the maximum velocity. In the definition of the control sequence, the efficiencies are assumed to be 1 (ideal efficiency).

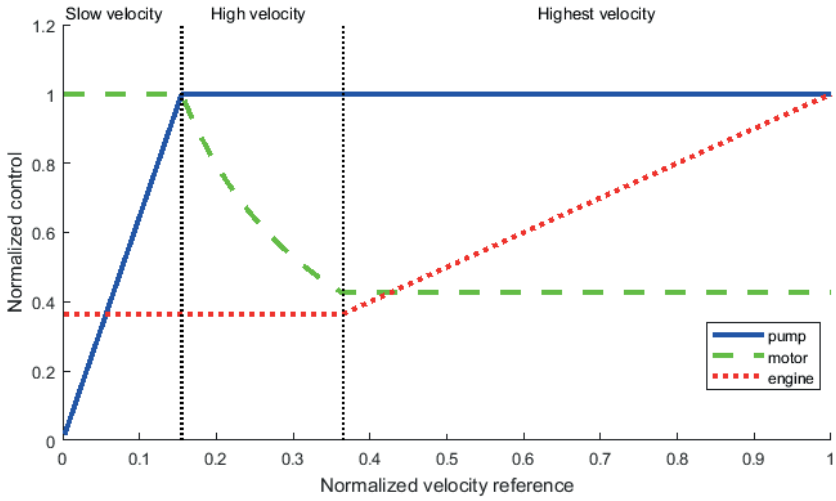

Figure 36. The drive module realizes the control sequence of the minimum rpm approach for the driving, where the control values are the normalized diesel engine speed reference and the hydraulic pump and motor displacement references.

Based on the control reference creation strategy defined in Figure 36, and given velocity reference (v_{ref}), the initial references ($\varepsilon_{\mathrm{p},0}, \varepsilon_{\mathrm{m},0}, \omega_{\mathrm{e},0}$) for the pump, motor and engine were defined. Based on the power limitations and interaction of other

modules, the initial references did not necessarily represent the final references. Therefore, the final references were compensated for based on the actual measurements:

$$\varepsilon_{\mathrm{m,ref}} = \frac{1}{c_0}\frac{\varepsilon_{\mathrm{p},0}\omega_{\mathrm{ICE},0}}{v_{\mathrm{ref}}} \tag{6.6a}$$

$$\varepsilon_{\mathrm{p,ref}} = c_0\frac{\varepsilon_{\mathrm{m,ref}}v_{\mathrm{ref}}}{\omega_{\mathrm{ICE,act}}} \tag{6.6b}$$

$$\omega_{\mathrm{ICE,ref}} = c_0\frac{\varepsilon_{\mathrm{m},0}v_{\mathrm{ref}}}{\varepsilon_{\mathrm{p},0}} \tag{6.6c}$$

where $c_0 = V_{\mathrm{m}}/\left(V_{\mathrm{p}}r_{\mathrm{eff}}\alpha_{\mathrm{gear}}\eta_{\mathrm{vol,p}}\eta_{\mathrm{vol,m}}\right)$, V_{p} and V_{m} are the maximum displacements of the pump and motor, r_{eff} is the effective tire radius, α_{gear} is the final gear ratio, and $\eta_{\mathrm{vol,p}}$and $\eta_{\mathrm{vol,m}}$ are the volumetric efficiencies of the pump and motor. Here, the effective tire radius is assumed to be constant, and the volumetric efficiencies are assumed to be ideal. Further, the final gear ratio between the tire and hydraulic motor can be shifted only when the machine is stopped, thus c_0 is constant while driving.

The displacement ratio of the motor and pump are controlled in the drive module, whereas the engine module controls the rotational speed of the engine within the request of other modules and power constraints. Therefore, the actual rotational speed of the engine can be higher from $\omega_{\mathrm{e},0}$, and the actual speed is used in Equation (6.6b) contrary to Equation (6.6a). Further, due to the traction control of the hydraulic motor, the final reference for the motor can be different to $\varepsilon_{\mathrm{m},0}$, and the reference of the motor used in Equation (6.6b) is contrary to Equation (6.6c). This means that the error in the velocity caused by the different rotational speed of the engine or the different displacement ratio of the motor was compensated for by controlling the displacement ratio of the pump.

Due to the limited power of the engine, the served power for driving is limited to prevent stalling of the engine and to ensure the proper function of the other modules. To prevent the drive module from exceeding the served power, the maximum limit is set for the displacement ratio of the pump:

$$\varepsilon_{\mathrm{p,max}} = \frac{P_{\mathrm{Drive,serv}}}{\omega_{\mathrm{ICE,act}}\Delta p}\frac{2\pi\eta_{\mathrm{hm,p}}}{V_{\mathrm{p}}} \tag{6.7}$$

where $P_{\mathrm{Drive,serv}}$ is the served power for driving, $\omega_{\mathrm{ICE,act}}$ is the rotational speed of the engine, Δp is the differential pressure of the pump, $\eta_{\mathrm{hm,p}}$ is the hydro-mechanical efficiency of the pump, and V_p is the maximum displacement of the pump. The served power for driving is based on the requested power from the engine module. This is defined from the current operation conditions by calculating the power that is currently required ($P_{\mathrm{Drive,act}}$)

$$P_{\mathrm{Drive,req}} = P_{\mathrm{Drive,act}} = \omega_{\mathrm{ICE}}\varepsilon_{\mathrm{p}}\Delta p\,\frac{V_{\mathrm{p}}}{2\pi\eta_{\mathrm{hm,p}}} \tag{6.8}$$

where ω_{ICE} is the actual rotational speed, and ε_{p} is the actual displacement ratio of the pump. In the acceleration phase, prediction of the required power would provide higher server power and faster reaction of the machine, as the amount of required power would be greater.

6.3 Power consumer: Implement module

The implement module realizes the interface of the consumer module by requesting the minimum rotational speed and the power from the engine module, similar to the drive module. The actual rotational speed of the engine and served power set constraints for the behavior and control of the implements. In the experimental wheel loader, the implements are realized with lift and tilt cylinders connected to the hydraulic circuit with proportional valves and displacement variable pumps, as described in Chapter 3.

The power request for the engine module is calculated from the supply pressure of the pump and the flow rate of the pump:

$$P_{\mathrm{Implement,req}} = \frac{Q_{\mathrm{p,ref}}p_{\mathrm{p}}}{\eta_{\mathrm{p,tot}}} \tag{6.9}$$

where $Q_{\mathrm{p,ref}}$ is the flow rate reference of the pump, which is a summation of the desired flow rates of the actuators; p_{p} is the supply pressure of the pump, and $\eta_{\mathrm{p,tot}}$ is the total efficiency of the pump, assumed to be constant. The desired flow rates of the actuators are derived from the joystick commands that represent the velocity command for the actuator.

The flow rate request of the actuators and the maximum delivery of the implement pump are used to define the minimum rotational speed request for the engine module:

$$\omega_{\mathrm{Implement,req}} = Q_{\mathrm{p,ref}} \frac{2\pi}{V_{\mathrm{p}} \eta_{\mathrm{p,vol}}} \tag{6.10}$$

where V_{p} is the displacement of the pump and $\eta_{\mathrm{p,vol}}$ is the volumetric efficiency of the pump (assumed to be constant). The control of the implement pump is similar to that in the standard ELS-system, where the highest actuator pressure defines the supply pressure for the pump. Therefore, the power of the implement module is restricted by setting the maximum limit for the flow rate of the pump:

$$Q_{\mathrm{p,max}} = \frac{P_{\mathrm{Implement,serv}} \eta_{\mathrm{p,tot}}}{p_{\mathrm{p}}} \tag{6.11}$$

where $P_{\mathrm{Implement,serv}}$ is the power served by the engine module. Restriction of the flow rate of the pump to the maximum limit is realized by restricting the opening of the proportional valves in the ratio of the flow rate requests:

$$Q_{\mathrm{Lift,req}} = \frac{Q_{\mathrm{Tilt,ref}}}{Q_{\mathrm{Lift,ref}} + Q_{\mathrm{Tilt,ref}}} Q_{\mathrm{p,max}} \tag{6.12a}$$

$$Q_{\mathrm{Lift,req}} = \frac{Q_{\mathrm{Tilt,ref}}}{Q_{\mathrm{Lift,ref}} + Q_{\mathrm{Tilt,ref}}} Q_{\mathrm{p,max}} \tag{6.12b}$$

where $Q_{\mathrm{Tilt,ref}}$ and $Q_{\mathrm{Lift,ref}}$ are the reference flow rates for the tilt and lift derived from the joystick commands. Control of the implement pump is similar to that in the ELS-system, so without the power restriction control of the implement module is similar to that in the ELS.

7 REALIZATION OF MACHINE FUNCTIONALITIES

The typical operation of non-road working machines contains highly transient operation conditions and control references. To handle a dynamic system with several natural frequencies, the controllers should be designed for robustness and immunity to disturbances. Therefore, the power management modules should handle the dynamics of the components, transient operation conditions and unpredicted operator commands. Here, the assumption is that commands from the operator and work cycle are not known in advance, so the control should be able to operate with present information. The functions are realized so that the machine has similar operation performance to the original series-production machine.

Further, control software is implemented in commercial PLC hardware with limited performance. Therefore, the highest control frequency is 100 Hz for the main PLC and 333 Hz for the implement PLC. The control frequency is high enough for most machine-related control and control logic. Closed-loop control with high transient and especially pressure control would still benefit from higher control frequency.

7.1 Engine control and power serving

The dynamic of the engine is not dependent only on the inertia: the engine controller and the turbocharger also have effects on the dynamics as well as the combustion and fuel systems. Therefore, power-based control should ensure that the engine has enough time to react to alternating power demand. Here, the engine is controlled with a rotational speed reference given to the engine's ECU that handles the closed-loop control of the rotational speed. The power based control is realised by defining the served power curve of the engine as function of the engine rotational speed and using that for defining the rotational speed reference for the engine.

The served power curve is shown in Figure 37 and is lower than the maximum power of the engine at low rotational speeds. The difference between the maximum power and the served power is the power reserve. The reserve is for variations in the

requested power, and for the acceleration of the engine (and connected subsystems) when the operation point of the engine is changed because of the increased power demand. At the highest rotational speeds shown in Figure 37, the served power curve is higher than the maximum power of the engine. The higher served power ensures that the consumers can exploit all power that the engine produces. Otherwise, due the control accuracy, the consumer modules might limit their power usage more than is needed. In the operation, the rotational speed of the engine decreases if the used power is higher than the maximum power at high rotational speeds. That results in a decrease in the served power until the system establishes an equilibrium in the engine load.

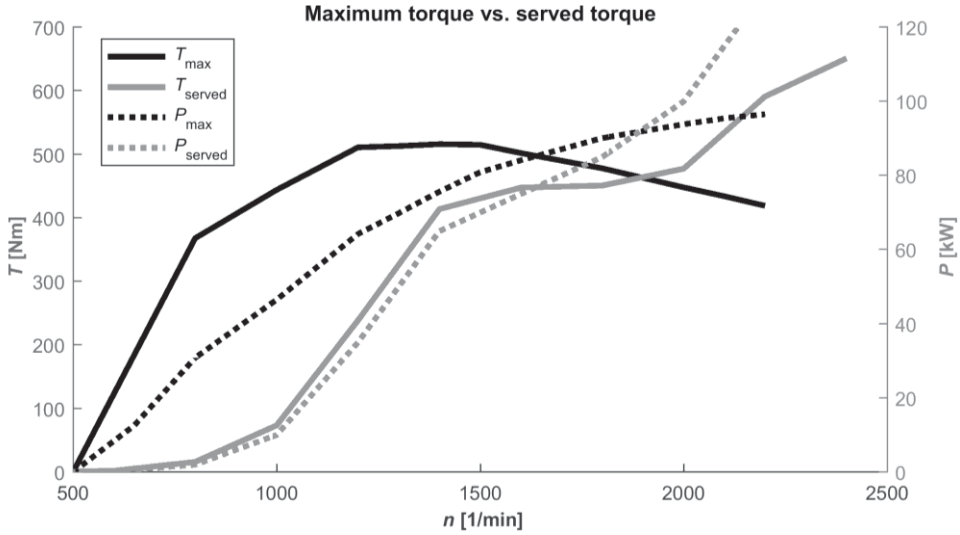

Figure 37. Without external energy storage, the torque/power reserve of the engine is needed for variations of the current torque/power conditions and for the acceleration of the engine when the power request increases.

To prevent a high increase rate in the power demand that can exceed the engine dynamics, the served power for consumers is limited to request. Then the served power of the consumers is not more than is actually used. The engine module can limit the increase rate of the power usage. Further, the increased rate of the served power is limited in the ratio of the available power of the consumer. That increased rate is tuned to the dynamics of the engine to ensure enough time for the engine controller to react to increasing power demand.

Figure 38 shows the realization of the control of the engine module. Lookup tables are used with the served power curve (see Figure 37) to convert requested power to requested rpm, as well as to define the available power of the engine. Final reference to the engine control unit is the rotational speed reference. That is the maximum value defined from the requested rpm of the consumer modules and rpm reference that is defined from the power requests of the consumer modules.

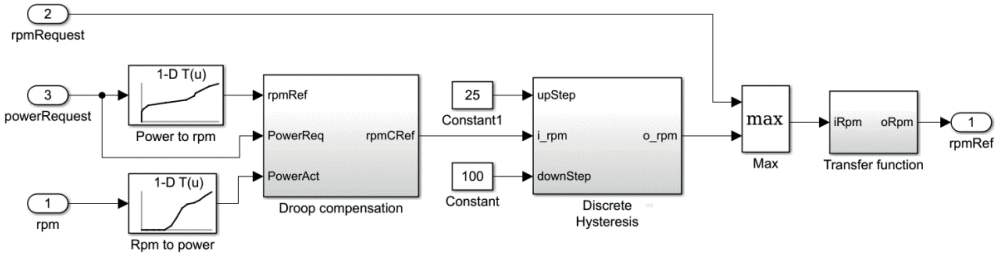

Figure 38. Control of the rotational speed of the engine is based on the requested power and the requested rotational speed.

The desired rotational speed of the engine is defined from the power requests (input 3) and the minimum rotational speed of the consumer modules (input 2). The actual rotational speed of the engine differs from that desired due to the droop of the engine. In modern diesel engines, the droop percentage can be given via CAN-interface and is therefore known. The rotational speed error caused by the droop percentage is compensated by requesting a higher rotational speed from the engine

$$\omega_{\mathrm{ICE,refC}} = \omega_{\mathrm{PowerCurve}}(P_{\mathrm{ICE,req}})(1 + \frac{P_{\mathrm{ICE,req}}}{P_{\mathrm{ICE}}(\omega_{\mathrm{ICE}})} d/100) \qquad (7.1)$$

where $P_{\mathrm{ICE,req}}$ is the requested power, $P_{\mathrm{ICE}}(\omega_{\mathrm{ICE}})$ is the actual power available from the engine with the current rotational speed, d is the droop percentage, and $\omega_{\mathrm{PowerCurve}}(P_{\mathrm{ICE,req}})$ is the non-compensated rotational speed reference for the engine that is calculated from the requested power.

To ensure a fast reaction of the engine when the requested power is increasing, and to prevent engine oscillation due to interaction with other modules, discrete hysteresis for the power request was introduced, as shown in Figure 38. Hysteresis

realizes the functionality where the rotational speed of the engine is increased with small steps, but decreased only when the step is high enough:

$$\omega_k = \omega_{k-1} + \tau(\omega_k - \omega_{k-1}), \qquad k \in \mathbb{N} \tag{7.2}$$

where $\tau = 1$ if $(\omega_k - \omega_{k-1})$ is higher than the predefined increment step, or if $(\omega_k - \omega_{k-1})$ is smaller than the predefined deduction step; otherwise, $\tau = 0$, ω_k is the current rotational speed and ω_{k-1} is the previous rotational speed. The engine control with hysteresis ensures that the requested rotational speed of the engine does not oscillate due to power requests but reserves enough power for the consumers.

Due to the variation of the rotational speed request and discrete hysteresis, the output of the maximum operator in Figure 38 is not smooth and stable in all operation conditions. Therefore, a first-order transfer function is used to smooth and filter the final reference signal to the engine. When the engine speed is rising, the time constant is 0.2, and when lowering, the time constant is 1.5.

7.2 Traction force control

When the tires are not slipping, the maximum traction force of the wheel is produced when the torque of the hydraulic motor is maximized. This is gained with the full displacement ratio and the highest allowed pressure, as Equation (3.8b) shows. When the pressure rises to the maximum level of the system, the traction force can be increased only by increasing the displacement ratio of the motor. Therefore, when operating close to the maximum pressure, the reference of the displacement ratio of the motor is increased, deviating from the predefined control sequence defined in Chapter 6.2. Typically, this happens during fast acceleration or when driving on a steep slope. To increase the displacement ratio of the motor from the predefined control sequence, the defined gain is applied as follows:

$$\varepsilon_{\mathrm{m,ref}} = C_{\mathrm{press}}(\varepsilon_{\mathrm{m,0}} - \varepsilon_{\mathrm{m,min}}) + \varepsilon_{\mathrm{m,min}} \tag{7.3}$$

where $\varepsilon_{\mathrm{m,0}}$ is the initial reference for the motor derived from the predefined control sequence, $\varepsilon_{\mathrm{m,min}}$ is the mechanical limited minimum displacement ratio of the motor, and C_{press} is the gain that increases the displacement ratio when the pressure reaches the cut-off pressure as defined by:

$$C_{\text{press}} = \max(0, \min\left(1, \frac{p_{\max} - p_{\text{act}}}{p_{\max} - p_{\text{cut-off}}}\right)) \tag{7.4}$$

where p_{act}, $p_{\max}$ and $p_{\text{cut-off}}$ are, respectively, the actual pressure, the maximum pressure of the system and the cut-off pressure. The cut-off pressure is defined so that the displacement ratio begins to increase when the actual pressure is higher. To prevent oscillation, both references $\varepsilon_{\text{m,init}}$ and C_{press} are filtered with a first-order transfer function:

$$y_{\text{filt}} = \frac{1}{\tau s + 1} y \tag{7.5}$$

where τ is time constant, y is the input for the transfer function and y_{filt} is the filtered value. For filtering reference $\varepsilon_{\text{m,init}}$, the time constant ($\tau = 0.5$ s) is fixed. For pressure-based compensation, the transfer function is designed so that the displacement ratio is increased faster than it is decreased. This is realized with the smaller time constant (τ) value when C_{press} is decreasing ($\tau = 20$ s), and the greater time constant ($\tau = 1$ s) when C_{press} is increasing. This ensures a rapid increase of the traction force when needed, but prevents oscillations when the machine accelerates with the maximum pressure of the drive system.

The error of the velocity caused by the difference in the initial reference ($\varepsilon_{\text{m,0}}$) and final reference ($\varepsilon_{\text{m,ref}}$) is compensated for in the pump with Equation (6.6b), as that equation uses the final reference of the motor instead of the initial reference defined from the predefined control sequence.

7.3 Hydrostatic braking with overspeed protection of the engine

The velocity reference arising from the accelerator pedal was modified to provide convenient drive behavior. In the experimental machine, the brake pedal was mechanical and was not measured. Therefore, the braking force was not separated from the drive resistance, and the activity of the mechanical brakes was unknown.

In general, it would be useful to know the position of the brake pedal. Then, hydrostatic braking could be used in parallel with mechanical brakes. This would

reduce fuel consumption, as the hydrostatic power would be returned to the engine. Further, the control of the drive system could be designed differently when the brakes are activated. When the position of the brake pedal is not known, the deceleration should be designed so that the following functionalities are realized:

- The wheels should not be locked or braking too rapid when releasing the accelerator pedal. This is dangerous, especially on slippery roads in winter.
- The drive system should not produce high power against mechanical brakes when the accelerator pedal is released (throttle-braking).
- The machine should not accelerate without pressing the accelerator pedal after mechanical braking.
- The hydrostatic braking should not race the engine above the overspeed limit.

To meet these requirements, the deceleration rate of the velocity reference was limited to the maximum value of two functions: the function of the differential pressure of the pump, and the function of the rotational speed of the engine. These functions are shown in Figure 39. The non-limited velocity reference of the machine is received from the accelerator pedal of the machine.

The function of the differential pressure is defined experimentally so that the hydrostatic braking force is similar to the original series-production machine. That ensures a carlike engine braking where the negative torque of the hydrostatic drive pump is transferred to the engine shaft. If the braking pedal is activated during hydrostatic braking, the differential pressure rises and the velocity reference will decrease faster due to the function.

The function of the rotational speed is experimentally defined when the engine is operating close to the overspeed limit. It prevents overspeed of the engine due the returned torque from drive to the engine shaft by limiting the deceleration rate of the machine. The function is used only when the differential pressure is negative to avoid limiting the deceleration rate in situations where the rotational speed of the engine is high due to the power demand.

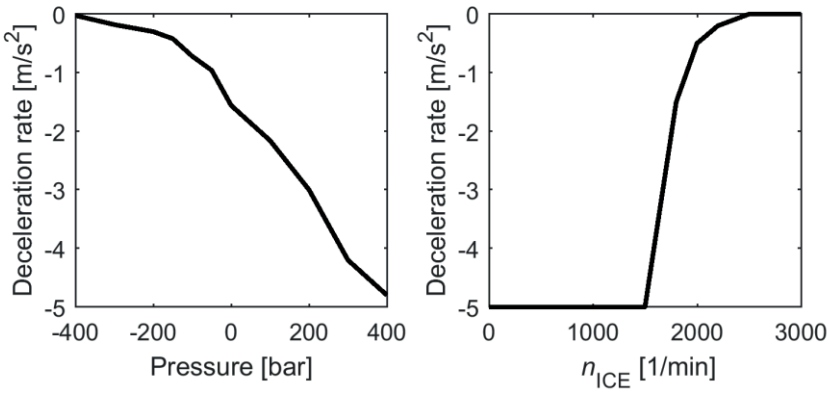

Figure 39. The deceleration rate is controlled in the function of the differential pressure and the rotational speed of the engine.

The maximum value of these two functions defines the allowed deceleration rate of the velocity reference during hydrostatic braking. As the increasing rate of the velocity reference is not limited when the accelerator pedal is depressed for a short period, the velocity reference reaches a high value, although the actual velocity of the machine is lower. To ensure that the velocity reference does not remain in the high value, it is always reset to the actual value when it falls below the actual velocity. Here, the actual velocity of the machine was calculated from the control signals with Equation (3.10).

7.4 Prediction of the requested drive power

To ensure the fast reaction of the machine in all operation conditions, the prediction of the requested drive power is proposed. With the prediction of the power request, the engine module has more time to react to the increasing power demand at the beginning of the acceleration. In this way, the served power for the drive increases faster than it would without predictions. Therefore, the requested drive power is the maximum of the actual power and the predicted power:

$$P_{\mathrm{Drive,req}} = \max(P_{\mathrm{Drive,act}}, P_{\mathrm{Drive,pred}}) \tag{7.6}$$

where $P_{\mathrm{Drive,act}}$ is the actual power derived from Equation (6.8) and $P_{\mathrm{Drive,pred}}$ is the predicted power. The prediction was implemented in the drive module and is based on the velocity reference from the drive:

$$P_{\mathrm{Drive,pred}} = P_{\mathrm{acc}} + P_{\mathrm{st}}(v_{\mathrm{act}}) = m\dot{v}_{\mathrm{pred}}v_{\mathrm{ref}} + P_{\mathrm{st}}(v_{\mathrm{act}}) \tag{7.7}$$

where P_{acc} is the power required for acceleration, $P_{\mathrm{st}}(v_{\mathrm{ref}})$ is the power required for steady-state velocity when the reference velocity is achieved, $\dot{v}_{\mathrm{pred}}$ is the predicted acceleration of the machine and v_{ref} is the velocity reference from the driver. The power required for steady-state velocity was calculated by using the steady-state model of the machine defined in Chapter 3.

The predicted acceleration was defined from the difference of the actual velocity and the predicted velocity and with the given time constant for acceleration:

$$\dot{v}_{\mathrm{pred}} = \frac{v_{\mathrm{ref}} - v_{\mathrm{act}}}{t_0} \tag{7.8}$$

where v_{ref} and v_{act} are the reference and actual velocity of the machine, and t_0 is the time constant given to the acceleration. The time constant here is 3.5 seconds and it represents the estimation of the time required to accelerate from the actual velocity to the reference velocity. The value of the time constant was experimentally tuned based on the machine dynamics and was set at the constant value in all operation conditions. Further, the actual velocity of the machine was calculated from the control signals with Equation (3.10).

To achieve an accurate prediction for the acceleration rate and required power, the dynamic model from the machine was needed. Nevertheless, the simplified equations are enough for a rough estimate for the predicted power. That improves the reaction of the machine compared with the system without prediction, as the prediction provides a rapid increase in the request power when the velocity reference rises from the actual velocity.

8 EXPERIMENTAL TESTS: COMPARISON OF FUEL ECONOMY AND PERFORMANCE WITH DESIGNED SYSTEM ARCHITECTURE

This chapter provides a detailed analysis and measurements of the fuel consumption from the real machine. The comparison of the fuel consumption was done between two control strategies realized in the experimental machine: the first was the modular power management architecture with the minimized rpm approach (MinRpm), and the second was the emulated series-production machine (ESM). The ESM has an emulated hydro-mechanical DA-control for the driving and ELS-system without power management for the implements.

The machine used in the study was rebuilt from scratch with electrified components. The maximum displacements of the hydraulic pumps and drive motor were slightly different in comparison with the original series-production machine. The sizes of the cylinders in the boom and bucket were smaller in the studied machine, because it was originally equipped with digital hydraulic valves and higher pressure levels. Further, the original series-production machine was not instrumented with all sensors that are available for the studied machine. Because of the discrepancies, emulation was used in the experimental test instead of the original series-production machine. Nevertheless, the series-production machine was compared with the studied machine in the earlier study [136].

As all components of the studied machine are electronic-controlled, the control strategy can be changed without any mechanical changes. This ensures that the properties and efficiencies of the components are the same with both tested strategies. DA-control was selected for the driving, as it is used in commercially available series-production machines. Therefore, it represents a current approach to commercial machines with hydrostatic transmission. Further, DA-control provides functions such as preventing engine stall and maximising the torque of the hydraulic motor when necessary. The emulation of DA-control was done with Simulink as presented in Chapter 4.2.2.

In the measurements, the same operator was driving the same cycle with both control methods. At first, the cycle was driven with the first control method and then the control method was changed and the cycle was repeated immediately. Therefore, the environmental conditions were similar in both control methods. Before each measurement, the machine was warmed up in normal operation conditions.

8.1 Realization of alternative control methods with designed system architecture

Both control methods (MinRpm and ESM) are realized in the same machine with the system architecture that is adaptable for alternative control flows. In the ESM control, the acceleration pedal signal directly controls the rotational speed of the engine. Figure 40 shows the control flows of the ESM control. When the drive gear is selected, the actual rotational speed of the engine defines the control signals for the hydraulic pump and motor displacements, as described in Chapter 4.2.2.

The ESM does not have power management for implements, so the control does not require any power or rpm. With ESM control, the valve openings are directly based on the joystick position, as shown in Figure 40. If higher velocity is required for the lift or tilt, the operator must press an accelerator pedal to increase the velocity of the actuators. The control of the implements is similar to the control of a standard ELS system.

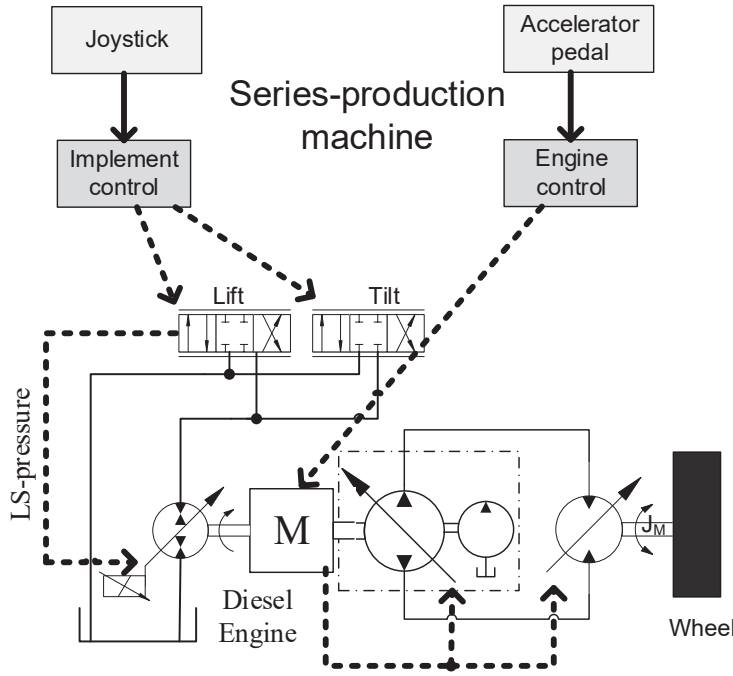

Figure 40. The control flows of the EMS show that there is no technical feedback signal from the drive or implement control to the engine control. Only the human operator observations are used as feedback.

The control flows of the modular power management with MinRpm approach designed in Chapter 6 are shown in Figure 41. The engine module defines the control signal for the engine ECU based on the signals from the consumer modules. The consumer modules try to fulfil the operator commands based on the limits that the engine module sets (the served power and rotational speed). The signals from the joystick and accelerator pedal are connected to the implement and drive modules and define the reference velocities for the actuators. MinRPM and EMS have the same ELS control for the implement pump, but MinRpm approach restricts the valve openings based on the power limitations from the engine module.

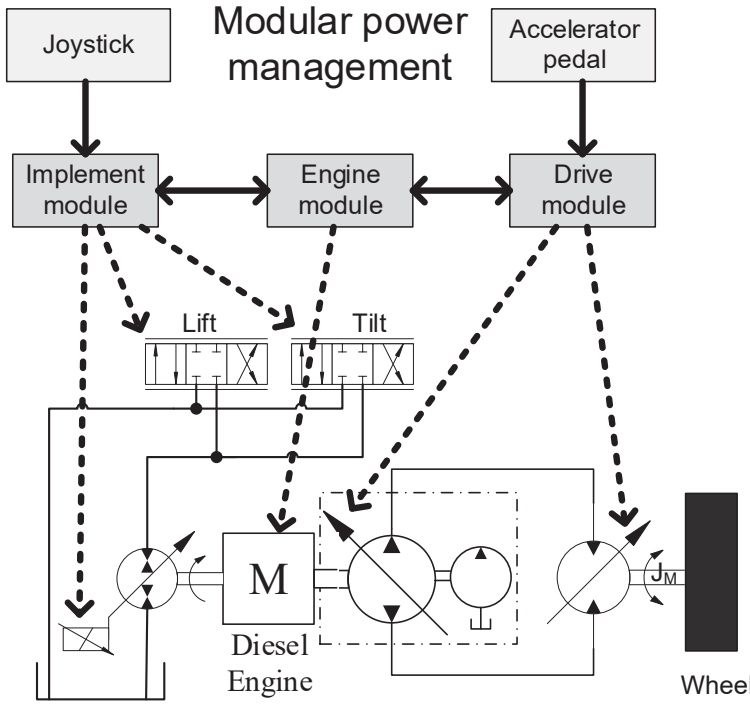

Figure 41. The controls flow with the modular power management and MinRpm approach shows that the engine is controlled based on the signals from the Implement and Drive module.

In the designed modular abstraction layer architecture, the control flows can be easily rerouted, as the inputs are defined in the isolated input handler. Therefore, both control methods can be realized in parallel in the same controller, and a parameter can be used to select the active control method. Further, the supervisory control of the system can be used to define the operation conditions when the parameter change is safe.

8.2 Data acquisition and sensors

All the machine data were collected from the CAN-busses with a data logger (Kvaser Memorator). The data logger recorded the signals from the CAN-busses to the memory card with a time stamp, which allowed for analysis of the data in Matlab. Some sensors were connected to the controllers of the machine with analog signals, so the controllers transmit that data to the CAN-bus, enabling the recording. The

sampling rate of the signals was related to the sensors and varied between 333 and 10 Hz.

The fuel consumption of the machine was measured with the instantaneous fuel consumption measurement device, AVL KMA Mobile. This device measures the flow rate of the fuel between a mechanical feed pump and a common rail pump of a diesel engine, as shown in Figure 42. The system can measure the fuel rates from 0.16 to 75 l/h with a response time below 125 ms [137]. The mass flow of the fuel can be calculated from the measured density and flow rate.

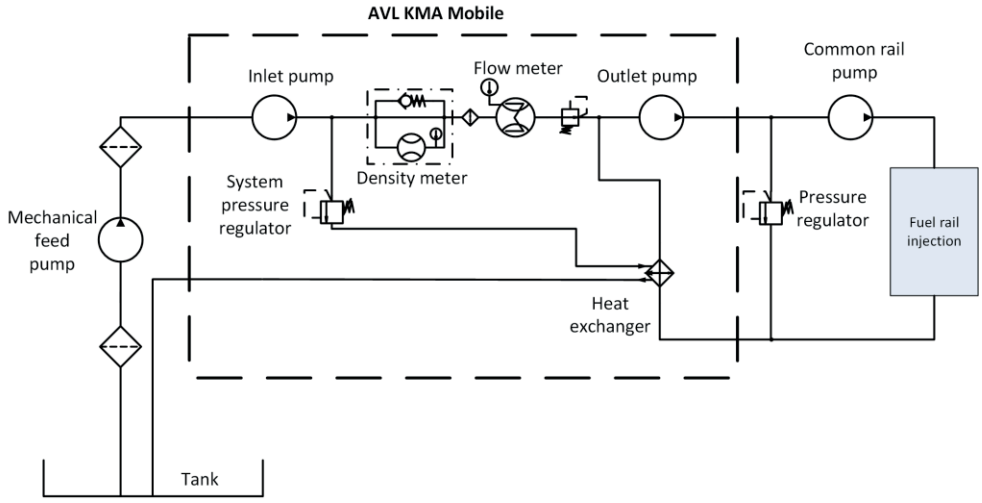

Figure 42. AVL KMA Mobile measuring principle and mounting to the fuel system of the experimental machine.

The external measurement provides a higher accuracy for fuel consumption than the data from the diesel ECU, which is based on the predefined fuel injection maps or the modeled fuel consumption from the torque and rotational speed. Further, the weighted fuel consumption from the work cycle was not enough to analyze the potential of fuel consumption in different operation points.

Figure 43 shows a short sample of the fuel rate measurements with AVL KMA and diesel ECU. The integrated fuel rate value of AVL KMA is higher than the value recorded from the ECU. Further, the response time of the ECU was better in rapid changes. This is a result of the dynamics of the flow meter and the capacity after the

flow meter. Nevertheless, the fuel measurement of AVL KMA is used in the experimental tests as it has higher accuracy in absolute value.

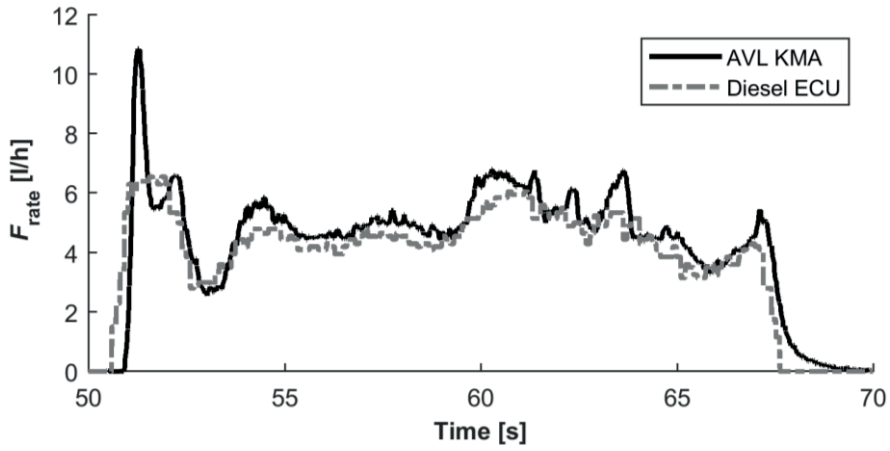

Figure 43. A short sample of measured fuel rates recorded from AVL KMA and Diesel ECU.

In the machine, all actuators were powered by the pumps: the auxiliary pump for the brakes and steering, the work pump for the implements, the drive pump for the hydrostatic drive, and the boost pump supporting the drive system. Therefore, the majority of the output power from the engine was shared between the pumps. Here, the energy used by the pumps was calculated from the flow rate and measured pressures, the resulting output power and the output energy of the engine. For the calculations, the efficiencies of the pumps were assumed to be ideal ($\eta \approx 1$), as accurate efficiency data is not available for the boost and auxiliary pumps. Further, the energy density of the diesel was assumed to be 42.7 MJ/kg when the energy efficiency of the engine is calculated from the fuel consumption.

In the scooping and transferring of gravel, the mass of the bucket was estimated from the position measurements of the tilt and lift and from the measured cylinder pressures. Due to the hydro-mechanical self-level stabilization feature, the stabilizer cylinders affected the lifting force of the boom. The mass estimation of the bucket was calibrated with different weights and was valid only when the boom was not moving.

The machine was equipped with a Global Navigation Satellite System (GNSS) receiver, including the correction signal. This provided accurate information about

the position and altitude of the machine during the work cycles. For the calculations of the travel distance, the wheel velocity was applied. The wheel velocity was measured from the rotational speed of the hydraulic motor. Therefore, the tire slippage and slide of the differential gear can affect the travel distance.

8.3 Comparative analysis of machine functions

In this chapter, the functions of the MinRpm approach are compared with the emulated series-production machine (ESM) without power management for the implements. A short drive cycle that contained a 20-degree uphill, 15-degree downhill, and level asphalt route was used to analyze the drive functions. For comparison, the route was driven using a similar speed profile with both control methods. The power management for implements was analyzed by lifting the bucket with gravel.

Figure 44 is separated into segments to emphasize different functionalities. At phase 1, the machine accelerated to the reference speed. The acceleration time was almost identical for both control methods. Due to the power demand, the MinRpm approach increased the rotational speed of the engine higher than in the steady state.

In phases 2, 4 and 6, the machine was driving at steady-state velocity with relatively level ground. In the steady state, the rotational speed of the engine was lower with the MinRpm approach, and it was compensated for with a higher hydrostatic gear ratio by decreasing the displacement ratio of the hydraulic motor more than the ESM. At phase 4, the machine was turning with a short turning radius that increased the pressure level of the drive.

At phase 3, the machine was driving uphill, so the hydrostatic pressures increased, as did the engine load. Both control methods increased the displacement ratio of the hydraulic motor to ensure enough drive torque. For the MinRpm approach, the displacement ratio of the pump compensated for both the increased rotational speed of the engine and the increased hydrostatic motor displacement, resulting in a displacement ratio of the pump that followed the reference velocity for the machine.

At phase 5, the machine was driving downhill, so the engine was racing from the reference due to engine braking. This can be seen in Figure 44, where the rotational

speed of the engine rises from the reference with both control methods. Further, the load percentage and fuel rate of the engine decreased to zero.

At phase 7, the machine braked with hydrostatic braking. The ESM with DA-control decreased the reference rotational speed of the engine, and the hydrostatic gear ratio followed smoothly. With the MinRpm approach, the rotational speed of the engine increased at the beginning due to engine braking. This is because the kinetic energy from the driving was returned to the transmission shaft of the engine. The deceleration rate was then controlled as a function of the pressures and maximum allowed rotational speed of the engine, as explained in Chapter 7.3.

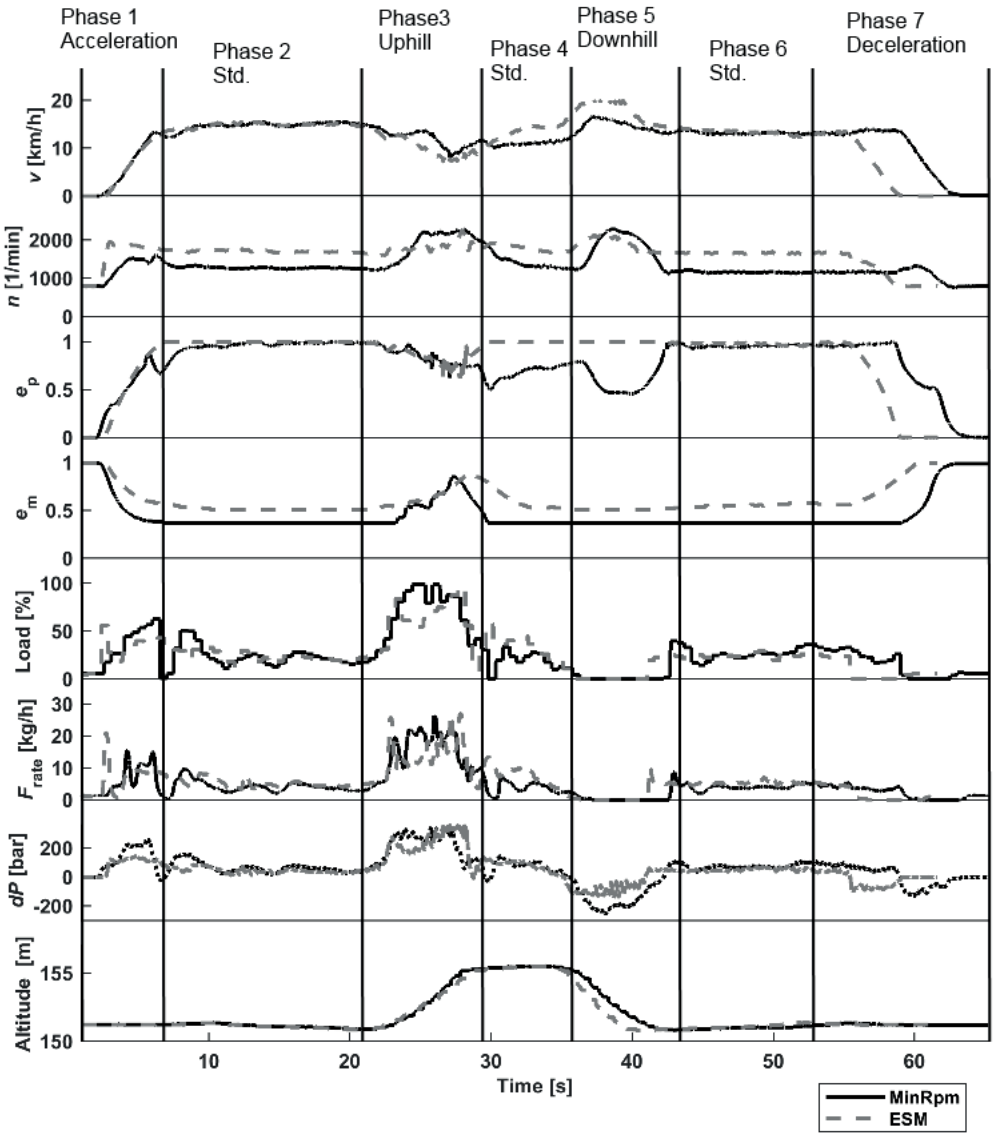

Figure 44. Short drive cycle with emulated DA-control and MinRpm control is divided into segments to demonstrate the differences of the drive functionalities.

The short drive cycle with varied terrain shows that the MinRpm approach is capable of providing similar drive functionalities to the ESM with DA-control. Further, the fuel rate in the MinRpm approach was lower than in the ESM in steady-state driving, but in the acceleration and deceleration the difference was not significant. At the beginning of the uphill, the fuel rate of the MinRpm approach was higher than in

ESM, as the kinetic energy of the engine was increased due to the increased rotational speed.

Originally, the series-production machine with DA-control did not have power management for the implements. Instead, the driver used an inch pedal with an accelerator pedal to provide enough power for the implements by increasing the rotational speed of the engine. As the studied machine was equipped only with accelerator pedal, the operator could not increase the rotational speed of the engine separately.

With ESM, the control of implements was realized with the same controller as in the MinRpm approach. Instead of power management, the maximum power was served to the implements all the time. Further, the requested power and requested rpm were not connected. Therefore, the implements behaved similarly to the original series-production machine. Figure 45 shows how the rotational speed of the engine drops with the ESM approach compared with the MinRpm that limits the power of the implements.

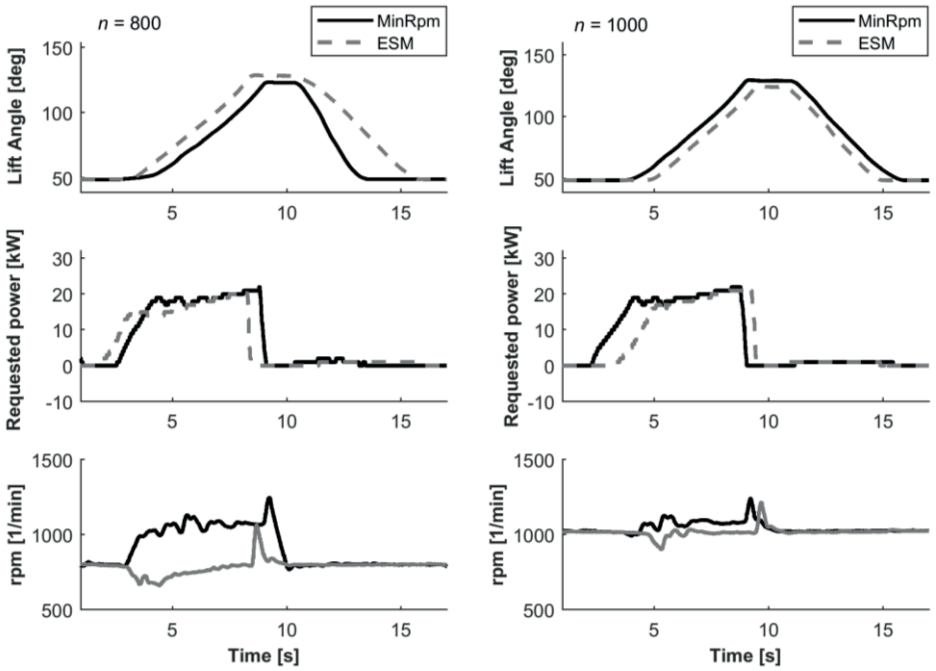

Figure 45. Comparison of the MinRpm and DA-control approaches when lifting the bucket with gravel. The rotational speed of the engine is 800 rpm (left) and 1000 rpm (right).

Further, the rotational speed of the engine increased with the MinRpm approach due to the requested power from the implement module. The ESM emulates hydro-mechanical DA-control for driving, and the work hydraulics behave like a standard ELS-system. The comparison of the drive and work functions shows that MinRpm is capable of the same performance as ESM.

8.4 Drive cycle on asphalt road

The driving behavior of the control methods (MinRpm and ESM) was compared on a route that contained an uphill, downhill and level road. The variation allowed comparison in different driving conditions. The length of the drive was about 1.9 km, and was driven in both directions (separated into two test cases) on an asphalt road. The maximum velocity of the machine was limited to the legal maximum: 40 km/h. The drive cycle represents a case when the machine is moved from one worksite to another.

The measurement started about two seconds before the machines started moving and stopped two seconds after the velocity reached zero. In the beginning, the machine accelerated to the target velocity as soon as possible. At the end, hydrostatic braking was used to slow down. Figure 46 shows the measurement from the first test case: Drive 1.

The velocity of the machine was almost the same with both control methods: the variation mainly resulted from hydrostatic efficiencies. Therefore, the machine slowed down a little when driving uphill (at 60–80 seconds), and the actual velocity rose downhill (at 100–130 seconds). Further, in the beginning, the road had a low-gradient uphill, while at the end the road was almost level to that shown with altitude in the lowest part of Figure 46.

At the beginning, when the machine accelerated to the low-gradient uphill, the engine load of both control methods was close to 100%, and the fuel rates were almost at the same level. When the engine load was lower, the MinRpm approach decreased the rotational speed of the engine compared with the DA-control of ESM, resulting in a lower fuel rate. At the end, the fuel rate of both control methods reached zero when slowing down with hydrostatic braking.

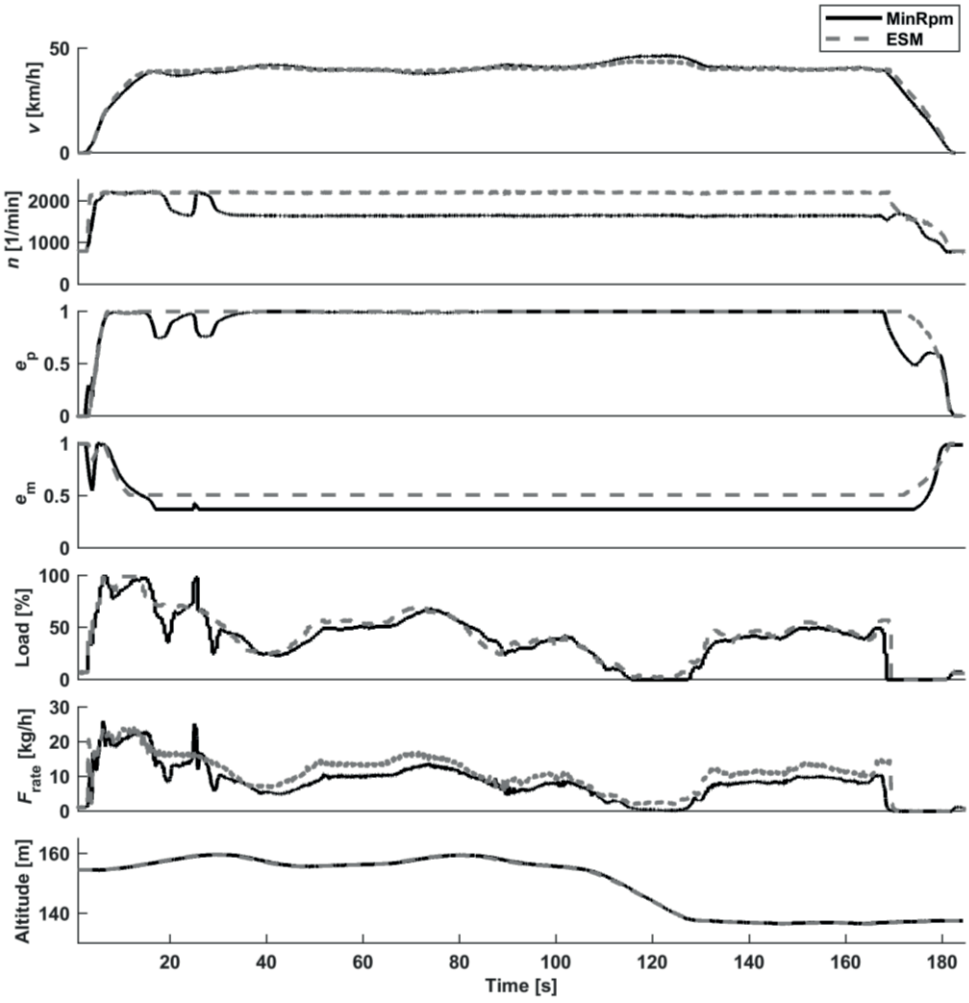

Figure 46. In the test (Drive 1), DA-control and MinRpm control are compared in terms of functions and fuel economy when driving on the public road.

The second drive test (Drive 2) was driven instantly after the first test (Drive 1) on the same route, but the other way around, so that the terrain and altitude were the opposite. The comparison of the control methods in Drive 2 test is shown in Figure 47.

At the beginning, the machine accelerated on the relative flat terrain so that the acceleration time was shorter than in the first test (Drive 1), where the machine

accelerated uphill. After the acceleration, the MinRpm approach lowered the rotational speed of the engine, as the power needed was lower.

In the steep uphill part (at 60–80 seconds), the needed power was close to the maximum, as the load percentage was over 90%. Therefore, the MinRpm approach increased the rotational speed of the engine to fulfil the power needed. Further, the displacement ratio of the hydraulic motor was increased to provide enough torque for the driving. The displacement ratio of the pump compensated for the velocity error when the rotational speed of the engine or the displacement ratio of the motor deviated from the predefined control sequence.

At the end, the deceleration started about 30 meters earlier with the MinRpm approach due to other traffic on the road. Further, the brakes were activated briefly, producing an external load for the driving. This can be seen in Figure 47, where the fuel rate and the load of the engine increased at the end of the drive cycle. However, the drive distances covered differed only by 1.6%, so the results are still comparable.

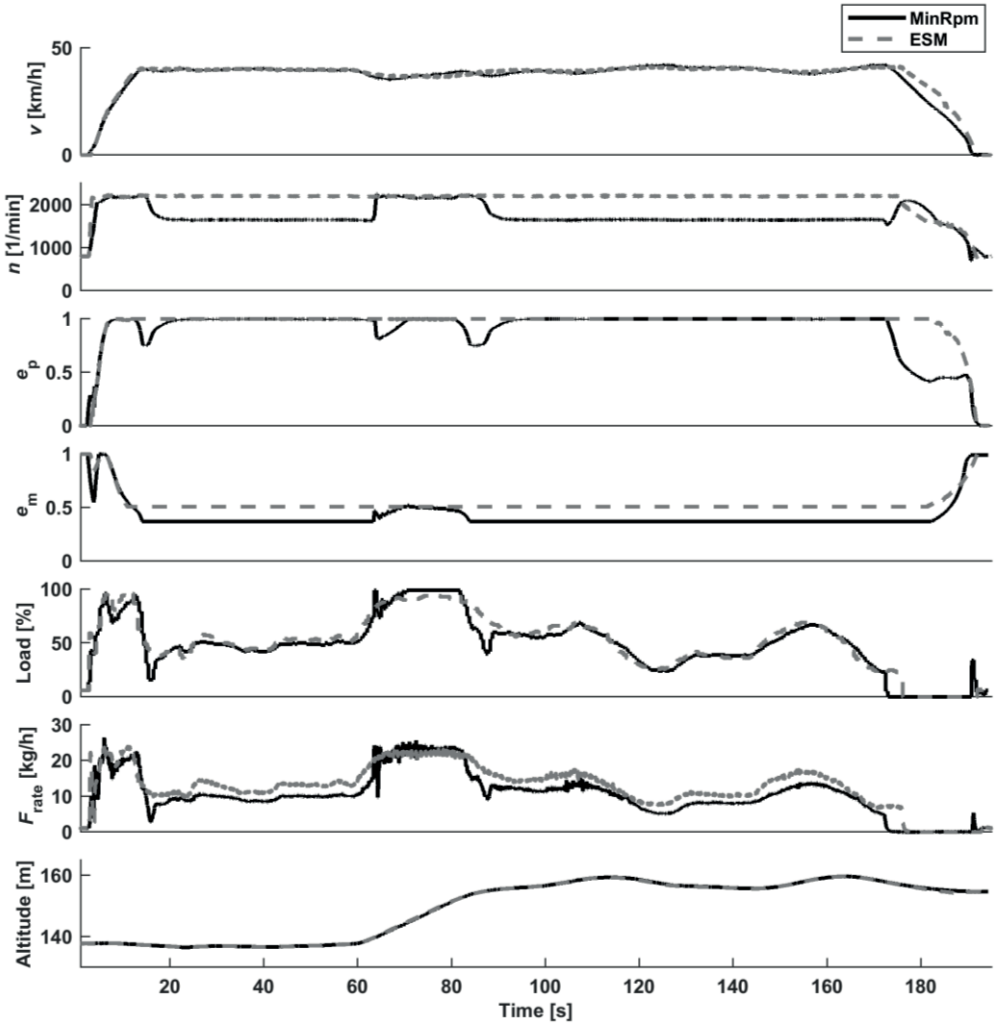

Figure 47. In the test (Drive 2), DA-control and MinRpm-control are compared in terms of functions and fuel economy when driving on the public road.

The comparison results of Drive 1 and Drive 2 are shown in Table 8. The total time and travel distance of the control methods differed only slightly. In the fuel economy, the difference was 22.0% and 15.5% depending on the drive cycle. The second drive cycle (Drive 2) contained a steep uphill, where the fuel rates were similar, resulting in a smaller difference in fuel economy.

Table 8. Comparison results of two drive cycles: Drive 1 and Drive 2.

Test case:	**Drive 1**			**Drive 2**		
Control method	**MinRpm**	**ESM**	**Diff [%]**	**MinRpm**	**ESM**	**Diff [%]**
Total time [s]	184.3	184.7	-0.2%	194.4	195.1	-0.4%
Travel distance [m]	1895	1893	0.1%	1933	1964	-1.6%
Avg. speed [km/h]	37.0	36.9	0.3%	35.8	36.2	-1.1%
Avg. engine rpm [1/min]	1650	2100	-21.4%	1720	2100	-18.1%
Output energy of the engine [MJ]	5.02	5.49	-8.6%	7.42	7.98	-7.0%
Energy efficiency of engine [%]	28.4	24.3	16.9%	30.6	27.4	-11.7%
Avg. fuel rate [kg/h]	8.1	10.3	-21.4%	10.5	12.6	-16.8%
Fuel consumption [g]	414	530	-21.9%	567	683	-17.0%
Fuel consumption (ECU) [ml]	479	618	-22.5%	652	786	-17.1%
Fuel economy [l/100km]	27.1	34.8	-22.1%	36.5	43.2	-15.5%

The output energy of the engine was 8.6% and 7.0% smaller with the MinRpm approach compared with the ESM. That was mainly because the average power consumption of the auxiliary and boost pump were lower when the rotational speed of the engine was lowered. Here, all output energy of the engine was shared with the pumps.

8.5 Pile to pile cycle with Y-pattern

The pile to pile work cycle represents a cycle with a high power transient, as the loading and unloading contain power transient of the implements and acceleration and deceleration of the machine. The work cycle was driven by the same operator, and the objective was to drive with similar route and lifting profile for the boom with both control methods.

The work cycle can be divided into the following phases: reaching the pile, filling the bucket, leaving the pile, reversing, towards the load receiver (other pile), bucket emptying, leaving the receiver, and reversing. The driving follows a Y-pattern and is repeated six times to ensure that small variations between cycles do not affect the

results. The drive paths are recorded from the GNSS and are shown for both control methods in Figure 48.

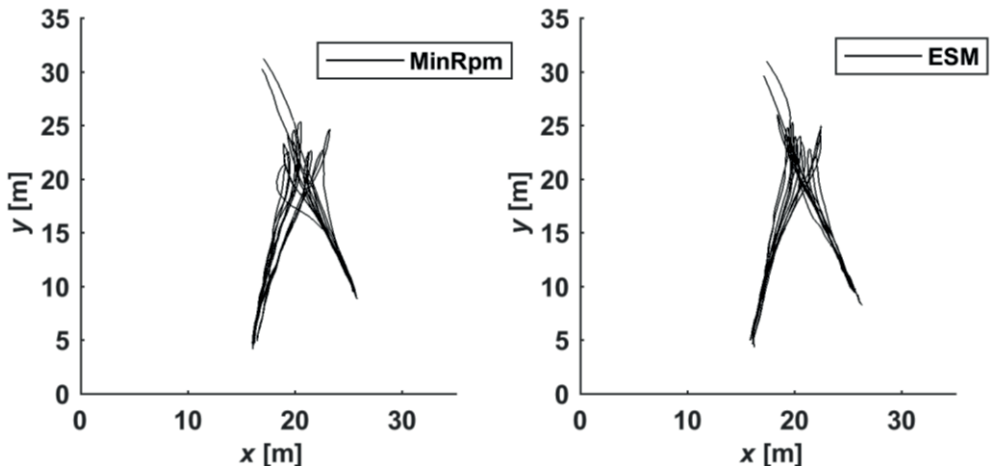

Figure 48. The drive path in the pile to pile work task is shown for both control methods in following the Y-pattern recorded from the GNSS.

The transferred load (gravel) was estimated by using the tilt and lift angles of the boom and the measured pressure of the cylinders. With the MinRpm approach, the estimated mass of the transferred load was 5600 kg, and with the ESM the mass was 5200 kg. The mass estimation of the load was calculated from the pressure when implements were not used. The accuracy of the steady-state mass estimation was about ±100 kg at each time, resulting in 10% accuracy for the estimation.

The studied wheel loader was equipped with the smaller lifting cylinders and smaller hydraulic motor for the driving in comparison with the series-production machine. Therefore, the lifting capacity of the studied wheel loader with the full bucket was close to the maximum limit and the maximum drive force was used in the loading phase. That hindered the filling process of the bucket and resulted in variations in the productivity.

The velocity of the machine and the lift and tilt angles of the boom are shown in Figure 49. Due to the small variations of the cycle, the curves were not identical phases. However, the total time and distance travelled were close between cycles. Further, the lifting angle (height of the bucket) is almost the same level in the unloading phases.

Most of the time, the rotational speed of the engine was lower in the MinRpm approach compared with the ESM. Nevertheless, the MinRpm approach yielded high peaks and transients for the rotational speed of the engine due to the variations in the required power. Further, the peaks in the fuel rate and load of the engine are a consequence of the transient rotational speed and power of the engine.

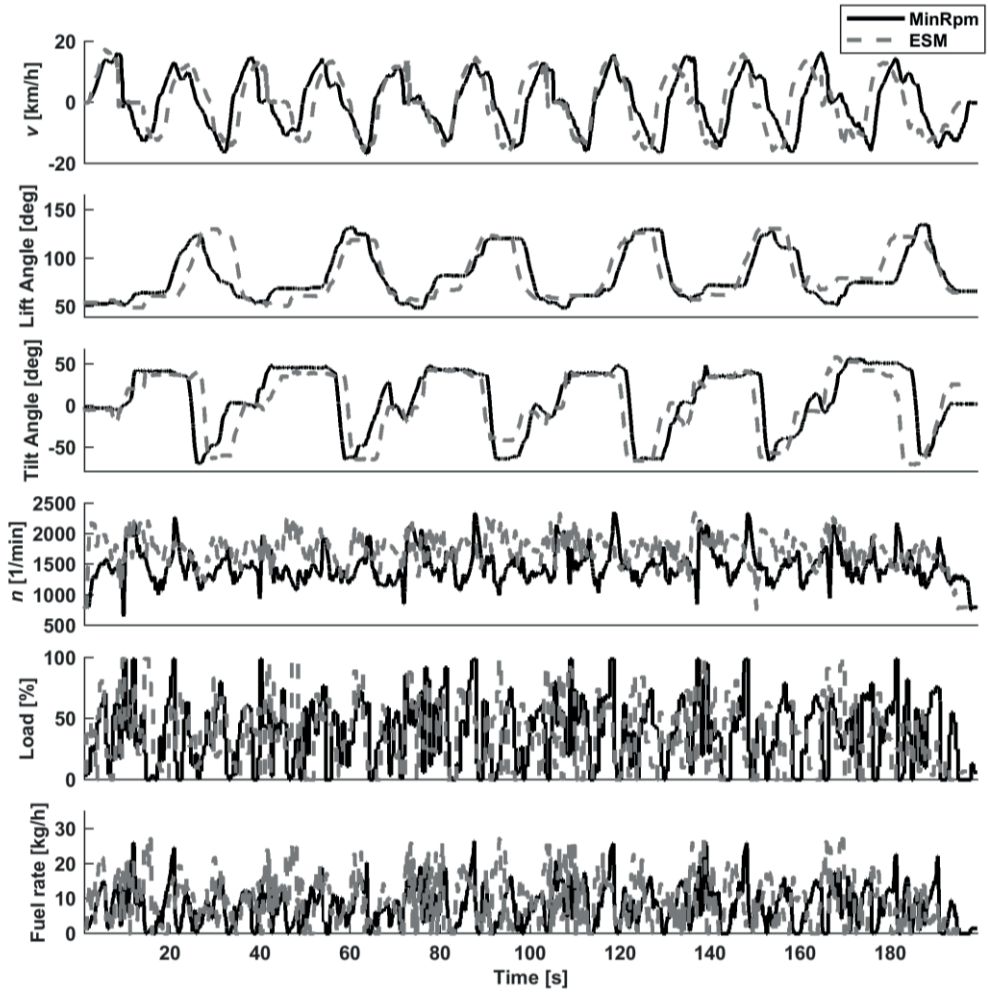

Figure 49. The velocity of the machine and the lift and tilt positions of the boom are compared as a function of time in the pile to pile work cycle.

The energy share between subsystems is shown in Figure 50. The pressure sensor of the auxiliary pump had a failure during the measurement. Therefore, the energy for the auxiliary system could not be defined accurately. Based on the earlier

measurements, the average value of the auxiliary pressure varies between 25 to 40 bar and is therefore assumed to be 32 bar all the time. With the MinRpm approach, a higher share of the energy goes to the drive and work (implements) compared with DA-control. The total energy is 4.2% smaller than with DA-control.

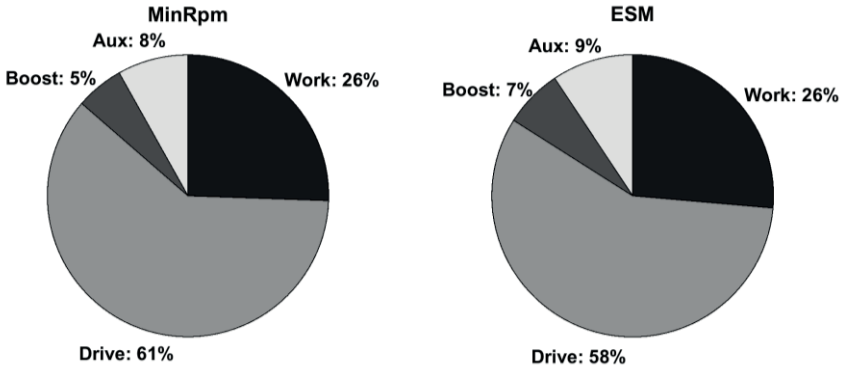

Figure 50. Energy share of the subsystems is calculated from the pump powers by assuming ideal efficiency. The total energy of the MinRpm approach is 4.81 MJ, and the total energy of DA-control is 4.91 MJ

Table 9 shows the comparison results of the pile to pile cycle. The fuel consumption is 14% smaller with the MinRpm approach. This is a result of the overall lower rotational speed of the engine. Due to the failure of the pressure sensor of the auxiliary pump, the output energy and energy efficiency of the engine are influenced by the estimation of the auxiliary energy.

Table 9. Comparison results of the pile to pile cycle shows 14% fuel savings with the MinRpm approach.

Test case:	**Pile to pile**		
Control method	**MinRpm**	**ESM**	**Diff [%]**
Total time [s]	199.3	197.0	1.2%
Travel distance [m]	428.6	445.3	-3.8%
Avg. engine rpm [1/min]	1470	1750	-16.0%
Output energy of engine [MJ]	4.81	4.92	-2.2%
Energy efficiency of engine [%]	28.6	25.1	13.9%
Avg. fuel rate [kg/h]	7.11	8.37	-15.1%
Fuel consumption [g]	394	458	-14.0%
Fuel consumption (ECU) [ml]	441	519	-15.0%

Total transferred gravel [kg]	5600	5200	7.7%
Productivity (tons/h)	101.2	95.0	6.5%

The fuel economy in the work cycle could be calculated in the ratio of consumed fuel and transferred gravel, which would result in 29% higher economy with the MinRpm approach. However, the difference of the transferred gravel relates here more to the performance of the driver between cycles than to the control method.

8.6 Short loading cycle with fork attachment

The short loading cycle with fork was selected, as it has good repeatability when moving a fixed mass; here, the loading pallet had a 1500-kg mass. In the cycle, the load was moved between two places: at ground level, and to a rack 1.9 meters in height. The starting and ending point of the cycle are in the middle without the loading pallet. The cycle can be separated into different phases:

1. The machine is driving to loading point 1 and the pallet is picked up
2. The machine is reversing to the starting point with the pallet
3. The machine is driving to loading point 2 with the pallet
4. The pallet is left on a rack (1.9-meter height)
5. The machine is reversing without the pallet to the starting point
6. The machine is driving to loading point 2 and the pallet is picked up
7. The machine is reversing to the starting point with the pallet
8. The machine is driving to loading point 1 with the pallet
9. The pallet is left on the ground
10. The machine is reversing without the pallet to the starting point

The cycle is repeated five times, and the drive path is shown in Figure 51.

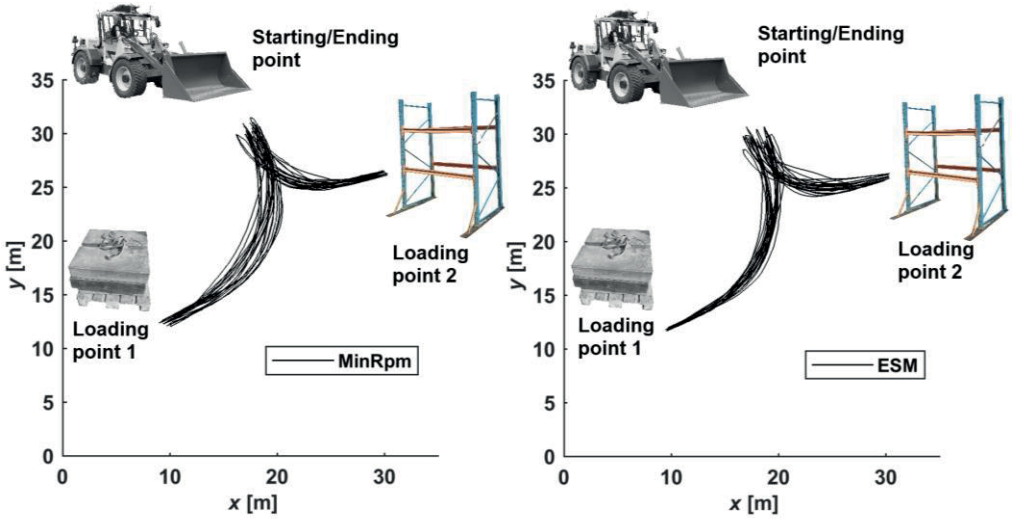

Figure 51. The drive path recorded from GNSS when the loading pallet with a 1500-kg mass is moved between the loading points.

The lift and tilt angles with the machine velocity are shown in Figure 52. The difference between cycles occurs because leaving the pallet on the rack requires accuracy. Therefore, the cycles are hard to repeat similarly. Nevertheless, the overall time of both control methods has only a 1.3% difference, and the travelled distance a 0.4% difference, so the results are comparable. Further, the velocity peaks and lift heights are have similar levels to both control methods.

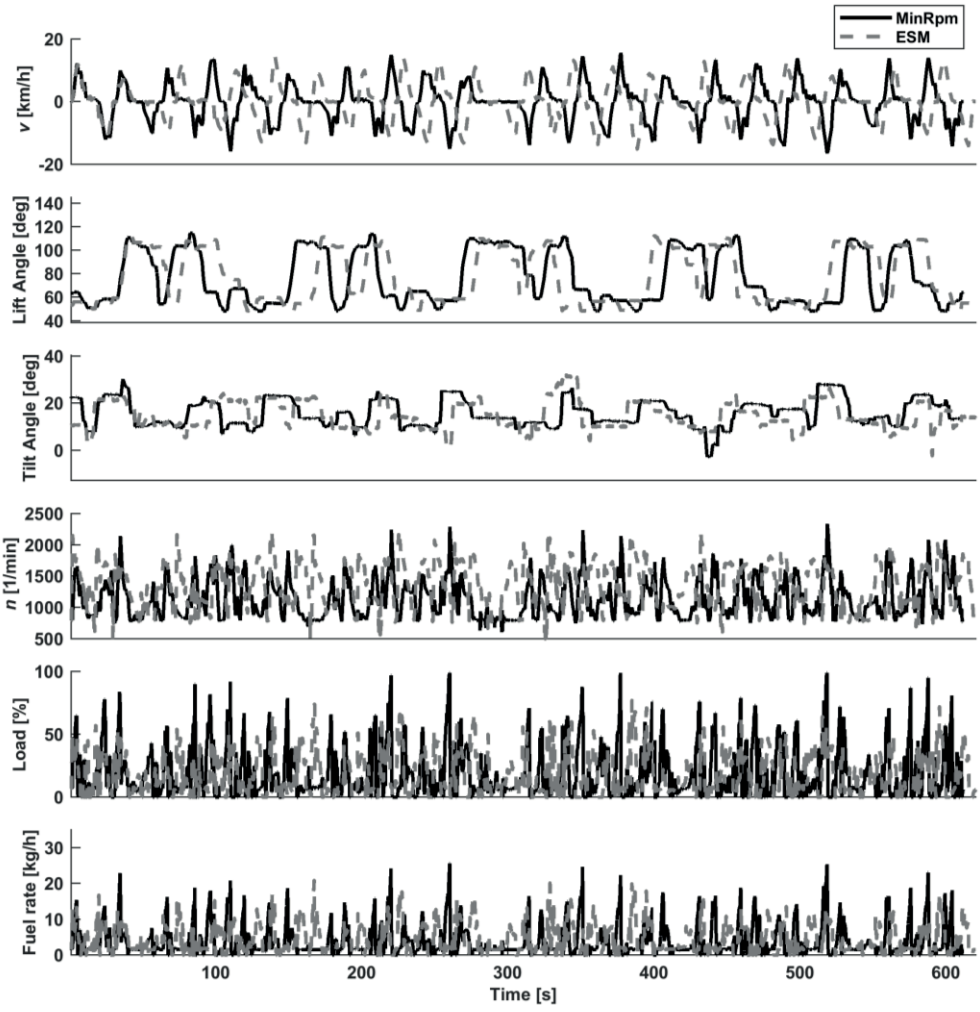

Figure 52. Lift and tilt positions of the boom and the machine velocity when moving the loading pallet.

The average rotational speed of the engine and the fuel rate are slower in the MinRpm approach compared with ESM. Nevertheless, the load and fuel rate have higher peaks in the MinRpm approach than in ESM. This is because the rotational speed of the engine is increased at the same time the load is increasing or when the prediction is assuming an increase in the loading conditions. The energy share of the subsystems is shown in Figure 53. The energy share of the subsystems with a fixed displacement pump (boost and auxiliary) is higher for the ESM.

The drive system has higher energy consumption with the MinRpm approach. The travelled distance or the operation time does not explain the difference in the energy consumption of the drive system. The difference is obtained also from the drive power of the MinRpm approach, which has more power peaks than ESM. Further, the acceleration distribution of MinRpm is spread more from zero. Therefore, the assumption is that the work cycle of the MinRpm approach contains a greater amount of velocity transients that raise the energy consumption.

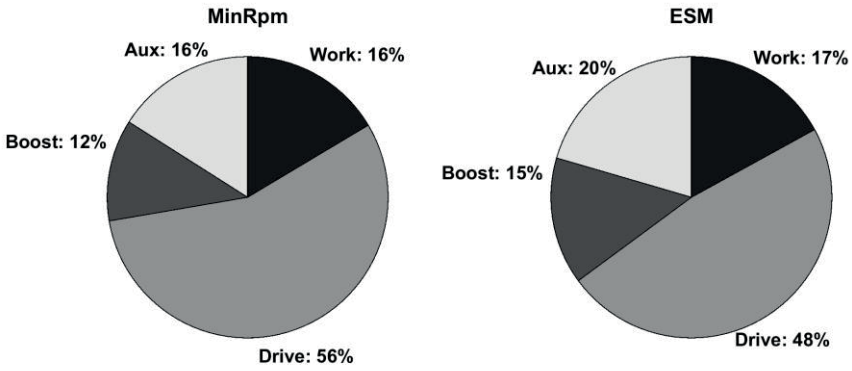

Figure 53. Energy share of the subsystems is calculated from the pump powers by assuming ideal efficiency. The total energy of the MinRpm approach is 5.34 MJ, and the total energy of the ESM is 5.39 MJ.

Table 10 shows the comparison results of a short loading cycle with forks. The average rpm of the engine is 1150 with the MinRpm, and 1360 with ESM. The fuel consumption is 11.5% higher with the ESM compared with the MinRpm approach.

Table 10. Comparison results of the pile to pile cycle show 11.5% fuel savings with the MinRpm approach.

Test case:	**Short loading cycle with forks**		
Control method	**MinRpm**	**ESM**	**Diff [%]**
Total time [s]	612.0	620.3	-1.3%
Travel distance [m]	740.4	737.6	0.4%
Avg. engine rpm [1/min]	1150	1360	-15.4%
Output energy of engine [MJ]	5.34	5.39	-0.9%
Energy efficiency of engine [%]	22.1	19.6	12.6%

Avg. fuel rate [kg/h]	3.33	3.71	-10.2%
Fuel consumption [g]	566	639	-11.4%
Fuel consumption (ECU) [ml]	657	734	-10.5%
Weight of loading pallet [kg]	1500	1500	0.0%

The output energy of the engine has only a 0.9% difference between these control methods. However, the engine is operating with a higher fuel efficiency area in the MinRpm approach.

8.7 Summary

The summary of the fuel consumption in the work cycles is shown in Figure 54. The experimental measurements show that fuel savings of 11 to 22% can be reached when the proposed power management architecture with the MinRpm control approach is compared with the emulated series-production machine.

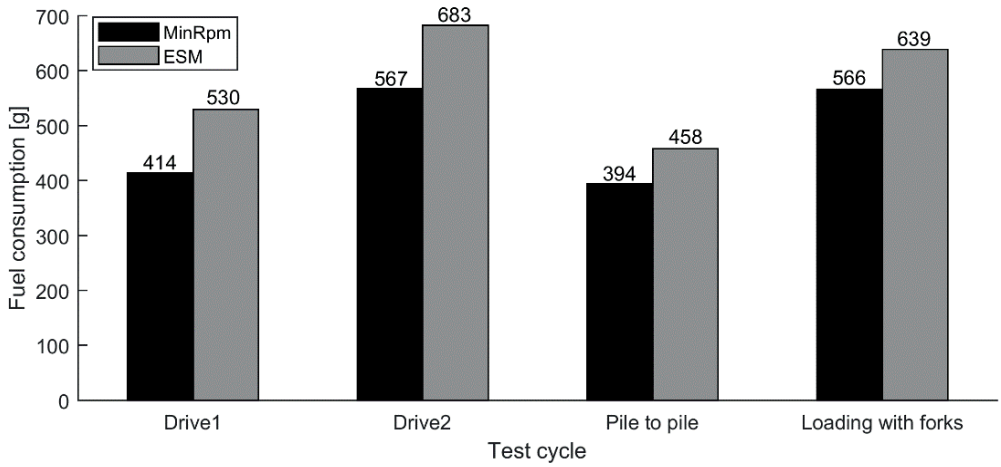

Figure 54. The fuel consumption of the MinRpm approach and the ESM are measured for different test cycles.

The measurements contain a slight variation in the time and travelled distance. Therefore, the fuel consumption differs a little from fuel economy, which is the relationship between travelled distance and fuel consumption in the drive cycles. As

the drive cycles (drive 1 and 2) were driven without an external mass and loading with the forks was done with fixed mass (1500 kg), the variation of the mass does not affect the fuel economy in the cycles.

The moved mass was estimated to be 5600 kg for MinRpm and 5200 kg for ESM in the pile to pile cycle. That results in a 29% difference in the fuel economy (tons/l), which is the relationship between the moved mass and consumption, and a 6.4% difference in productivity (tons/h). However, due the accuracy of the mass estimation and limited force capacity of the machine while loading, the difference in the variation of the moved mass in the pile to pile cycle was also dependent on factors other than the selected control method.

The drive cycles are comparable, as they are very similar in terms of time, distance, route travelled and velocity. The pile to pile and short loading cycle with fork contain more variations, although the target was to repeat the cycles in a similar way. The variations are rather related to repeatability than the control method, which makes it hard to estimate how much the selected control method affects the way of driving. Nevertheless, in terms of travel distance, acceleration rate or lift height, both control methods perform the cycles without significant difference. Therefore, all the cycles are comparable in terms of fuel consumption.

The main reason for the fuel saving of MinRpm is that the engine is operating with lower rotational speeds. Therefore, the engine has higher fuel efficiency compared with ESM. Further, the boost and auxiliary pumps have lower energy consumption when the engine rotational speed is decreased. Figure 55 shows the operation points of the engine in the pile to pile cycle.

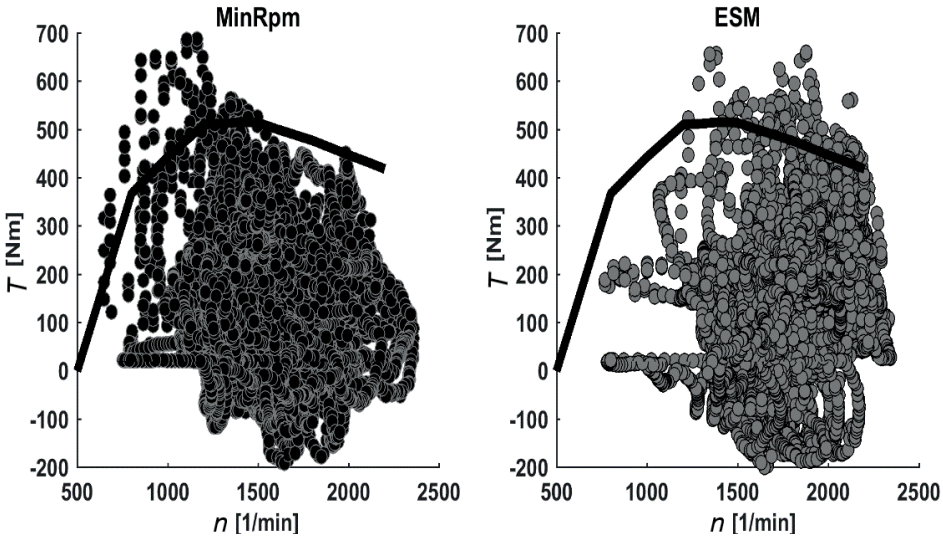

Figure 55. The operation points of the engine recorded from the pile to pile work cycle with MinRpm and EMS control methods.

In ESM control, the engine is mainly operating in an area where the maximum torque curve is decreasing. That ensures enough power and prevents engine stalling. With MinRpm, the rotational speed of the engine is lower, and it is operating in a wider area. MinRpm reserves the power margin of the engine for the increasing power demand, especially when operating with low rotational speed. That is seen from Figure 55, where the engine is not operating close to the maximum torque. Further, the maximum torque of the engine is exceeded temporarily with both control methods as the cycle contains high power peaks.

9 DISCUSSION

This thesis proposes a system architecture for machine-level control. Further, the thesis shows how improvements in fuel economy can be achieved by separating the control architecture into different modules. The implementation of the subsystems shows how the constraints of the system and the challenges involved with a distributed system can be handled at the modular level. The machine level architecture was compared with alternative approaches by using trade-off analysis and scoring functions. The system was tested on the experimental wheel loader with a relatively small set of work cycles, so the applicability of this system in other types of machines and under different test cycles requires further study.

The answers to the research questions of this thesis are addressed in this section.

RQ1: *How can the system architecture support the development of automation and fuel economy of a non-road working machine?*

In many autonomous applications, operator actions are still needed to perform tasks when autonomous functions cannot reach the required safety or performance levels. Therefore, machines operate in different operating modes such as manual, semi-autonomous or fully autonomous. Because of these requirements, the system architecture should be flexible to adapt alternative control methods and operating modes, not only in research and prototyping.

This study proposes a system architecture for machine level control that is capable of the required characteristics. The modular abstraction layer architecture abstracts machine level functions from the higher level systems. That allows redesign or adaptations of alternative control algorithms while the interfaces at the higher levels are static. The hardware abstraction and abstraction layers are successfully applied in several control systems. Here, the abstraction was realized in the low level functionalities with selected hardware and communication design.

The modular abstraction layer architecture was compared with alternative architectural approaches in the trade-off analysis based on the designer's point of view during the design and implementation. Scoring functions were defined and used for the evaluation of different architectural characteristics. Based on the scoring functions and use cases, alternative architectures were evaluated and the most suitable approach was selected.

The modular abstraction layer architecture has several benefits in the development and management of the control systems. The architecture provides static interfaces for the control of the higher levels. The required sensor and actuator information can be transferred to the higher levels for the co-coordinate control of the subsystems. The operation mode is changed in a controlled way by rerouting signals, while the supervisory module takes care of safety such as ensuring that the wireless emergency stop is active when the machine is operated in remote or autonomous mode.

The requirements for the control methods vary when the machine is operated in various control modes. In manual mode, an operator controls the deceleration with engine braking or can predict the increase of the power usage before the bucket fill by using the accelerator pedal. In autonomous operation, these can be predicted from the known work cycle, or the low-level control takes care of the power constraints. Depending on the design and control mode, the requirements for the low-level control and control methods are different.

Therefore, the control methods of the subsystem should be adaptable or must be changed when the control mode varies from manual to operator assistance systems or autonomous systems. In this thesis, the fuel economy comparison requires that the control methods are changed from MinRpm approach to the EMS. Chapter 8.1 shows how the control flows are different with different control methods. Nevertheless, for higher level systems and data acquisition the control interface was invariable.

For cost saving, general purpose mobile controllers are widely used for the control of non-road working machines. Therefore, the usage of I/Os and communication interfaces is not optimal for each application. Instead, several functions are realized in the same controller, or the functionalities can be distributed based on the hardware limits and not only as logical entities. Chapter 5 shows how the system architecture can be designed, although the hardware layer has divergence from the logical entities.

The designed system has different functional layers for remote and autonomous operation. The lowest level layer, the machine level, realizes the modular abstraction layer architecture that combines the robotic architectures with the requirements of non-road working machines. The architecture can be adapted to different control modes and alternative control methods. The machine level layer realizes the reactive behavior and close feedback loops with bandwidths from 333 Hz to 10 Hz. It has been shown that the low level system is capable of rerouting signals and control flows, adapting alternative control methods and modes, capable of mastering the required response times, consistency and complexity, and can be expandable with new functionalities.

RQ2: *How can the control methods be realized in the architecture and what are improvements that can be achieved in a wheel loader with a hydrostatic drive?*

It is well known that lowering the rotational speed of an internal combustion engine with given power typically improves the fuel economy as the engine operates within a higher fuel efficiency region [47, 103]. Furthermore, a system which applies almost constant torque for an engine uses more power when the rotational speed of the engine is higher. For example, the closed circuit pump of the hydrostatic drive has a boost pump that exerts almost constant torque, so the power consumption increases when the rotational speed of the engine is higher.

The simulation study in Chapter 4 showed the fuel saving potential for hydrostatic driving with different control methods. The displacement control of the pump and the engine speed-related DA control represented two commercially available control methods, while the minimized rotational speed control was the proposed control method. These three control methods were compared with the optimal operation points in steady-state driving conditions. The study shows that the minimized rotational speed approach was close to optimal. Furthermore, the most significant potential for fuel saving with the minimized rotational speed was with relatively slow velocities (5 to 25 km/h) compared to the pump displacement control and DA control methods used in commercial vehicles.

However, the simulation study did not take into account the power constraints of real-world driving, such as uphill motion or operation of the implements. Furthermore, unless the work cycle is known beforehand, the reserved power of the engine may be needed for unpredictable operation conditions. Therefore, power

management is needed, and the full potential for fuel saving is hard to reach in real-world driving.

Therefore, a comparative study between the proposed control method (MinRpm) with the power management and conventional control method (DA-control) with emulated series-production was performed in the experiments with a real machine. The power management was comparable with the approaches patented by Volvo using a wheel loader as a pilot machine [118] and Caterpillar using a hydraulic excavator as a pilot machine [117]. Further, Danfoss, Bosch Rexroth and Linde Hydraulics have presented concepts and systems with power management functions [92, 94, 96]. However, to the author's best knowledge, no reports of the operation of these systems in real machines and under realistic work cycles have been published.

The modular power management architecture with the proposed control method (MinRpm) can improve the fuel economy in comparison with the series-production machine. The MinRpm with the power management architecture was tested and measured in earlier studies by the author with another wheel loader, called IHA-machine. The hydraulic transmission of the IHA-machine was implemented with a variable displacement pump coupled with four hub motors. The drive tests showed about 15% fuel savings compared with the constant rpm approach, where only the pump displacement was varied [134].

The experimental machine used in this study with the designed power management algorithm was compared with a non-modified series-production machine in an earlier study. In that case, the experimental machine had digital hydraulics technology for the implements. The drive hydraulics of the series-production machine was realized with hydro-mechanical DA-control, and the hydraulics were realised with proportional valves and an LS-pump. The diesel engine was similar in both machines. The fuel economy measurements showed that the experimental machine used 15 – 35% less fuel than the series-production machine, depending on the work-cycle [136]. Further, in the earlier study, the power management approach was compared to the constant rpm approach, with the drive and work cycle providing a 25% reduction in the fuel consumption [135].

Based on earlier studies by the author and the fuel economy comparison shown here, fuel savings of between 10 and 22% can be achieved with a modular power-management architecture by minimizing the rotational speed of the engine. In this

thesis, the control system was defined so that the machine fulfilled the same performance requirements as the series-production machine, but with clearly reduced fuel consumption. If the operating requirements for the machine were slightly reduced, the fuel economy could be even higher.

For comparison, MinRpm and EMS control methods were realized in the modular abstraction layer architecture. Although the control flows of the methods differ, the system architecture with electrified components makes the change of the control method effortless. In addition, the comparison requires recording multitude signals from the control system. The realized CAN interfaces for communication with the system design make it possible to use sufficient measuring frequency for the recording measurements.

Although simulation techniques were used, real-time debugging and real-time data transmission are worthwhile for developing the control system. For that, development tools such as Simulink with code generation and designed higher level control systems originally developed for autonomous operation support easy access to the parameters, controllers and online measurements.

RQ3: *How are typical functionalities of the wheel loader realized in the designed architecture?*

There is a wide variety of functions and characteristics that are typical for the wheel loader. These have influence on the operational performance, the usage of components, and the fuel economy. In the designed system architecture with the power management and MinRpm approach, these functions are realized with various modules. Filtering the operator's input signals was realized at the input handler that uses different filters for the manual and remote operation modes. In the autonomous mode, filters are not required, as controllers are then at the higher layers in the system architecture.

Without external energy storage for hybrid vehicles, the power margin of the engine will be reserved for acceleration, increasing power requests and disturbances in the required power. The power margin is gained by operating the engine in the region where the maximum power of the engine is above what is required. This results in the engine operating at lower efficiency [47], which reduces the potential for fuel savings.

The power margin for the studied machine was experimentally defined as the function of the rotational speed of the engine, as described in Chapter 7.1. At low rotational speeds, the margin is high as the power reserve is needed for the acceleration of the engine (and connected subsystems). At the highest power, the served power is higher than that available, resulting in a negative power margin. The negative margin ensures that the consumers exploit all the power that the engine can produce. Otherwise, the consumer modules might not use all the power from the engine that is available due to the control accuracy. The defined power margin provides performance that is comparable with the serial-production machine. The power margin ensures fast reaction times of the engine in the low power range, and the consumers exploit all the power that engine provides in the high power range.

Further, the series-production machine realizes many functionalities that relate to operating performance, such as the anti-stall feature of the engine, engine braking, or ensuring maximum tractive force. The proposed control architecture shows how these properties can be realized in the independent modules of the system. The anti-stall function of the engine was realized in the engine module by requesting the engine to operate in the region where it has enough power, and reserving the power margin. Further, the served power for the consumer modules was limited to the current power capacity of the engine. If the consumer modules required more power from the engine than the maximum power available at that moment, the available power of the engine was served to the consumers in proportion to their requests.

When the control of the hydrostatic drive was decoupled from the engine, engine braking was realized in the drive module. The realization was shown in Chapter 7.3 by controlling the deceleration rate of the machine. Chapter 7.2 shows how the maximum traction force of the hydrostatic drive was ensured by increasing the displacement ratio of the hydraulic motor if the drive pressure reaches the maximum set point. The error in the velocity was then compensated by increasing the displacement ratio of the pump.

With these functionalities, the machine with the modular power management performed the work cycles similarly to the series-production machine, as shown in Chapter 8.3. This demonstrates that the modular power management architecture with MinRpm control approach is capable of providing the required performance.

Nevertheless, it should be noted that the modular power management with invariable interfaces between the power producer and consumers has some

restrictions for the control. As the reference of the rotational speed of the engine is not known in the consumer modules, the actual rotational speed was used. In some functions, such as the velocity compensation of the machine with alternating engine speed, the usage of engine reference could reduce response times and remove the feedback loop from actual engine speed. These limitations should be taken account when the system is applied to the control of non-road working machines.

10 CONCLUSIONS

Non-road road working machines are considered as complex systems combining hydraulics, electronics, control and software. This study shows the benefits of the modular abstraction layer architecture at the machine level control compared with alternative approaches. It has been shown that abstracted functionalities and layered architecture are capable of alternative control modes, from manual to autonomous, and can operate with different control methods and control flows.

At the machine level control, the modular abstraction layer architecture supports the development and usage of alternative control methods with a variety of control flows. In this study, alternative control methods are realized for the comparison of operational performance and fuel economy. Further, the control methods and control flows at the machine level differ from manual to autonomous operation. That requires rerouting of the control signals, the usage of alternative filtering and a variety of safety features.

The power management architecture with MinRpm control was realized in the system architecture. MinRpm was based on the knowledge that the lowering rotational speed of the engine and operating with higher partial loads will improve fuel economy. The realization guarantees the operational performance and therefore requires a power management system. The power management has independent modules for power providers and consumers and is integrated with the system architecture. Further, the emulated series-production machine was realized with the same system architecture for the fuel comparison study.

The simulation of hydrostatic drive in steady-state conditions shows that minimizing the rotational speed of the engine has a significant effect on the efficiencies and fuel consumption. The real-world measurement with the experimental machine shows that the fuel consumption can be improved by 11 to 22% compared with the series-production machine. Further, the experimental tests were analyzed to reveal the operating conditions where fuel savings were possible.

This research shows that without external energy storage such as batteries or hydraulic accumulators in the hybrid vehicles, the power margin of the engine will be reserved for engine acceleration, increasing power requests and disturbances of the required power. This reduces the potential for fuel savings. Further, the series-production machine realizes many functionalities that relate to operating performance, such as the engine anti-stall, engine braking or ensuring maximum tractive force. The system architecture with both control methods (MinRpm and EMS) shows how these properties can be realized in the system level modules. As both control methods are realized in the same machine and integrated into the designed systems architecture, the comparison is not related to discrepancy of the machine components.

The designed system architecture for the machine level control was compared with alternative architectures by using trade-off analysis. When the architectures were evaluated, the assumption was that mobile PLCs on the market were used. Nevertheless, the recent development of industrial PLCs and I/O modules on the market makes it possible to use these in non-road working machines. Taking these into consideration with high capacity fieldbus technologies, the results of scoring functions and trade-off analysis would be updated. High capacity PLCs with communication interfaces of high data transfer rates could make centralized system architecture reasonable.

Modular abstraction layer architecture with fully electrified control of components creates new facilities to develop machine functionalities. In driving, the reference can be based on the velocity, torque or power demand for the drive system, which could have a variant for different control modes and operating conditions. Further, combining autonomous functionalities with operator assistance and manual operation that is supported in the designed system architecture could improve the drive experience.

REFERENCES

[1] G. Archer, 2025 CO2 Regulation. The next step to tackling transport emissions, Briefing paper, Transport & Environment., 2015.

[2] M.A. Hannan, M.M. Hoque, A. Mohamed, A. Ayob, Review of energy storage systems for electric vehicle applications: Issues and challenges, Renewable and Sustainable Energy Reviews, Vol. 69, 2017, pp. 771-789.

[3] R. Vijayagopal, K. Gallagher, D. Lee, A. Rousseau, Comparing the powertrain energy densities of electric and gasoline vehicles), SAE Technical Papers, 2016.

[4] Z. Quan, L. Quan, J. Zhang, Review of energy efficient direct pump controlled cylinder electro-hydraulic technology, Renewable and Sustainable Energy Reviews, Vol. 35, 2014, pp. 336-346.

[5] M. Erkkilä, Model-based design of power-split drivelines, Tampere University of Technology, Publication 825, 2009, 102 p.

[6] M. Huova, M. Karvonen, V. Ahola, M. Linjama, M. Vilenius, Energy efficient control of multiactuator digital hydraulic mobile machine, 7th International Fluid Power Conference (7th IFK), 22-24 March, 2010, Aachen, Germany, pp. 1-12.

[7] P. Immonen, P. Ponomarev, R. Åman, V. Ahola, J. Uusi-Heikkilä, L. Laurila, H. Handroos, M. Niemelä, J. Pyrhönen, K. Huhtala, Energy saving in working hydraulics of long booms in heavy working vehicles, Automation in Construction, Vol. 65, 2016, pp. 125-132.

[8] N. Daher, M. Ivantysynova, Energy analysis of an original steering technology that saves fuel and boosts efficiency, Energy Conversion and Management, Vol. 86, 2014, pp. 1059-1068.

[9] J. Gong, Q. He, D. Zhang, Y. Zhang, X. Liu, Y. Zhao, C. Liu, Power system control strategy for hybrid excavator based on equivalent fuel consumption, 2012 IEEE International Conference on Mechatronics and Automation, ICMA 2012, pp. 1097-1102.

[10] S. Grammatico, A. Balluchi, E. Cosoli, A series-parallel hybrid electric powertrain for industrial vehicles, IEEE Vehicle Power and Propulsion Conference, Lille, France, pp. 1-6.

[11] T. Lin, Q. Wang, B. Hu, W. Gong, Development of hybrid powered hydraulic construction machinery, Automation in Construction, Vol. 19, Iss. 1, 2010, pp. 11-19.

[12] G. Stein, A. Froberg, J. Martinsson, B. Brattberg, R. Filla, J. Unnebäck, Fuel efficiency in construction equipment - optimize the machine as one system, 7th AVL International Commercial Powertrain Conference Proceedings, Helmut-List-Halle, Graz Austria, May 22nd–23rd, 2013, SAE International and AVL List GmbH, pp. 1-8.

[13] V. Nezhadali, B. Frank, L. Eriksson, Wheel loader operation - Optimal control compared to real drive experience, Control Engineering Practice, Vol. 48, 2016, pp. 1-9.
[14] B. Frank, L. Skogh, R. Filla, A. Froberg, M. Alaküla, On increasing fuel efficiency by operator assistance systems in a wheel loader, International Conference on Advanced Vehicle Technologies and Integration (VTI 2012), 2016, Changchun, China.
[15] M. Hafner, M. Schüler, O. Nelles, R. Isermann, Fast neural networks for diesel engine control design, Control Engineering Practice, Vol. 8, Iss. 11, 2000, pp. 1211-1221.
[16] T. Nilsson, A. Fröberg, J. Åslund, Predictive control of a diesel electric wheel loader powertrain, Control Engineering Practice, Vol. 41, 2015, pp. 47-56.
[17] V. Nezhadali, L. Eriksson, A. Fröberg, Modeling and optimal control of a wheel loader in the lift-transport section of the short loading cycle, IFAC Proceedings Volumes, Vol. 46, Iss. 21, 2013, pp. 195-200.
[18] M. Schneider, O. Koch, J. Weber, Green Wheel Loader – improving fuel economy through energy efficient drive and control concept, 10th International Fluid Power Conference, 2016, Dresden, Germany, pp. 63-78.
[19] H.C. Pedersen, T.O. Andersen, R.H. Hansen, Power management in open circuit hydraulic systems, Proceedings of the 4th FPNI – PhD Symposium, Vol. 1, 2006, Sarasota, Florida, USA, pp. 65-76.
[20] T. Kim, H. Kim, Performance of integrated engine - CVT control considering powertrain loss and CVT response lag, Proceedings of the Institution of Mechanical Engineers, Part D: Journal of Automobile Engineering, Vol. 216, Iss. 7, 2002, pp. 545-553.
[21] H. Durrant-Whyte, An autonomous guided vehicle for cargo handling applications, The International Journal of Robotics Research, Vol. 15, Iss. 5, 1996, pp. 407-440.
[22] J. Kalmari, T. Pihlajamäki, H. Hyyti, M. Luomaranta, A. Visala, ISO 11783 Compliant forest crane as a platform for automatic control, IFAC Proceedings Volumes, pp. 164-169.
[23] L. Yang, Development of control system of wheel type backhoe loader, Proceedings of International Conference on Soft Computing Techniques and Engineering Application, December 2013, Springer India, New Delhi, India, pp. 87-95.
[24] Y. Li, W. Liu, L. Yang, Z. Ji, Y. Zhao, P. Wang, L. Zhang, Development of electro-hydraulic proportion control system of track-laying machinery for high speed railway construction, Mechatronics, Vol. 40, 2016, pp. 167-177.
[25] J.P. Hespanha, P. Naghshtabrizi, Y. Xu, A survey of recent results in networked control systems, Proceedings of the IEEE, Vol. 95, Iss. 1, 2007, pp. 138-162.
[26] C. Willimanson, M. Ivantysysnova, The effect of pump efficiency on displacement controlled actuator systems, The Tenth Scandinavian International Conference on Fluid Power, May 21-23, 2007, Tampere, Finland, pp. 301-326.
[27] Q. Xiao, Q. Wang, Y. Zhang, Control strategies of power system in hybrid hydraulic excavator, Automation in Construction, Vol. 17, Iss. 4, 2008, pp. 361-367.
[28] Einola Kalle, Prestudy on power management of cut-to-length forest harvester with a hydraulic hybrid system, Proceedings of the 13th Scandinavian International Conference on Fluid Power SICFP'13, June 3-5, 2013, Linköping, Sweden, pp. 71-83.

[29] M. Ryu, M. Kabir, Y. Choo, S. Chung, Y. Kim, J. Ha, K. Lee, Pre-processing of load data of agricultural tractors during major field operations, Korean Journal of Agricultural Science, Vol. 42, Iss. Issue 1, 2015, pp. 53-61.
[30] T. Nilsson, A. Fröberg, J. Åslund, Minimizing fuel use during power transients for naturally aspirated and turbo charged diesel engines, Report, 2014, 13 p.
[31] R. Filla, B. Frank, Towards finding the optimal bucket filling strategy through Simulation, Proceedings of 15th Scandinavian International Conference on Fluid Power (SICFP17), Linköping, Sweden, June 7-9, 2017, Linköping University Electronic Press, Linköpings universitet, Linköping, Sweden, pp. 402-417.
[32] S. Tikkanen, V. Ahola, E. Koskela, Effect of driver and work cycle on losses of a loader, Proceedings of the BATH/ASME 2018 Symposium on Fluid Power and Motion Control FPMC2018, Bath, UK, September 12-14, 2018, ASME, Bath, UK, pp. 1-8.
[33] R. Filla, Quantifying operability of working machines, Linköping University, Linköping Studies in Science and Technology. Dissertations, 0345-7524, 2011, 263 p.
[34] EPA Nonregulatory nonroad duty cycles, United States Environmental Protection Agency, web page. Available (accessed 2 July 2018): https://www.epa.gov/moves/epa-nonregulatory-nonroad-duty-cycles.
[35] K. Oh, H. Kim, K. Ko, P. Kim, K. Yi, Integrated wheel loader simulation model for improving performance and energy flow, Automation in Construction, Vol. 58, 2015, pp. 129-143.
[36] P. Immonen, Energy efficiency of a diesel-electric mobile working machine, Lappeenranta University of Technology. ISBN 978-952-265-415-1, 2013, 138 p.
[37] D. Friso, Brake thermal efficiency and BSFC of diesel engines: mathematical modeling and comparison between diesel oil and biodiesel fueling, Applied Mathematical Sciences, Vol. 8, 2014, pp. 6515-6528.
[38] A. Thiruvengadam, S. Pradhan, P. Thiruvengadam, M. Besch, D. Carder, O. Delgado, Heavy-duty vehicle diesel engine efficiency evaluation and energy audit, Final Report, The International Council on Clean Transportation, Washington, DC, 2014, 62 p.
[39] J.M. Cullen, J.M. Allwood, Theoretical efficiency limits for energy conversion devices, Energy, Vol. 35, Iss. 5, 2010, pp. 2059-2069.
[40] U. Asad, R. Kumar, M. Zheng, J. Tjong, Ethanol-fueled low temperature combustion: A pathway to clean and efficient diesel engine cycles, Applied Energy, Vol. 157, 2015, pp. 838-850.
[41] E. Cauda, D. Fino, G. Saracco, V. Specchia, Preparation and regeneration of a catalytic diesel particulate filter, Chemical Engineering Science, Vol. 62, Iss. 18, 2007, pp. 5182-5185.
[42] P.K. Sahoo, L.M. Das, M.K.G. Babu, P. Arora, V.P. Singh, N.R. Kumar, T.S. Varyani, Comparative evaluation of performance and emission characteristics of jatropha, karanja and polanga based biodiesel as fuel in a tractor engine, Fuel, Vol. 88, Iss. 9, 2009, pp. 1698-1707.
[43] M. Lindgren, P.-. Hansson, Effects of transient conditions on exhaust emissions from two non-road diesel engines, Biosystems Engineering, Vol. 87, Iss. 1, 2004, pp. 57-66.

[44] P. Hansson A., M. Lindgren, M. Nordin, O. Pettersson, A methodology for measuring the effects of transient loads on the fuel efficiency of agricultural tractors, Applied Engineering in Agriculture, Vol. 19, 2003, pp. 251-257.
[45] K.K. Yum, N. Lefebvre, E. Pedersen, An experimental investigation of the effects of cyclic transient loads on a turbocharged diesel engine, Applied Energy, Vol. 185, 2017, pp. 472-481.
[46] J. Backas, Modelling of efficiencies of hydraulic pump with neural computation, Tampere University of Technology, Department of Intelligent Hydraulics and Automation, Tampere, 2010, 77 p.
[47] B. Vanwalleghem, C. Dousy, G. Pinte, B. Vanseveren, Optimization of the efficiency of hydrostatic drives, 8th International Fluid Power Conference, March 26-28, Dresden, Germany, pp. 12.
[48] Eaton® Medium Duty Piston Pumps, Eaton Corporation. Hydraulics Division. Form No. 03-206, 1992, 28 p.
[49] L. Wang, W.J. Book, J.D. Huggins, Application of singular perturbation theory to hydraulic pump controlled systems, IEEE/ASME Transactions on Mechatronics, Vol. 17, Iss. 2, 2012, pp. 251-259.
[50] M. Axin, B. Eriksson, P. Krus, Flow versus pressure control of pumps in mobile hydraulic systems, Proceedings of the Institution of Mechanical Engineers, Part I: Journal of Systems and Control Engineering, Vol. 228, Iss. 4, 2014, pp. 245-256.
[51] M. Huova, Energy efficient digital hydraulic valve control, Tampere University of Technology. Publication 1298, 2015, 158 p.
[52] N. Srivastava, I. Haque, A review on belt and chain continuously variable transmissions (CVT): dynamics and control, Mechanism and Machine Theory, Vol. 44, Iss. 1, 2009, pp. 19-41.
[53] H. Saha, Some methods to improve life cycle manageability of low-volume mobile processing platforms, Tampere University of Technology. Publication 899, 2010, 175 p.
[54] N. Mohammed, A. Munassar, A. Govardhan, A comparison between five models of software engineering, International Journal of Computer Science Issues (IJCSI), Vol. 7, Iss. 5, 2010, pp. 94-101.
[55] M. Shahbakhti, J. Li, J.K. Hedrick, Early model-based verification of automotive control system implementation, 2012 American Control Conference (ACC), pp. 3587-3592.
[56] R. Isermann, J. Schaffnit, S. Sinsel, Hardware-in-the-loop simulation for the design and testing of engine-control systems, Control Engineering Practice, Vol. 7, Iss. 5, 1999, pp. 643-653.
[57] G. Ao, J. Qiang, Z. Chen, L. Yang, Model-based energy management strategy development for hybrid electric vehicles, 2008 IEEE International Symposium on Industrial Electronics, pp. 1020-1024.
[58] A.R. Mayyas, S. Kumar, P. Pisu, J. Rios, P. Jethani, Model-based design validation for advanced energy management strategies for electrified hybrid power trains using innovative vehicle hardware in the loop (VHIL) approach, Applied Energy, Vol. 204, 2017, pp. 287-302.
[59] T. Park, C. Han, S. Lee, Development of the electronic control unit for the rack-actuating steer-by-wire using the hardware-in-the-loop simulation system, Mechatronics, Vol. 15, Iss. 8, 2005, pp. 899-918.

[60] S. Jeong, Y. Kwak, J.L. Woo, Software-in-the-loop simulation for early-stage testing of AUTOSAR software component, 2016 Eighth International Conference on Ubiquitous and Future Networks (ICUFN), pp. 59-63.
[61] O. Gietelink, J. Ploeg, B. De Schutter, M. Verhaegen, Development of advanced driver assistance systems with vehicle hardware-in-the-loop simulations, Vehicle System Dynamics, Vol. 44, Iss. 7, 2006, pp. 569-590.
[62] Home - dSpace, dSPACE GmbH, Available (accessed 28 August 2018): https://www.dspace.com/en/pub/home.cfm.
[63] What is LabVIEW, National Instruments, web page. Available (accessed 11 August 2018): http://www.ni.com/en-us/shop/labview.html.
[64] Simulink - Simulation and Model-Based Design, The MathWorks, Inc., web page. Available (accessed 11 August 2018): https://se.mathworks.com/products/simulink.html.
[65] Simcenter Amesim, Siemens Product Lifecycle Management Software Inc., web page. Available (accessed 11 August 2018: https://www.plm.automation.siemens.com/global/en/products/simcenter/simcenter-amesim.html.
[66] Embedded Code Generatio, The MathWorks, Inc., web page. Available (accessed 11 August 2018: https://se.mathworks.com/solutions/embedded-code-generation.html.
[67] Simulink PLC Coder, The MathWorks, Inc., web page. Available (accessed 11 August 2018: https://se.mathworks.com/products/sl-plc-coder.html.
[68] S. Shafer, A. Stentz, C. Thorpe, An architecture for sensor fusion in a mobile robot, Proceedings.1986 IEEE International Conference on Robotics and Automation, pp. 2002-2011.
[69] R. Brooks, A robust layered control system for a mobile robot, IEEE Journal on Robotics and Automation, Vol. 2, Iss. 1, 1986, pp. 14-23.
[70] R. Peter Bonasso, R. James Firby, E. Gat, D. Kortenkamp, D.P. Miller, M.G. Slack, Experiences with an architecture for intelligent, reactive agents, Journal of Experimental & Theoretical Artificial Intelligence, Vol. 9, Iss. 2-3, 1997, pp. 237-256.
[71] E. Gat, Integrating planning and reacting in a heterogeneous asynchronous architecture for controlling real-world mobile robots, Proceedings of the Tenth National Conference on Artificial intelligence (AAAI'92), July 12 - 16, 1992, AAAI Press, San Jose, California, pp. 809-815.
[72] T. Taira, N. Yamasaki, Functionally distributed control architecture for autonomous mobile robots, Journal of Robotics and Mechatronics, Vol. 16, 2004, pp. 217-224.
[73] J.L. Posadas, J.L. Poza, J.E. Simó, G. Benet, F. Blanes, Agent-based distributed architecture for mobile robot control, Engineering Applications of Artificial Intelligence, Vol. 21, Iss. 6, 2008, pp. 805-823.
[74] A.R. Khan, D.M. Asghar, An intelligent agent for a vacuum cleaner, International Journal of Digital Content Technology and its Applications, Vol. 3, 2009, pp. 143-146.
[75] M. Waibel, M. Beetz, J. Civera, R. D'Andrea, J. Elfring, D. Gálvez-López, K. Häussermann, R. Janssen, J.M.M. Montiel, A. Perzylo, B. Schießle, M. Tenorth, O. Zweigle, R.V. De Molengraft, RoboEarth, IEEE Robotics & Automation Magazine, Vol. 18, Iss. 2, 2011, pp. 69-82.

[76] S. Dersten, J. Axelsson, J. Fröberg, An analysis of a layered system architecture for autonomous construction vehicles, 2015 Annual IEEE Systems Conference (SysCon) Proceedings, pp. 582-588.
[77] L. Zhang, H. Gao, O. Kaynak, Network-induced constraints in networked control systems - a survey, IEEE Transactions on Industrial Informatics, Vol. 9, Iss. 1, 2013, pp. 403-416.
[78] T. Nolte, Share-driven scheduling of embedded networks, Mälardalen University. Press Dissertations No.26, 2006, 314 p.
[79] B.L. Steward, L. Tang, S. Han, A design framework for off-road equipment automation, Proceedings of the 2015 Conference on Autonomous and Robotic Construction of Infrastructure, Ames, IA, USA, June 2-3, 2015, Ames, IA, pp. 180-196.
[80] S. Blackmore, S. Fountas, H. Hawe, Proposed system architecture to enable behavioral control of an autonomous tractor, Proceedings of Automation Technology for Off-Road Equipment, Chicago, USA, July 26-28, 2002, American Society of Agricultural and Biological Engineers, pp. 13-23.
[81] R. Gu, R. Marinescu, C. Seceleanu, K. Lundqvist, Formal verification of an autonomous wheel loader by model checking, 018 IEEE/ACM 6th International FME Workshop on Formal Methods in Software Engineering (FormaliSE), Gothenburg, Sweden, 27 May-3 June 2018, IEEE, pp. 74-83.
[82] O. Koch, B. Beck, G. Heß, C. Richter, V. Waurich, J. Weber, V. Werner, U. Aßmann, Cloud-based system architecture for driver assistance in mobile machinery, Proceedings of 15:th Scandinavian International Conference on Fluid Power, Linköping, Sweden, June 7-9, 2017, Linköping University Electronic Press, Linköpings universitet, Linköping, pp. 81-90.
[83] J.S. Albus, 4D/RCS: A reference model architecture for intelligent unmanned ground vehicles, Proceedings of the SPIE 16th Annual International Symposium on Aerospace/Defense Sensing, Simulation and Controls, Orlando, FL, USA, April 1 - 5, 2002.
[84] F. Rovira-Más, Sensor architecture and task classification for agricultural vehicles and environments, Sensors, Vol. 10(12), 2010, pp. 11226-11247.
[85] R. Hippalgaonkar, Power management strategies for hydraulic hybrid multi-actuator mobile machines with DC actuators, Purdue University. UMI Number: 3636124, 2014, 177 p.
[86] BOBCAT 853H SKID STEER LOADER Service Repair Manual, Melroe Company. S/N 509711001-509717999, 1999, 43 p.
[87] Avant 630/635 Operator's Manual 2008, AVANT Techno Oy, 2007, 28 p.
[88] Volvo Excavator EW140B, Volvo Construction Equipment. Ref No. 21 3 433 1150, 2006, 20 p.
[89] Easy Machine Operation with Rexroth Automotive Drive and Anti Stall Control, Bosch Rexroth AG. RE 98300/06.03, 2003, 7 p.
[90] M. Brand, Digital driving - scalable functions for electronified drives , Mobile 2017, Perspective and Dialogue: Next level of Safety, Efficiency and Automation, Augsburg, Germany, June 28–29, 2017, Bosch Rexroth AG., Elchingen, Germany, pp. 71-79.
[91] EATON ETAC control: electronic transmission automotive control user's manual, Eaton Corporation. Document No. E-HYOV-TM002-E, 2007, 20 p.

[92] Propel Application Software Best Point Control (BPC), Danfoss. AI00000272en-US0102, 2016, 2 p.
[93] G. LaFayette, S. Gruettert, M. Gandrud, B. Laudenbach, D. Koenemann, Integration of engine & amp: hydraulic controls for best operation, 52nd National Conference on Fluid Power, March 23-25, 2011, Las Vegas, Nevada USA, pp. 591-598.
[94] S. Mutschler, N. Brix, Y. Xiang, Torque control for mobile machines, 11th International Fluid Power Conference Vol. 3, Aachen, Germany, 19th - 21th March 2018, Aachen University, Aachen, pp. 187-195.
[95] Engine-Speed-Dependent Driving Control (CA), Linde Hydraulics GmbH & Co. KG, web page. Available (accessed 20 August 2018): https://www.linde-hydraulics.com/en-gb/catalogue/detail.aspx?pid=56847&gid=43798&pg=W9S81%2F6lacagmMoQxWjYxg%3D%3D.
[96] LinDrive. The unbeatable driving experience, Linde Hydraulics GmbH & Co. LHY.LinDrive.01/13.e, 2018, 12 p.
[97] K. Huhtala, J. Fonselius, M. Vilenius, Comparing different control strategies of hydrostatic transmissions, The Seventh Scandinavian International Conference on Fluid Power, SICFP´01, Linköping, Sweden, May 30 - June 1, 2001, pp. 191-204.
[98] M. Sannelius, J.-. Palmberg, Conceptual design of complex hydrostatic transmissions, Proc. Seventh Bath International Fluid Power Workshop, Bath, UK, 21st-23rd September 1994, Taunton, Somerset, England : Research Studies Press.
[99] R. Pfiffner, L. Guzzella, C.H. Onder, Fuel-optimal control of CVT powertrains, Control Engineering Practice, Vol. 11, Iss. 3, 2003, pp. 329-336.
[100] T. Nilsson, A. Fröberg, J. Åslund, Fuel potential and prediction sensitivity of a power-split CVT in a wheel loader, IFAC Proceedings Volumes, Vol. 45, Iss. 30, 2012, pp. 49-56.
[101] Y. Zhang, Z. Zhou, X. Zhou, Intelligent control rule for tractor with continuously variable transmission, 2006 International Conference on Mechatronics and Automation, pp. 1712-1716.
[102] R. Pfiffner, L. Guzzella, Optimal operation of CVT-based powertrains, International Journal of Robust and Nonlinear Control, Vol. 11, Iss. 11, 2001, pp. 1003-1021.
[103] J. Ossyra, M. Ivantysynova, Application for a direct optimization procedure for drive line control, Power Transmission and Motion Control: PTMC 2004, Bath, England, 1-3 September, 2004, Bath University, Bath, pp. 53-69.
[104] M. Heikkilä, M. Huova, J. Tammisto, M. Linjama, J. Tervonen, Fuel efficiency optimization of a baseline wheel loader and its hydraulic hybrid variants using dynamic programming, Proceedings of the BATH/ASME 2018 Symposium on Fluid Power and Motion Control FPMC2018, Bath, UK, September 12-14, 2018, ASME, Bath, pp. 1-10.
[105] L.V. Larsson, Control aspects of complex hydromechanical transmissions with a focus on displacement control, Linköping Studies in Science and Technology Licentiate Thesis No. 1781, 2017, 55 p.
[106] G. Palmgren, On secondary contolled hydraulic systems
, Linköping Studies in Science and Technology Thesis No. 144, 1988, 64 p.
[107] R.H. Hansen, T.O. Andersen, H.C. Pedersen, Development and implementation of an advanced power management algorithm for electronic load sensing on a

telehandler, Proc. FPMC 2010, Bath/ASME Symposium on Fluid Power & Motion Control, American Society of Mechanical Engineers, pp. 537-550.
[108] C. Williamson, Power management for multi-actuator mobile machines with displacement controlled hydraulic actuators, Purdue University. UMI Number: 3449412, 2010, 154 p.
[109] B. Saerens, J. Vandersteen, T. Persoons, J. Swevers, M. Diehl, E. Van den Bulck, Minimization of the fuel consumption of a gasoline engine using dynamic optimization, Applied Energy, Vol. 86, Iss. 9, 2009, pp. 1582-1588.
[110] Key Figure - Hitachi Construction Machinery, CSR & Financial Report 2015 for all stakeholders, Hitachi, 2015, 38-44 p.
[111] T. Cheng, B. O'Sullivan, LX1 prototype hybrid wheel loader delivers around 50% fuel efficiency improvement during customer testing, Volvo AB, Available (accessed 20 August 2019): https://www.volvoce.com/global/en/news-and-events/news-and-press-releases/2017/lx1-prototype-hybrid-wheel-loader-delivers-50-percent-fuel-efficiency-improvement/
[112] J. Wang, Z. Yang, S. Liu, Q. Zhang, Y. Han, A comprehensive overview of hybrid construction machinery, Advances in Mechanical Engineering, Vol. 8, Iss. 3, 2016, 15 p.
[113] R. Filla, Hybrid power systems for construction machinery: aspects of system design and operability of wheel loaders, ASME 2009 International Mechanical Engineering Congress and Exposition, Lake Buena Vista, Florida, USA, November 13–19, 2009, ASME, Florida, pp. 611-620.
[114] B. Wu, C. Lin, Z. Filipi, H. Peng, D. Assanis, Optimal power management for a hydraulic hybrid delivery truck, Vehicle System Dynamics, Vol. 42, 2004, pp. 23-40.
[115] H. Kim, S. Yoo, S. Cho, K. Yi, Hybrid control algorithm for fuel consumption of a compound hybrid excavator, Automation in Construction, Vol. 68, 2016, pp. 1-10.
. Zeng, N. Yang, Y. Peng, Y. Zhang, J. Wang, Research on energy saving control strategy of parallel hybrid loader, Automation in Construction, Vol. 38, 2014, pp. 100-108.
[117] J.W. Anders, C.L. Gorman, System and method for managing power in machine having electric and/or hydraulic devices, US 8606448B2, US8606448B2 29.06.2011, (10.12.2013), 20 p.
[118] R. Filla, Method for operating a working machine and a working machine, US9032725B2, US12444402, 2006-10-25, (2015-05-19), 11 p.
[119] U. Tietge, N. Zacharof, P. Mock, V. Franco, J. German, A. Bandivadekar, N. Ligterink, U. Lambrecht, From laboratory to road: a 2015 update of official and "real-world" fuel consumption and CO2 values for passenger cars in Europe, ICCT White Paper, International Council on Clean Transportation Europe, Berlin, 2015, 24 p.
[120] R. Filla, Representative testing of emissions and fuel consumption of working machines in reality and simulation, SAE 2012 Commercial Vehicle Engineering Congress, SAE Technical Paper, pp. 1-18.
[121] R. Filla, Optimizing the trajectory of a wheel loader working in short loading cycles, SICFP2013, June 3-5, 2013, Linköping, Sweden, pp. 307-317.
[122] J. Andersen, D. Ekenberg, K. Willner, L. Erlandsson, Methods to calculate and declare fuel consumption for heavy non road mobile machinery part II: literature and simulation study, Swedish National Road and Transport Research Institute (VTI), 2011, 26 p.

[123] K. Sud, Transient modeling and control of split cycle clean combustion diesel engine, University of Illinois at Chicago, 2013, 127 p.
[124] M. Ehsani, K.M. Rahman, H.A. Toliyat, Propulsion system design of electric and hybrid vehicles, IEEE Transactions on Industrial Electronics, Vol. 44, Iss. 1, 1997, pp. 19-27.
[125] K. Johanastrom, C. Canudas-de-Wit, Revisiting the LuGre friction model, IEEE Control Systems, Vol. 28, Iss. 6, 2008, pp. 101-114.
[126] H. Olsson, K.J. Åström, C. Canudas de Wit, M. Gäfvert, P. Lischinsky, Friction models and friction compensation, European Journal of Control, Vol. 4, Iss. 3, 1998, pp. 176-195.
[127] Axial Piston Variable Pump A4VG. Data sheet, Bosch Rexroth AG. RE92004/06.09, 2009, 60 p.
[128] Axial Piston Variable Motor A6VM. Data sheet, Bosch Rexroth AG. RE91610/01.12, 2012, 80 p.
[129] M. Ahopelto, K. Huhtala, Prediction of drive torque in hydraulic wheel loader, Bath, United Kingdom, September 10–12, 2014, The American Society of Mechanical Engineers ASME, pp. 1-8.
[130] Vilenius Jani, Raneda Albert, Huhtala Kalevi, Characteristics of teleoperated skid steered mobile machine, Proceedings of the 3rd FPNI-Phd Symbosium on Fluid Power, Terrassa, Spain, June 30-July 2, 2004, Fluid Power Net International, Spain, pp. 587-598.
[131] Karhu Otso, On-board electronic control systems of future automated heavy machinery, Tampere University of Technology. Publication 1352, 2015, 148 p.
[132] Uusisalo Jarno, A case study on effects of remote control and control system distribution in hydraulic mobile machines, Tampere University of Technology. Publication 960, 2011, 111 p.
[133] Ahopelto Miika, Design of the control system of the work machine, Tampere University of Technology, 2010, 73 p.
[134] M. Ahopelto, J. Backas, K. Huhtala, Power management in a mobile work machine: reduced diesel rpm for better energy efficiency, Proceedings of the 7th FPNI PhD Symposium on Fluid Power, Reggio Emilia, Italy, June 27-30, 2012, University of Modena and Reggio Emilia., Reggio Emilia, Italy, pp. 133-148.
[135] M. Ahopelto, J. Backas, R. Ghabcheloo, K. Huhtala, Improved energy efficiency and controllability of mobile work machines by reduced engine rotational speed, Proceedings of the ASME 2013 International Mechanical Engineering Congress and Exposition, IMECE2013, San Diego, California, USA, November 15–21, 2013, ASME, pp. 1-8.
[136] J. Tervonen, Researching the energy consumption of a wheel loader, Tampere University of Technology, Department of Intelligent Hydraulics and Automation, 2014, 105 p.
[137] AVL KMA Mobile, AVL LIST GmbH, web page. Available (accessed 12.7.2018): https://www.avl.com/-/avl-kma-mobile.